DOE/PC/93227--T11

ROLE OF CHAR DURING REBURNING OF NITROGEN OXIDES

Eleventh Quarterly Report
April 1, 1996 - June 30, 1996

Wei-Yin Chen[1]
L.T. Fan[2]
Te-Chang Lu[1]
Lin Tang[1]
Fang Meng[2]

1. Department of Chemical Engineering
Anderson Hall
University of Mississippi
University, MS 38677-9740

2. Department of Chemical Engineering
Durland Hall
Kansas State University
Manhattan, KS 66506-5102

Submitted to

U.S. Department of Energy
Pittsburgh Energy Technology Center
P.O. Box 10940-118
Pittsburgh, PA 15236-0940

July 30, 1996

Work Performed under the Grant DE-FG22-93PC93227

ROLE OF CHAR DURING REBURNING OF NITROGEN OXIDES

Eleventh Quarterly Report
April 1, 1996 - June 30, 1996

Wei-Yin Chen[1]
L.T. Fan[2]
Te-Chang Lu[1]
Lin Tang[1]
Fang Meng[2]

1. Department of Chemical Engineering
Anderson Hall
University of Mississippi
University, MS 38677-9740

2. Department of Chemical Engineering
Durland Hall
Kansas State University
Manhattan, KS 66506-5102

Submitted to

U.S. Department of Energy
Pittsburgh Energy Technology Center
P.O. Box 10940-118
Pittsburgh, PA 15236-0940

July 30, 1996

Work Performed under the Grant DE-FG22-93PC93227

ACKNOWLEDGMENTS

Substantial contribution to this report were made by Jeremy Milum, undergraduate assistant.

ABSTRACT

Reburning is an emerging three-stage combustion technology designed for the reduction of NO by introducing a small amount of reburning fuel above the primary flame where the majority of NO is chemically reduced to nitrogen. While coal, in general, has not been considered an effective reburning fuel, research at the University of Mississippi suggested that lignite has a reburning efficiency even higher than that of methane. Furthermore, heterogeneous mechanisms are more important than homogeneous mechanisms for char/NO reaction. The objectives of this research are to investigate 1) implications of pore structure analysis, 2) parameters governing heterogeneous reactions, and 3) estimation of rates of NO reduction and mass transfer limitations. Experiments have been performed in a flow reactor with a simulated flue gas at a stoichiometric ratio (SR) 1.1. Reburning fuels in this study include chars derived from Pittsburgh #8 bituminous coal and Mississippi lignite. Chars were produced in N_2 by suspending a sample basket in a tube furnace. Pore structure analyses include BET-N_2, BET-CO_2, and DR-CO_2 surface areas, pore size distribution, micropore volume, total pore volume, and average pore radius. These studies suggest that neither BET-N_2 nor DR-CO_2 surface area is a normalization factor of chars of different origin. Reaction with NO leads to closures of pores, which may be contributed by formation of surface complexes.

Parameter study reveals that the effectiveness of heterogeneous reburning strongly depends on variables in three areas: (1) the origin of char, (2) char devolatilization temperature and time, and, (3) the competition of NO with CO_2 and O_2 for the active sites on the char surface. Without any oxidants in the feed, char derived from Pittsburgh #8 bituminous coal is more reactive than char derived from Mississippi lignite. Chars derived from less severe pyrolysis, 950°C and zero holding

time, are significantly more reactive than chars derived from pyrolysis, 1100°C, 5 min holding time and 1100°C, 2 h holding time. Active sites for the generation of CO_2-gasification products can be destroyed easier than those accessible to NO and O_2; however, within certain levels of severity, CO_2 seems to form stable surface complexes on bituminous coal char derived from 1100 °C and 5 min holding time. Fundamental understanding of these mechanisms has practical importance to the production of activated carbon for flue gas cleanup.

Justification of the laminar flow for the plug flow reactor has been well estiblished Estimation of the rate of NO reduction has been established to include the conversion in the nonoisothermal and isothermal regions of the flow reactor and internal mass transfer limitations. Solving a set of equations simultaneously with MathCad gives the frequency factor, activation energy, Thiele modulus, and effectiveness factor. The calculated results imply that internal mass transfer limitations exist only when the temperature is close to 1100°C. External mass transfer rate is of the same order of magnitude as reaction rate at 1100°C. Possible reasons for the higher intrinsic rates obtained from the present study are discussed. The present study also suggests that the gasification rate for char/NO reaction is about the same or even higher than the rate for char/O_2 reaction.

TABLE OF CONTENTS

ACKNOWLEDGMENTS ii

ABSTRACT iii

I. INTRODUCTION 1

II. EXPERIMENTAL 5
A. Flow Reactor 5
1. Experimental Apparatus 5
2. The Coal Feeder 7
3. Char/Ash Collection Unit 7
4. Product Analysis 8
B. Char Sample Preparation and Analysis 8
C. Surface Area and Pore Volume Analysis 9
D. Summary of Experimental Work 10

III. CHARACTERISTICS OF THE FLOW REACTOR SYSTEM . . 11
A. Justification of Laminar Flow and Dispersion Model . . . 11
B. Solid Mixing in Flow Reactor 14

IV. IMPLICATIONS OF PORE STRUCTURE ANALYSIS . . . 15

V. PARAMETERS GOVERNING HETEROGENOUS REBURNING . 18
A. Effects of Char Origin, Char History, and CO_2 and O_2 on NO Reduction 18
1. Effects of Char Origin on NO Reduction 18
2. Effects of Char History on NO Reduction 20
3. Effects of CO_2 and O_2 on NO Reduction 21
B. Yields of Carbon Oxides and Oxygen Balance 24
C. Yield of Nitrous Oxide 25

VI. RATES OF NO REDUCTION IN VARIOUS REACTING ENVIRONMENTS 25
A. Rate Expression for Data from Plug Flow Reactor 25
B. Reactions during Heat-up and Cooling 28
C. Estimations of Transfer Limitations 30
1. Rate Constants and Internal Mass Transfer Limitation . . 30
2. External Mass Transfer Limitation 34
D. Effects of Char Origin, History and Oxidants on Rate of NO/Char Reaction 36
E. Comparison with Published Data 36
F. Effect of Initial NO Concentration 37
G. Comparison of the Rates of NO/Char and O_2/Char Reactions . . 42

VII. CONCLUSIONS 45

REFERENCES 47
APPENDICES 52
APPENDIX A. Methods of Surface Area Calculation 52
APPENDIX B. Stoichiometric Ratio (SR) of Reburning Zone . . . 55
TABLES 58
FIGURES 71

I. INTRODUCTION

The regulations established in the United States by the Clean Air Act Amendments of 1990 mean that a single NO_x control technology is not likely to be sufficient for boilers in the ozone non-attainment areas. Reburning is an emerging three-stage combustion technology designed for the reduction of NO by introducing a small amount of reburning fuel above the primary flame where the majority of NO is chemically reduced to nitrogen in this fuel rich environment. The concept of reburning was first introduced by Wendt *et al.* (1973). Tests on a full-scale boiler at Mitsubishi Heavy Industries (Takahashi *et al.*, 1983) resulted in over 50% NO_x reduction.

Coals, including lignites, are an economical source of the carbon required for NO reduction in the fuel rich environment. Their effectiveness as a reburning fuel seems to depend on two ambivalent factors in their early stage of development. First, the conversion of the nitrogen in coal to NO in the reburning and burnout stages is not clear. Nevertheless, through an isotopical tracing technique, it has been revealed that conversion of volatile nitrogen in coal to NO during reburning is very low (Burch *et al.*, 1994). It is also known that conversion of char nitrogen to NO during combustion is less than 50% of that of volatile nitrogen (Pershing and Wendt, 1979). Second, while the homogeneous gas phase NO reduction in the fuel rich environment is relatively well understood (see, e.g., Miller and Bowman, 1989), NO reburning by chars of diverse origin and history has not been considered a viable NO reduction route until very recently.

Our initial studies of simulated reburning with reactors of two scales (Burch *et al.*, 1991a,b; 1994) have demonstrated that lignites are more effective than methane as reburning fuel. The two lignites tested were selected from Mississippi and North Dakota; both lignites have a high calcium content. Screening with the North Dakota lignite indicated that the lignite char surface participates

in heterogeneous/catalytic NO reduction to HCN, while lignite ash enhances catalytic HCN reduction to NH_3. Both reactions are important in the overall NO reduction scheme. The effectiveness of heterogeneous reburning has recently been demonstrated in a 1.0 and a 0.1 MMBtu/hr pilot scale test facility (Payne *et al.*, 1995; Pershing, 1995).

Detailed kinetic analysis of homogeneous phase NO reduction in a fuel rich environment indicates that the majority of NO is reduced by hydrocarbon radicals C, CH and CH_2 to HCN and amine radicals (NH_i) (Miller and Bowman, 1989). The amine radicals, in turn, can be converted to N_2 or NO. The yields of these desirable hydrocarbon radicals from lignite during reburning are not known. Nevertheless, coal and lignite produce only about 50% of the volatile carbons which methane produces at the same stoichiometry, which leads to the speculation that the lignite char participates in considerable heterogeneous reactions with NO.

Although NO reburning by char has not been a major area of research, investigating the interaction of NO with various carbonaceous and metallic materials has been the objective of a number of studies. An extensive review has been conducted by De Soete (1990). It has been shown that carbonaceous materials can be gasified by NO to form CO, CO_2 and N_2 (Bedjai *et al.*, 1958; Smith *et al.*, 1959; Furusawa *et al.*, 1980; Levy *et al.*, 1981; Chan *et al.*, 1983; Suuberg *et al.*, 1990; Teng *et al.*, 1992; Chu and Schmidt, 1993; Illan-Gomez *et al.*, 1993). The gasification reaction can be promoted by the addition of reducing agents, such as CO and H_2, and inhibited by O_2 when the CO_2/CO ratio is higher than one (De Soete, 1990). In addition to gasification, reaction of NO with CO on various surfaces, including char, ash and soot, can also be a major route of heterogeneous NO reduction mechanisms (De Soete, 1990). Catalytic decomposition of NO on various metallic oxides, some of which are common constituents in the lignite, has been reported by Winter (1971).

Huffman *et al.* (1990) reported that calcium is dispersed in coal macerals and is bonded to the oxygen anions. During combustion, the calcium present in lignite agglomerates, and eventually forms CaO and CaS. Recent lab-scale investigations of fluidized bed combustion (FBC) and circulating FBC (CFBC) have shown that calcium sulfide (Hansen *et al.*, 1992), CaO (Allen, 1991; Hansen *et al.*, 1992; Hansen and Dam-Johansen, 1993; Shimizu *et al.*, 1993; Lin *et al.*, 1993) and Fe_2O_3 (Allen, 1991) serve as catalysts for NO reduction in various environments. While most of these researchers claimed the catalysts enhanced the gasification or the conversion of NO + CO to form CO_2 and N_2, Lin *et al.* indicated that CO decreases the NH_3 conversion to NO. Lin *et al.* also claimed that NO may oxidize NH_3 to form nitrogen through homogeneous and heterogeneous mechanisms in FBC or CFBC. These char gasification and mineral-catalyzed reactions in reburning environments have not been fully investigated, but can certainly be enhanced by the highly porous nature of lignite char. Various calcium-NO surface complexes have been identifiedby infrared studies (Low and Yang, 1974; Allen, 1991).

In the early period of this project (Chen and Ma, 1995; Chen *et al.*, 1995a, 1995b), we have been examining the reactivities of selected chars with NO. Some of the findings from the project are summarized below.

1. Heterogeneous mechanisms contribute higher NO reduction than homogeneous mechanisms over a wide range of stoichiometric ratios when lignite is used as reburning fuel;
2. Lignite char alone can be an effective reburning fuel;
3. Surface area, estimated either by the Dubinin-Radushkevich (D-R) equation with CO_2 as adsorbate or by BET- N_2 method, is not a normalization factor of char reactivity;
4. Based on limited experiments, NO reduction by bituminous coal char can be somewhat improved

by impregnating the char with CaO;

5. Unlike the homogeneous phase mechanisms, oxidants, including CO_2 and O_2, inhibit the surface NO reduction over the entire range of reburning stoichiometric ratio (SR2) studied, 0.6 to 1.1.

Our observation of the heterogeneous mechanisms along with the impregnation approach discussed herein may have profound impacts on the practice of coal-fired boilers in utilities and industries. First, previous studies (Pohl, 1976; Pershing and Wendt, 1979) have indicated that conversion of char nitrogen to NO is less than 50% of the conversion of volatile nitrogen. This suggests only a small fraction of the char nitrogen will be converted to NO in the burnout stage. Second, impregnation/ion-exchange technique is expected to increase the value of bituminous coal as a reburning fuel. Third, the presence of calcium compounds may also enhance sulfur capture, both in the reburning and in the burnout stages. Although SO_2 may compete with NO in the reburning zone for CaO, it has been established that CaS and $CaSO_4$ also catalyze the oxidation of char (Gopalakrishnan *et al.*, 1994, Hansen *et al.*, 1992). Fifth, earlier work (Burch *et al.*, 1991b) has demonstrated that lignite ash contains minerals which catalyzes HCN conversion to NH_3, a desirable reaction step when volatile reburning fuel is used.

The objectives of this study focus on the variables which are potentially significant to heterogeneous reburning, including the effects of char origin, pyrolysis severity and oxidants. Product distributions of NO reaction with chars of two different origins have been examined by sequentially adding the three major oxidants in reburning: NO, O_2, and CO_2. Internal pore structures of chars before and after the reactions have been determined to assist the interpretations of experimental results. Rates of NO reduction have estimated; implications of Langmuir-Hinshelwood mechanisms

and mass transfer limitations have been examined in detail.

II. EXPERIMENTAL

Reburning experiments were conducted with Mississippi lignite char and Pittsburgh #8 bituminous coal char in a wide range of reburning stoichiometric ratios. The major experimental apparatus follows Chen *et al.* (1991). For completeness, it is discussed in the following sections.

A. Flow Reactor

1. Experimental Apparatus

The experimental apparatus is shown in Figure 1. The experiments were carried out in a ceramic flow reactor with a simulated flue gas consisting of 16.8% carbon dioxide, 1.95% oxygen, and 0.1% NO in a helium base. The above concentrations were chosen to be consistent with those of a coal primary flame operated at a stoichiometric ratio of 1.1. Helium, instead of nitrogen, was used as the carrier gas to minimize the heating time. The reburning temperatures are from 800 °C to 1100 °C. The estimated residence time is about 0.2 s in this temperature range.

The flow reactor used for this research was an alumina tube (Coors Ceramic Co.) with an inside diameter of 1.91 cm and an overall length of 64 cm. The central portion of the reactor tube was enclosed in a 30 cm long, electrically heated Lindberg Model 55035 tube furnace. The low thermal mass moldatherm^R insulation and helically coiled alloy heating element composite in the furnace enables rapid duty cycles, conservation of energy, and improved program efficiencies.

Furnace temperature profiles were determined by both centerline traverse and wall mounted type K thermocouples (Burch, 1991a). These two methods agreed within ±5°C. The furnace produces a parabolic axial temperature profile with a relatively flat peak (±20°C) over approximately

10 cm of the heated length. Outside the zone of maximal heating, the temperature falls rapidly at a rate of approximately 60°C/cm. For typical flow conditions, this corresponds to heating and cooling rates on the order of 2000°C/s. Furnace temperature profiles with and without combustion produced identical temperature profiles except for a narrow zone of maximum heat release where both wall mounted and centerline thermocouple exhibited an approximate 10°C rise.

The centerline temperature measurements were taken using a 0.32 cm o.d. sheathed but unshielded thermocouple (Burch, 1991a). Due to high radiation from the walls, the temperature profiles obtained by this method are more representative of the wall temperature than the mean gas temperature at any given location. Using property data for the simulated flue gas composition and the method of Sellars *et al.* (1956) the maximum gas temperature is estimated to be 50°C lower than the maximum wall temperature and to be maintained for only 10 cm of the furnace length (Figure 2). The estimated average gas temperature profile is used in the estimation of the rate constant, which is discussed in detail in section V.B.

All of the gas flows were measured individually with rotameters, as shown in Figure 1. These rotameters are calibrated periodically using a wet test meter. The gas mixtures, with certified compositions, were purchased from Matheson Gas Products Inc., Liquid Air Corp., and Liquid Carbonic.

The reactor tube was cleaned after each run to minimize wall buildup of soot or ash. To eliminate any transient phenomena due to adsorption/desorption, operating conditions were stabilized for at least fifteen minutes before data collection began.

The reactor tube was directly connected with a coal feeder at the inlet of the tube and a char/ash collection unit at the exit of the tube. The coal feeder provided a supply of reburning fuel

to the reactor. The effluent from the reactor is first allowed to pass through the char/ash collection unit in which most of char/ash particles are removed. Then, fine particles are filtered off by a NUPRO filter (60 micron) and the flue gases are allowed to pass through either the impinger or the impinger bypass. The sampling train consisted of 0.635 cm stainless steel transfer lines and a switching manifold with stainless steel valves. The effluent was finally transferred to the instrument package through 0.635 cm Teflon tubing. The coal feeder and char/ash collection unit will be discussed in detail in the following sections.

2. The Coal Feeder

For experiments with coal as the reburning fuel, the delivery system is shown schematically in Figure 3 and Figure 4. Details of this device and it's modification have been documented elsewhere (Chen *et al.*, 1991; Chen, 1994). Part of the gas flow (usually helium) was diverted through the coal feeder as a carrier gas. The coal feeder carriage and drive mechanism are shown in Figure 4. It relies on stable aero-striping of a small amount of coal particles by a high velocity carrier gas entering from the top around a piston guide. The diameter of the piston guide is only about 0.0076 cm smaller than the inside diameter of the coal reservoir. Stable aero-striping, in turn, depends on the precision and uniformity of this small opening, a narrow range of coal particle size and gas flow rate. The acrylic sample reservoir has a capacity of only about 10 cm^3, and can be pressed hard to ensure perfect sealing when assembled.

3. Char/Ash Collection Unit

The stainless steel char/ash collection unit is based on inertia and gravity separation principles (Chen, 1994). As illustrated in Figure 5, the sharp change of the flow direction and decrease in gas velocity facilitate the settlements of the particles. The collection unit is 10.16 cm i.d. × 20.32 cm

height and is able to reduce the gas velocity after the 180 degree turn due to an enlarged cross-sectional area. The flange at the bottom of the collection unit allows frequent opening and easy cleanup. The test runs showed that the reasonable response time of the flow system is about 12 minutes.

After the char/ash collection unit, the flue gases were directed to three analyzers; an NO/NO_2 analyzer, CO/CO_2 analyzer, and N_2O analyzer.

4. Product Analysis

The three major nitrogenous species, nitrogen oxide (NO), carbon dioxide (CO_2), carbon monoxide (CO), and nitrous oxide (N_2O) were routinely analyzed by the procedure described by Chen *et al.* (1995). NO was analyzed by a Thermal Electron Model 10A chemiluminescent $NO-NO_x$ analyzer. CO_2 and CO were analyzed by a California Analytical Instruments, Inc. Model ZRH $CO-CO_2$ infrared gas analyzer. The N_2O was analyzed by a Horiba Model VIA-510 infrared analyzer. The analyzers were all calibrated with a gas mixture representative of the feed gas composition. When volatile fuels are used, the yields of HCN and NH_3 are determined by ion detectors, which is well documented in Chen & Ma (1995).

B. Sample Preparation and Analysis

In order to determine the importance of heterogeneous NO/char reaction mechanisms from the homogeneous phase reaction mechanisms during reburning, and to evaluate the effectiveness of different chars as reburning fuels, chars were prepared in a stainless tube (5.3 cm i.d.) electrically heated by a split tube furnace. This char preparation system is shown in Figure 6. The furnace (Thermcraft Model # 23-18-12H) is a single zone furnace with a heating chamber three inches inside diameter and eighteen inches long. A 50 mesh stainless steel screen was installed as the distributor

6" above the bottom of the furnace. To provide effective heat transfer to the gas, a silicon sand layer was placed on the distributor. The coal/char basket assembly consisted of a stainless steel handle (0.635 cm stainless steel tubing) and a stainless steel basket (serving as the coal/char container 2.2 cm o.d.× 15 cm height). The basket is equipped with a mesh screen cover. During the pyrolysis in nitrogen, the sample basket with only two thirds of its volume filled with sample (about 12g), was lowered into the ceramic tube furnace just above the sand bed. Volatile products were carried away by nitrogen. The set temperature of the furnace was then raised from room temperature to a target temperature (1100 °C or 1150 °C) with a 0.28°C/s heating rate. The measured sand temperatures are about 50 °C lower than the set temperatures. After the furnace reached the set temperature, the sample was kept in the furnace for another pre-determined time period, 0, 5 min or 2 h. Quenching was achieved by raising the sample basket to a water-cooled, reversed-nitrogen gas flow section. The sample was kept in the quenching zone for about 25 minutes before removal from the furnace. The char samples were stored in glass bottles sealed with caps. This procedure generates char with a weight percentage (dry basis) of 45% of the Mississippi lignite, 61.8% of Pittsburgh #8 bituminous coal. The ultimate analysis results of the lignite and coal chars were reported by Huffman Laboratory and are listed in Table 1.

C. Suface Area and Pore Structure Analysis

The char samples were sent to Kansas State University for pore structure analysis. Table 2 lists the char origin and history of these samples. The measurements were carried out with Quantachrome NOVA-1200. The samples were measured by both the BET-N_2 method and the CO_2 D-R equation. The BET-surface area was determined by using nitrogen (N_2) as the adsorbate at a temperature of 77 K. The CO_2 D-R equation analysis was conducted with CO_2 at 273 K, which will

be discussed in details in Chapter IV and Appendix A.

D. Summary of Experimental Work

The investigation of the effects of feed NO concentration on the rate of NO reaction was conducted with chars of two different origins. From the standpoint of reburning practice, these rate data are desirable because recent successful developments in low NO_x burners have significantly lowered the NO concentration of flue gas coming into the reburning stage. From the standpoint of basic research, these rate data are needed for the understanding of the heterogeneous reburning mechanisms in various periods of reburning.

Five series of experiments with chars of two different origins were conducted with feed NO at 200, 400, 600, 800, and 1000 ppm and in the temperature range from 800 to 1100°C. To be consistent with other experiments, the chars were produced from the Pittsburgh #8 bituminous coal and Mississippi lignite at 1100°C and 5 min holding time. No oxidants are included in the feed during their reactions with NO.

In order to study the effects on char severity and oxidants for the NO reduction, we carefully designed the pyrolysis temperature and holding time for both chars as follows; (a) char pyrolyzed at 950°C and 0 holding time, (b) char pyrolyzed at 1100 °C and 5 min holding time, (c) char pyrolyzed at 1100°C and 2 h holding time. All chars were subject to reactions at 1100°C with three types of gaseous environments, NO , $NO+CO_2$, $NO+CO_2+O_2$.

III. CHARACTERISTICS OF THE FLOW REACTOR SYSTEM

A. Justification of Laminar Flow and Dispersion Model

It is known that measurement of reaction rate can be profoundly influenced by the flow pattern inside a laminar flow reactor. To estimate of the extent of such effects, the flow region based on the Peclet number is estimated first, and the choice of axial dispersion model is justified. Based on the dispersion model, the extents of radial and axial diffusion are estimated and the deviation from plug-flow in the estimation of rate constant is assessed.

Although the reaction in a tubular flow reactor can be affected by a number of variables, the flow pattern has been conveniently categorized into three regions (e.g., Wen and Fan, 1975): pure convection, axial dispersion, and intermediate region . The two factors governing the flow regions are: Peclet number (Ru/D_M) and dimensionless time ($D_M t/R^2$), where R is the tube radius, u is the average fluid velocity, D_M is the molecular diffusivity, and t is the average fluid residence time in the reactor. Our experiments have been conducted with a tubular reactor with i.d. 1.91 cm, at 1100°C, and with a volumetric flow rate of 2000 cm^3/min (measured at 25°C). The reactor is placed in a electric furnace with a 12 in. heating element. Using property data for the simulated flue gas composition and the method of Sellars *et al.* (1956), the maximum gas temperature is estimated to be 50°C lower than the maximum wall temperature and maintained for only 4 in. of the tube length. The estimated average gas temperature and reaction time for this 4 in. zone are the basis for the analysis presented below. At 1100°C, the flow rate and average residence time of gas in the tube are 153.6 cm^3/s and 0.2 s respectively. The diffusivity of NO in He can be estimated based on molecular theory (Bird *et al.*, 1960)

$$\frac{P\,D_{AB}}{(P_{cA}P_{cB})^{\frac{1}{3}}(T_{cA}T_{cB})^{\frac{5}{12}}\left(\frac{1}{M_A}+\frac{1}{M_B}\right)^{\frac{1}{2}}} = a\left(\frac{T}{\sqrt{T_{cA}T_{cB}}}\right)^{b} \qquad \text{(III-A-1)}$$

in which D_{AB} [=]$cm^2\ sec^{-1}$, p [=] atm, and T [=] K. Analysis of experimental data gave the following values of the constants: a = 2.745 x 10^{-4} and b = 1.823 (Bird *et al.*, 1960). This formula suggests that the diffusivity varies from 0.84 to 13.7 cm^2/s when temperature increases from 25 to 1100°C. Based on the system parameters obtained above, the Peclet number and dimensionless reaction time at 1100 °C are estimated

$$\frac{Ru}{D_M} = 3.72 \qquad \text{(III-A-2)}$$

$$\frac{D_M t}{R^2} = 2.99 \qquad \text{(III-A-3)}$$

The values of these factors imply that the axial dispersion model is appropriate in the subsequent analysis of deviations from a plug flow reactor (e.g., Wen and Fan, 1975).

Based on the dispersion model, the pertinence of reaction rate measurements using a laminar flow reactor can be assessed. Dispersion model is an effective approach for handling the combined effects of radial dispersion, axial dispersion, and axial convective flow, either laminar or turbulent. The effective axial dispersion coefficient under influences of radial dispersion and axial dispersion in a laminar flow has been theoretically derived (Taylor, 1953; Aris, 1956)

$$E_z = D_M + \frac{R^2 u^2}{48 D_M} \qquad \text{(III-A-4)}$$

Substituting the known values into the right hand side of Eq. (III-A-4) we obtain

$$E_z = 17.1 \frac{cm^2}{s} \qquad \text{(III-A-5)}$$

Equation (III-A-4) is valid when (Wissler, 1969)

$$\frac{kR^2}{(3.8)^2 D_M} < 1 \qquad \text{(III-A-6)}$$

where k is the first order reaction rate constant; or, after substituting the system parameters,

$$k < 216\ s^{-1} \qquad \text{(III-A-7)}$$

For the study of NO reduction on the char surface, the feeding rate of char can be controlled to ensure that the rate constant is below the limit in Eq. (III-A-7). In fact, the limiting rate constant stated in Eq. (III-A-7) corresponds to an extremely fast reaction and low output to input NO ratio which rarely happens in our experimental system (t = 0.2 s)

$$\frac{[NO_{out}]}{[NO_{in}]} = e^{-kt} = 10^{-19} \qquad \text{(III-A-8)}$$

From the effective axial dispersion coefficient, the Peclet number for the axial direction, Pe_z, can be

estimated

$$\frac{1}{Pe_z} = \frac{E_z}{uL} = 3.38 \times 10^{-2} \qquad \text{(III-A-9)}$$

where L is length, cm. This is a very small number, implying only small deviation from plug flow (Levenspiel and Bischoff, 1959). Levenspiel and Bischoff provided both a graphic representation and equation for correction of the rate measurement

$$\frac{[NO_{out}]}{[NO_{in}]} = \exp\left[-kt + (kt)^2 \frac{E_z}{uL}\right] \qquad \text{(III-A-10)}$$

The correction term in Eq. (III-A-10) indicates that the error in measurement of the rate constant will not be over 5% when the conversion is below 95%. This justifies the use of our laminar flow reactor for the measurement of reaction rate.

B. Solid Mixing in Flow Reactor

When the char particle reaches the terminal velocity under free fall conditions, the weight of the particle is balanced by the sum of buoyant force and total drag, i.e.,

$$\frac{\pi}{6} d_s^3 \rho_s g = \frac{\pi}{6} d_s^3 \rho_g g + 3\pi \mu_g d_s u_s \qquad \text{(III-B-11)}$$

where d_s, ρ_s, g, ρ_g, μ_g, and u_s are char particle diameter, char nominal density, gravity, gas density, viscosity of gas, and particle velocity, respectively. Substituting the system parameters, we obtain

$$u_s = 0.56 \frac{cm}{s} \qquad \text{(III-B-12)}$$

which is much smaller than the average gas velocity, 11 cm/s. This suggests good particle entrainment in the gas.

It is worth mentioning that the char/gas mixture goes through a two-stage expansion before it reaches the reactor tube. From the reservoir, char particles are swept by a gas stream with a flow rate at 1000 cm^3/min vertically into a 0.3175 cm tube. The tube expands to an 0.635 cm i.d. tube about 5.08 cm above the reactor tube (1.9 cm i.d). At the second expansion point, a gas stream of 1000 cm^3/min flow rate is fed horizontally. The two streams merge at a 90 degree angle, which produces rigorous mixing of solids in the gas stream.

IV. IMPLICATIONS OF PORE STRUCTURE ANALYSIS

A detailed description of surface area measurement has been included in Appendix A. The BET-surface areas of samples were measured with nitrogen (N_2) as the adsorbate at a temperature of 77 K. Table 2 lists the origin and history of these samples. Let P be the partial pressure of the adsorbate, and P_0, the saturation vapor pressure of the adsorbate at the operating temperature, then the relative pressure is P/P_0. Measurements were carried out under six different relative pressures, P/P_0, with the multi-point method. The values of P/P^0, ranging from 0.05 to 0.30, comprised the linear region of the multi-point BET equation. The experimental results are summarized in Table 3. This table also lists results previously obtained with CO_2 as the adsorbate at 273K. Additional measurements were carried out with nitrogen (N_2) as the adsorbate at 77 K to evaluate the micropore volume and total pore volume of the eight samples.

Measurements for the micropore volume were carried out under five different levels of P/P^0. The values of P/P_0, ranging from 0.02 to 0.1, comprised the linear region of the Dubinin-

Radushkevich (DR) equation (Dubinin and Radushkevich, 1947). The total pore volume was measured directly when P/P_0 was close to 1. The average pore radius evaluated from the total pore volume and surface area has been computed:

$$r = \frac{2V_T}{S} \qquad \text{(IV-1)}$$

where V_T is the total pore volume; and S, the surface area. The results are summarized in Table 4. Micropore volume with adsorbate CO_2 at 273K is also listed in the same table for comparison.

Pore-size distributions were determined from the desorption isotherm. Nitrogen (N_2) served as the adsorbate, and the desorption was conducted at 77K. The results are plotted in Figures 9 and 10.

The review by Mahajan and Walker (1978) summarized a number of interesting conclusions concerning observed discrepancies of pore analyses when N_2 and CO_2 were used as adsorbates. Micropore volume and surface area with N_2 at 77K are always considerably lower than those with CO_2 at 273K. It has been suggested that at 77K the micropore system is not completely accessible to N_2 molecules due to an activated diffusion process and/or shrinkage of pores. Adsorption of N_2 is considered to measure the area of the macropores, mesopores, and the larger micropores in chars. CO_2 adsorption at 273K should measure the total surface area of chars. These observations will be used in the interpretation of our experimental data discussed below.

Data in Table 3 show that the raw lignite char after pyrolysis has a much higher surface area than bituminous coal char, either by the BET/N_2 or by the DR/CO_2 method. A comparison of surface areas of chars at different pyrolysis temperatures and holding times is shown in Figure 7 and 8. From these figures, the observed decrease in surface areas of chars during reburning may be due to a

structure ordering of carbon, or graphitization, taking place at elevated temperatures (Radovic *et al.*, 1983a,b; Sahu *et al.*, 1988; Wong *et al.*, 1995). The structure reorganization of the carbon matrix at higher pyrolysis temperature, up to 1300°C, leads to closure of pore mouths and pore coalescence, thus reducing surface area. The reasons for the increase in surface area need further investigation.

Since NO reduction by lignite char in the absence of CO_2 and O_2 is less severe than that by bituminous coal char (to be discussed in a subsequent section), this observation confirms the earlier claim (Chen and Ma, 1995) that surface area is not a normalization factor of char reactivity. Indeed, as we will discuss later in Chapter V, the effectiveness of heterogeneous reburning depends on: (1) the origin of char, (2) char devolatilization temperature and time, and (3) the competition of NO with CO_2 and O_2 for the active sites on the char surface.

When either N_2 or CO_2 is used as adsorbate, micropore (<10Å) volumes of both chars decrease after their reactions with NO (Table 4). The decrease in micropore volume becomes a prominent feature of lignite char during its reaction with NO, CO_2 and O_2 (see samples 4-1L and 4-4L in Table 4). On the contrary, the micropore volume of the bituminous coal char increases during its reaction with NO, CO_2 and O_2, see samples 4-1P and 4-4P in Table 4. Pore volume distributions of these chars are presented in Figure 9 and 10, which clearly suggest that closures of micropores of both chars during their reactions with NO. Both chars have major a peak at about 20Å and a second peak below 15Å in the measured range of pore size distributions, 15 to 70Å. The pore structure of the bituminous coal char, however, is relatively insensitive to the reaction with NO.

The decreases in micropore volumes are likely caused by formation of surface oxygen complexes at the mouths of micropores. This observation is comparable to a char gasification study by Lizzio *et al.* (1990), in which techniques for the determination of both stable and reactive surface

oxygen complexes were developed. Reactive surface complexes were determined by transient kinetics, i.e., by measuring the decay of CO yield after the oxidant in the feed (CO_2) is switched to N_2. The decay had a time scale on the order of minutes. The stable oxygen complex was determined by temperature-programmed desorption (TPD) of quenched char after the reactive complex was removed. It was shown that the lignite char has a higher amount of stable and reactive oxygen complexes than those of bituminous coal char. In our study, char sample undergoes rapid quenching at the exit of the flow reactor and both stable and reactive surface oxygen complexes are expected to remain on the char. Therefore, due to the formation of both reactive and stable surface complexes and closures of pores, neither the surface area before the reaction nor the surface area after the reaction can be a good normalization factor for the reactivity of a specific char. For the calculations to be discussed in the subsequent sections, we will report rate constants based on the surface areas of chars before their reaction with NO.

For future study, transient kinetics and TPD experiments should be potentially important approaches for the correction of the aforementioned problem. Surface areas of chars after these experiments should give the estimated quantities of reactive surface areas and the surface areas occupied by complexes. Furthermore, these experiments should assist the construction of a Langmuir-Hinshelwood model which is, in turn, a critical missing element in the evaluation of boiler performance when heterogeneous reburning is to be incorporated.

V. PARAMETERS GOVERNING HETEROGENEOUS REACTIONS

A. Effects of Char Origin, Char History, and CO_2 and O_2 on NO Reduction

1. Effects of Char Origin

Figures 11 and 12 present the series of fourteen experiments conducted with chars derived from bituminous coal and lignite. Comparison of results in these figures reveals several interesting observations. The two interesting observations about the bituminous coal char were that its reactivity increases drastically above 950°C, and addition of CO_2 in the feed shifts this transition in char activity to higher temperature. The shapes of the these curves in Figure 11 suggest that NO reduction on char surface follows two or three different mechanisms, or has different controlling steps over the temperature region 800 to 1100°C. The abrupt change in NO/char reactivity has been reported earlier by many researchers (Farusawa *et al.*, 1980; Chan, 1980; Teng *et al.*, 1992), and the temperature at which the change takes place is called a "breaking point" (Teng *et al.*, 1992). Based on the yields of gasification products, CO and CO2, and products from temperature-programmed desorption of surface complexes, Teng *et al.* (1992) constructed a Langmuir-Hinshelwood model whcih involves NO attack of rapid turnover sites at high temperature. Since NO is also involved in dissociative adsorption on the char surface, the overall NO reduction rate is, therefore, nonlinear with respect to NO contration. This model will be discussed in detail in section VI.F.

A number of potentially significant statements can be made when the reactivities of chars of two different origin are compared. At high temperatures and in the absence of CO_2 and O_2, the reactivity of the bituminous coal char is comparable, or higher than that of lignite char. Second, when 16.8 % (by volume) of CO_2 and 1.95% (by volume) are introduced into the feed stream, the reactivities of bituminous coal char are affected more severely than those of lignite char. Since the reburning stage also contains about 1.95 % (by volume) of O_2, the effects of CO_2 discussed above inspired our study of O_2 effects, which is discussed in section V.A-3.

2. Effects of Char History

To study char history, we have conducted experiments with three different pyrolysis temperatures and holding times; (a) 950°C, 0 holding time,(b) 1100°C, 5 min holding time, and (c) 1100°C, 2 h holding time. For series (a) and (b), we found that the Arrhenius rates of NO/char reaction obtained (see section VI.C) were consistently higher than the data reported in the literature. After extensive review of the experimental procedures adopted by various groups, we noted that most literature values have been reported by using char produced with 1 to 3 h holding time. Although devolatilization of coal completes within a fraction of second (see, e.g., Howard, 1981), our chars for series (a) and (b) were significantly "younger" than chars produced by others. Since devolatilization severity has been demonstrated to be detrimental to char gasification in carbon dioxide (see, e.g., Radovic *et al.*, 1983a), the finding about the difference in holding time prompted our decision to measure the rate of "older" chars: 1100°C and 2 h holding time. Chars derived from Mississippi lignite and Pittsburgh #8 bituminous coal have been tested in three different gaseous environments: NO+char, NO+char+CO_2, and NO+char+CO_2+O_2.

The results from the experiments with three different pyrolysis temperatures and holding time are shown as Figures 13 through 15. The exit NO concentrations presented in Figure 13 suggest that the holding time is indeed a very significant variable in the determination of char activity. Long pyrolysis time severely destroys the char reactivities, particularly the reactivities of bituminous coal char. Since most published rate data for the NO/char reaction were collected from experiments where chars were prepared with 1 to 3 h pyrolysis time, their rates are expected to be higher than ours. Furthermore, since devolatilization completes within a fraction of a second, our study implies that future studies on NO/char interactions should focus on "young" chars.

The observed dependence of char reactivity on pyrolysis severity is certainly related to the physical and chemical structure of the chars. The loss of reactivity of high severity char could be caused by a number of reasons. First, it has been reported that pyrolysis of Pittsburgh #8 coal generates a small amount of H_2 (<0.4 wt % of as received coal) in the temperature range of 950 to 1100°C (Howard, 1981) and this hydrogen yield may assist the removals of oxidants, CO_2 and O_2, and direct reduction of NO. The ultimate analyses shown in Table 1, however, demonstrate that the elemental compositions of high and low temperature bituminous coal chars are about the same; the low temperature lignite char does have a slightly higher atomic H/C ratio than that of the high temperature char. Second, it has been speculated that a hydrogen complex forms on the partially devolatilized char, which also assists the removal of oxidants and NO (De Soete, 1990). Third, high temperature causes closure of pores due to a structure ordering of carbon, or graphitization, as discussed in the previous chapter. The low temperature lignite char does have higher CO_2 surface area, but lower N_2 surface area, than those of the high temperature lignite char (Chen *et al.*, 1996).

3. Effects of CO_2 and O_2 on NO Reduction

Figure 13 presents the exit NO concentrations from runs where the major oxidants in reburning, CO_2 and O_2, are sequentially added. The exit NO concentrations suggest two interesting observations. First, the reactivity of the bituminous coal char is comparable or even higher than lignite char when CO_2 and O_2 are absent, as stated in section VI.A-1. Second, CO_2 and O_2 are more detrimental to the bituminous coal char than that to the lignite char.

Figure 14 illustrates the net yields of gasification products, CO_2 and CO, from the experiments discussed above. Addition of 16.8 volume % of CO_2 in the feed does not seem to increase the total yields of these gasification products from reburning either with the lignite char or with the bituminous

coal char. But the presence of CO_2 results in notably higher NO concentration from reburning with bituminous coal char, and results in only a small increase in NO from reburning with lignite char. Using the Langmuir-Hinshelwood interpretation, this seems to suggest that NO adsorption on lignite char is much faster than CO_2 adsorption, but CO_2 and NO are competitive for the active sites on the char derived from the bituminous coal.

The exit concentrations of NO, CO_2, and CO from reactions of lignite char appear to be insensitive to the presence of 16.8 volume % of CO_2. This observation may be rather important to NO reburning with mixed fuels containing both volatile and solid carbon. Since the volatile fuels usually burn much faster than char, CO and CO_2 produced from burning of mixed fuels is not expected to compete with NO for the active sites on lignite char. Furthermore, we have observed the catalytic conversion of HCN to NH_3 by lignite char or ash (Burch *et al.*, 1991b), which is a desired reaction when volatile fuel is used in reburning. Thus, with O_2 already depleted, the NO/char reaction will take place in an environment "richer" in NO than normally observed, and the NO reduction should not be the sum of the reduction from each fuel taken separately.

When both O_2 and CO_2 are added in the feed (Figures 14 and 15) the yields of gasification products and oxygen balance notably increase, and more carbon is gasified from lignite char than from bituminous coal char. Again, using Langmuir-Hinshelwood kinetics, the observed NO concentrations imply that NO competes with O_2 for the formation of surface complexes on lignite char, but NO can not compete with O_2 on the bituminous coal char. Furthermore, due to the formation of a large amount of gasification products, turnover of the oxygen surface complex on the lignite char seems to be faster than that on the bituminous coal char. The accelerated desorption is likely a result of catalysis.

Interestingly, the char gasification literature has offered some helpful support to what we have observed here, particularly through the concepts of "stable oxides," "labile oxides," and "reactive surface area" which have been well documented by Laine *et al.* (1963), Lizzio (1990) and Radovic *et al.* (1991). In a study of gasification of carbon by N_2O, Strickland-Constable (1938) distinguished two types of surface oxides: 1) stable oxides, i.e., those C-O complexes which accumulate on the surface and inhibit oxidation, and 2) labile oxides, i.e., those C(O) complexes which have a shorter lifetime and are active in the combustion mechanisms. Lizzio (1990), Lizzio *et al.* (1990), and Radovic *et al.* (1991) developed temperature-programmed desorption techniques for the quantification of both C-O and C(O) complexes. They concluded that the surface area occupied by the labile oxides, i.e., C(O), is a better normalization parameter for char reactivity and called it "reactive surface area (RSA)." This technique is tested in the determinations of CO_2-gasification rates of chars derived from lignite and bituminous coal (Lizzio *et al.*, 1990).

The yields of gasification products, CO and CO_2, presented in Figure 14 suggest a number of interesting phenomena. First, pyrolysis severity, in terms of time and temperature, reduces the rates of gasification of both chars with NO, CO_2 and O_2. Second, only the char derived from the least severe conditions, i.e., 950°C and zero holding time, is reactive with CO_2. The chars derived at the next level of severity (series B and E), i.e., 1100°C and 5 min holding time, however, produce very low levels of gasification products when CO_2 is present in the reactive gas stream. Figure 15 presents the total oxygen in the gasification products normalized to the converted NO, which indicates the competition of various oxidants and the levels of active sites accessible to NO, CO_2 and O_2. Third, exit NO data in Figure 13 suggests that increasing pyrolysis time from 5 min to 2 h seriously destroys the reactivities of both chars with NO. Fourth, both CO_2 and O_2 are detrimental to NO reduction,

for chars produced under all severities. Fifth, the effects of CO_2 on NO reduction is less serious for younger lignite char. These observations seem to imply that there are two, not quite mutually exclusive, kinds of active sites: one is more accessible to NO and the other is more accessible to CO_2. Active sites accessible to CO_2 can be destroyed easier than those accessible to NO; however, at the first two levels of severities, CO_2 forms stable surface complexes on bituminous coal char. Fundamental understanding of these mechanisms has practical importance to the production of activated carbon for flue gas cleanup.

B. Yields of Carbon Oxides and Oxygen Balance

Carbon monoxide and carbon dioxide are the principal products of the NO/char reaction. Figures 16 and 17 illustrate the yields of these two components, in volume percentages, from the reaction of NO with the bituminous coal char and the lignite char, respectively. The molar CO/CO_2 ratio is higher than 1.0 under all test conditions. These figures also include the net yields of CO and CO_2 from experiments with both CO_2 and O_2 in the feed.

It is very interesting to note that there is no clear excess yield of CO or CO_2 when oxygen is added introduced in the feed containing bituminous coal char (Figure 16). Nevertheless, significant excess yields of CO or CO_2 are observed when oxygen is included in the feed containing lignite char (Figure 17). These observations suggest the gasification of lignite carbon by oxygen during reburning, however, gasification of the bituminous coal char does not take place under similar experimental conditions. Since oxygen clearly retards the NO reduction of the char surface, as shown in Figure 13, our observations discussed above strengthen the conclusion that stable oxygen complexes form on the bituminous coal char surface while CaO on the lignite char surface accelerates the decomposition of these stable oxygen surface complexes. The runs with CO_2 only do not result

in notable yields of gasified carbon from char. The oxygen conversions from NO to CO and CO_2 are presented in Figures 18 and 19 for the bituminous coal char and the lignite char, respectively. Although the data scatter, they fluctuate around complete recoveries.

C. Yield of Nitrous Oxide

The possibility of NO conversion to N_2O in reburning was first discussed by Kramlich *et al.* (1989). Therefore, the concentration of N_2O was routinely monitored during this study. The yields of nitrous oxide (N_2O) from all the experiments have always been very low. As an example, for NO reaction with the chars form two different origins with NO initial concentration at 1000 ppm, the yield of N_2O has always been below 14 ppm, see Figure 20 and Table 5. Lower temperature favors slightly higher of N_2O.

VI. RATES OF NO REDUCTION IN VARIOUS REACTING ENVIRONMENTS

A. Rate Expression for Data from Plug Flow Reactor

We have discussed the justification of using conversion data from a laminar flow system in the estimation of NO reduction rate in section III.A. In this section, the rate expression for conversion data generated from a nonisothermal flow reactor is derived.

Carbon in the char can be gasified by NO to form CO and CO_2. The first order NO reaction rate on char surface can be expressed as (see, e.g., De Soete, 1990)

$$r_{NO} = - kAP_{NO} \qquad \text{(VI-A-1)}$$

where r_{NO} is the rate of NO formation, in moles $(s)^{-1}$ (g of char)$^{-1}$
A is the specific, internal surface area of char, in $m^2(g)^{-1}$
P_{NO} is the partial pressure of NO, in atm,

k is the rate constant, in moles $(s)^{-1}$ $(m)^{-2}$ $(atm)^{-1}$.

Material balance over a small section of tubular reactor yields

$$F_{NO} + dF_{NO} = F_{NO} + (r_{NO})\, dW \qquad \text{(VI-A-2)}$$

where W is the char weight and F_{NO} is the molar flow rate of NO. By the definition of conversion we obtain

$$\begin{aligned} dF_{NO} &= d(F_{NO,\,in}(1-X)) \\ &= -F_{NO,\,in}\, dX \\ &= -F_{NO,\,in}\, d\left(1 - \frac{C_{NO}}{C_{NO,\,in}}\right) \\ &= +F_{NO,\,in}\, d\left(\frac{P_{NO}}{P_{NO,\,in}}\right) \end{aligned} \qquad \text{(VI-A-3)}$$

where X = conversion of NO.

Substituting Eqs. (VI-A-1) and (VI-A-2) into Eq. (VI-A-3) we obtain

$$F_{NO,\,in}\, d\left(\frac{P_{NO}}{P_{NO,\,in}}\right) = -k\, A\, P_{NO}\, dW_t \qquad \text{(VI-A-4)}$$

Rearranging the above equation we obtain

$$\frac{dP_{NO}}{P_{NO}} = \frac{-k\, A\, P_{NO,\,in}\, dW_t}{F_{NO,\,in}} \qquad \text{(VI-A-5)}$$

The char weight, dW_t, in Eq. (VI-A-4) can be expressed in terms of char feeding rate W_1

$$dW_t = W_1\,dt \tag{VI-A-6}$$

where W_1 is in g s^{-1}. Integrating Eq. (VI-A-5) above we obtain

$$\ln \frac{P_{NO}}{P_{NO,\,in}} = \frac{-k\,A\,W_t\,P_{NO,\,in}}{F_{NO,\,in}} \tag{VI-A-7}$$

where W_t is the total char in the reaction zone. Eq. (VI-A-7) can also be expressed in terms of conversion.

$$X = 1 - \exp\left(\frac{-k\,W_t\,A\,P_{NO,\,in}}{F_{NO,\,in}}\right) \tag{VI-A-8}$$

or

$$\ln(1 - X) = -\frac{k\,A\,W_t\,P_{NO,\,in}}{F_{NO,\,in}} \tag{VI-A-9}$$

Equation (VI-A-9) can be used either for the estimation of rate constant, or the conversion if k is known. By assuming the gas is an ideal gas mixture, the molar flow rate can be expressed as:

$$F_{NO,\,in} = \frac{P_{NO,\,in}}{P}\,\frac{v}{2.445 \times 10^4} \tag{VI-A-10}$$

where the constant in Eq. (VI-A-10) denotes the specific volume of gas at 25°C (in cm^3/mole), and v is the total inlet volumetric flow rate measured at 25°C (in cm^3/s). Substituting Eqs. (VI-A-1), (VI-A-6) into Eq. (VI-A-9) with P = 1 atm and v = 33.33 cm^3/s, we obtain:

$$\ln(1 - X) = \frac{-2.445 \times 10^4\,k\,A\,W_1\,t_h}{33.33}$$

$$= -7.34 \times 10^2\,k\,A\,W_1\,t_h \tag{VI-A-11}$$

The equation above is used in the estimation of rate constant k for the isothermal region. The flow reactor used for this research has an inside diameter of 1.91 cm and an overall length of 64 cm. The total flow rate in the flow reactor system is 2000 cc/min. The surface area of the ceramic tube is

$$A = 2\pi rL \tag{VI-A-12}$$

where A is the surface area, cm^2
r is the outer diameter of the tube, 1.91 cm
L is the length of the heating area, 4 in.

Assuming the gas is ideal,

$$\frac{V_1}{T_1} = \frac{V_2}{T_2} = \frac{\frac{V_1}{t}}{T_1} = \frac{\frac{V_2}{t}}{T_2} = \frac{G_1}{T_1} = \frac{G_2}{T_2} \tag{VI-A-13}$$

where G is the volumetric flow rate, cm^3/s, V is the volume of gas, cm^3.

At 1100°C, $G_2 = (G_1/T_1)T_2 = 153.579$ (cm^3/s), and the velocity of the gas in the reactor is

$$u = \frac{G}{A} = 53.61\ (cm/s) \tag{VI-A-14}$$

and the residence time in the isothermal region is $L/u \approx 0.1896$ sec.

B. Reactions During Heat-up and Cooling

The rate of reaction is corrected by considering the extents of reaction during heat-up and cooling. The gas mixture enters the tubular reactor with a flow rate of 2000 cm^3/min at 25°C. The cross section area of the tube is 2.865 cm^2. Assuming the gas is ideal, the gas residence time t in the heating up section can be expressed as a function of temperature and the traveled distance

$$dt = \frac{a}{G}\,dz = 25.62\,\frac{1}{T}\,dz \qquad \text{(VI-B-15)}$$

where t is the gas residence time in the tubular reactor, in s
a is the cross section area of the reactor tube, in cm^2
G is the gas volumetric flow rate, in $cm^3\ s^{-1}$
z is the longitudinal distance of gas traveled in the tubular reactor, in cm
T is the gas temperature in the tube, in °C.

The centerline temperature measurements were taken using a 0.32 cm o.d. sheathed but unshielded thermocouple. Due to high radiation from the walls, the temperature profiles obtained by this method are more representative of the wall temperature than the mean gas temperature at any given location which has been stated in section II.A-1. During the heating up period, the estimated temperature profile increases almost linearly with respect to z. Specifically, gas temperature increases from 700 to 1100°C in 11.9 cm, thus, the heating rate can be written as:

$$\frac{dT}{dz} = 33.51\ °C\ cm^{-1} \qquad \text{(VI-B-16)}$$

Substituting Eq. (VI-B-16) into Eq. (VI-B-15), we obtain

$$dt = \frac{0.765}{T}\,dT \qquad \text{(VI-B-17)}$$

For the cooling section, the gas temperature decreases along the tube length with the same rate, thus,

$$dt = -\frac{0.765}{T}\,dT \qquad \text{(VI-B-18)}$$

Assuming NO reduction follows first order kinetics, the equation for material balance of a plug flow tubular reactor is expressed as Eq. (VI-A-8)

$$\frac{dP_{NO}}{P_{NO}} = \frac{-kA\,P_{NO,in}\,dW}{F_{NO,in}} \qquad \text{(VI-A-8)}$$

The NO reduction rate, k, can be written as in the Arrhenius form

$$k = k_0 \exp\left(\frac{-E_a}{RT}\right) \qquad \text{(VI-B-19)}$$

where k_0 and E_a are the exponential factor and activation energy of NO reduction of char surface. Substituting Eqs (VI-B-17), (VI-B-18), and (VI-B-19) into Eq. (VI-A-8), and integrating the resultant expression over the heating up, isothermal and cooling sections, we obtain the following expression

$$\ln(1-X) = 733.6\left(-\int \frac{0.765}{T} W_1 A k_0 e^{-\frac{E_a}{RT}} dT - t_h W_1 A k_0 e^{-\frac{E_a}{RT}} - \int -\frac{0.765}{T} W_1 A k_0 e^{-\frac{E_a}{RT}} dT\right) \qquad \text{(VI-B-20)}$$

where t_h is gas residence time in the isothermal temperature region. The constants k_0 and E_a have been estimated by comparing the above equation with theexperimentally acquired NO conversions at various temperatures using MathCad.

C. Estimation of Transfer Limitations

1.Rate Constants and Internal Mass Transfer Limitation

Due to the low surface reaction rate of NO and char reported in the literature (see, e.g., De Soete, 1990), we have been assuming that mass transfer limitations are negligible and our interpretation of the reburning mechanisms has been based on Langmuir-Hinshelwood models (Chen

and Ma, 1995; Chen *et al.*, 1995b). Two of our recent findings, however, have revealed the need for further examination of the significance of mass transfer limitations. First, surface area of the high temperature bituminous coal char is much smaller than that of the low temperature char measured previously, yet the two chars demonstrate very similar reactivity with NO. The observed low surface area of high temperature char results in higher estimated NO activity per unit char surface area, and the reaction is more likely to suffer the mass transfer limitations. Second, as discussed in the last section, the internal surface areas of lignite char vary significantly when CO_2 and O_2 are introduced, and the pore-closure process can potentially lead to mass-transfer controlled mechanisms.

For a system involving internal mass transfer limitation, the observed Arrhenius rate in the above expression can be considered the product of the true surface reaction rate and the effectiveness factor, η, i.e., from Eq. (VI-B-20)

$$\ln(1 - X) = 733.6 \left(- \int \frac{0.765}{T} W_1 A \eta k_0 e^{-\frac{E_a}{RT}} dT - t_h W_1 A \eta k_0 e^{-\frac{E_a}{RT}} - \int - \frac{0.765}{T} W_1 A \eta k_0 e^{-\frac{E_a}{RT}} dT \right) \qquad \text{(VI-C-21)}$$

The effectiveness factor has been theoretically shown to be a function of the Thiele modulus, ϕ (see, e.g., Satterfield, 1970)

$$\eta = \frac{3}{\phi} \left[\frac{1}{\tanh \phi} - \frac{1}{\phi} \right] \qquad \text{(VI-C-22)}$$

where the Thiele modules is defined as

$$\phi = R \left[\frac{a\, k\, A\, \rho_P}{D_{eff}} \right]^{0.5} \qquad \text{(VI-C-23)}$$

and R is the radius of char particles, in cm,
a is the ideal gas conversion constant, 2.445×10^4 cm^3 $mole^{-1}$,
D_{eff} is the effective diffusion coefficient, in cm^2 s^{-1}, and,
ρ_p is the bulk density of char, in g cm^{-3}.

The mass transfer resistance in terms of the effective diffusivity can be considered a linear combination of the resistances contributed by the Knudsen and the bulk diffusivity (Satterfield, 1970),

$$\frac{1}{D_{eff}} = \frac{1}{D_{k,eff}} + \frac{1}{D_{12,eff}} \qquad \text{(VI-C-24)}$$

$$D_{k,eff} = 19400 \left[\frac{\theta^2}{\tau_m A \rho_p}\right]\left[\frac{T}{M}\right]^{0.5} \qquad \text{(VI-C-25)}$$

$$D_{12,eff} = \frac{0.001858\, T^{1.5}\left[\frac{M_1 + M_2}{M_1 M_2}\right]^{0.5}}{P \sigma_{12}^2 \Omega_D} \qquad \text{(VI-C-26)}$$

where $D_{k,eff}$ is the Knudsen diffusion coefficient for a porous solid, in cm^2 s^{-1},
$D_{12,eff}$ is the bulk diffusion coefficient of species 1 in species 2, in cm^2 s^{-1},
θ is the particle void fraction,
τ_m is the tortuosity factor based on the mean pore radius, assumed 2,
M, M_1 are the molecular weights of diffusing molecules, $M_{NO} = 30$, $M_{HE} = 4$,
M_2 is the molecular weight of the gas medium,
P is pressure, 1 atm,
Ω_D is the "collision integral", a function of $K_B T / \epsilon_{12}$, dimensionless,
ϵ, σ are the force constant of the Lenard-Jones potential function, ϵ in g cm^2 s^{-2}, σ in Å, and,
k_B is the Boltzmann constant, 1.38×10^{-16} g cm^2 s^{-2} K^{-1}.

Equations (VI-C-24) through (VI-C-26) allow the calculation of the effective diffusivity for the (NO +char) reaction at 1100°C. For instance, we have examined the pore volumes presented in Table 3, and obtained the average pore volumes for the MS lignite char and the Pitt#8 coal char, 0.07 cm^3/g

and 0.0065 cm^3/g, respectively. By the water displacement method, the bulk densities of the lignite char and bituminous coal char have been measured as 1.2 and 1.4 g/cm^3, respectively. Based on these values, we obtain the pore fraction

θ = pore volume × density
= 0.084 for the MS lignite char and 0.0091 for the Pitt#8 char.

From Bird *et al.* (1960),

$\epsilon_{He}/k_B = 10.2$ °K, $\sigma_{He} = 2.576$ Å,
$\epsilon_{NO}/k_B = 119$ °K, $\sigma_{NO} = 3.47$ Å,
$\sigma_{He\text{-}NO} = 1/2\ (\sigma_{He} + \sigma_{NO}) = 3.023$ Å,
$\epsilon_{He\text{-}NO} = (\epsilon_{He}\ \epsilon_{NO})^{0.5} = 34.84\ k_B\ g\ cm^2\ sec^{-2}$,
$k_B T/\epsilon_{He\text{-}NO} = 23.83$, $\Omega_D \approx 0.6776$.

Substituting the above constants into Eq. (VI C-24) through Eq. (VI C-26), we obtain

$D_{k,\,eff} = 3.98 \times 10^{-5}\ cm^2\ s^{-1}$ for lignite char at 1100°C,
$D_{12,\,eff} = 8.127\ cm^2\ s^{-1}$,
$D_{eff} = 3.98 \times 10^{-5}\ cm^2\ s^{-1}$ for lignite char at 1100°C.

These results show that Knudsen diffusion controls the overall diffusion rate.

Equations (VI-C-21) through Eq. (VI-C-23) can be solved simultaneously by MathCad for η, ϕ, k_0, and E_a. Since there are four unknowns, Eq. (VI- C-21) is used twice for two experimental data in each calculation. For reactions with varying activation energy in the temperature range 800 to 1100°C, such as the rate of bituminous coal char with NO, calculations have been conducted stepwise from lower temperatures to higher temperatures, and the new sets of η, ϕ, k_0, and E_a are recovered. Formation of both stable and reactive surface complexes cause closures of pores during the reaction, so neither the BET N_2 nor the DR CO_2 surface area provides a good measure of the actual reactive surface area; thus, in the present calculations, surface areas of raw chars are used in

the estimation of rate constants. The results of these calculations are shown in Tables 6 and 7.

2. External Transfer Limitation

The high activation energies shown in Tables 6 and 7 suggest that external mass transfer should not a limiting factor in determination of the rate constant. The following calculation provides justification of the estimation.

Under steady state conditions, the mass transfer rate of NO through the gaseous boundary layer equals to the surface reaction rate, i.e.,

$$k_c S(C_g - C_s) = (-r) W_p \qquad \text{(VI-C-27)}$$

where C_g = NO concentration in the mainstream of gas flow, moles cm^{-3}
C_s = NO concentration at the particles surface, moles cm^{-3}
k_c = mass transfer coefficient, cm s^{-1}
S = external surface area of a single particle, cm^2
- r = reaction rate, moles g^{-1} s^{-1}, and,
W_p = weight of a single particle, g

NO reduction on the char surface has been expressed in the following form

$$(-r) = \eta k A P_{NO} \qquad \text{(VI-C-28)}$$

The NO concentration gradient,

$$F = \frac{(C_g - C_s)}{C_s} \qquad \text{(VI-C-29)}$$

is an index of mass transfer limitations; that is, a large concentration gradient indicates large mass transfer resistance. If the gas follows the ideal gas law, i.e.,

$$P_{NO} = C_s R T \qquad \text{(VI-C-30)}$$

and the weight of a char particle can be expressed as

$$W_p = \rho_p \frac{1}{6} \Pi d_p^3 \qquad \text{(VI-C-31)}$$

so substituting Eqs. (VI-C-27), (VI-C-28), (VI-C-30) and (VI-C-31) into Eq. (VI-C-29), we obtain

$$F = \frac{C_g - C_s}{C_s} = \frac{\eta k A R T \rho_p \Pi d_p^3}{6 k_c S} \qquad \text{(VI-C-32)}$$

The mass transfer coefficient has been estimated based on the Frossling correlation with the Sherwood number (Sh) = 2, i.e.,

$$k_c = \frac{D_{AB} Sh}{d_p} = \frac{2 D_{AB}}{d_p} \qquad \text{(VI-C-33)}$$

The diffusivity, D_{AB}, at 1100°C has been estimated by the Chapman-Enskog equation, i.e., Eq. (VI-C-26),

$$D_{AB} = 13.7 \text{ cm}^2 \text{ s}^{-1}$$

The particles have mean diameter 0.0128 cm, therefore, from Eq. (VI-C-33),

$$k_c = 2.14 \times 10^3 \, cm \, s^{-1} \qquad \text{(VI C-34)}$$

Substituting the highest rate constant shown in Tables 6 and 7, i.e., the rate of the bituminous coal

char derived from pyrolysis at 1100°C and 5 min holding time followed by reaction with NO at 1100°C,

$$F = 1.62$$

This value suggests that external mass transfer rate is of the same order of magnitude of the reaction rate at the highest reaction temperature of this investigation. Intrinsic rates higher than what we have obtained may be distorted by mass transfer limitations.

D. Effects of Char Origin, History and Oxidants on Rate of NO/Char Reaction

As mentioned in section V.A, the NO conversion by Pittsburgh #8 bituminous coal char is more effective than that by Mississippi lignite char if the feed does not include CO_2 and O_2. Figure 21 illustrates that the rate of NO reduction by bituminous coal char is higher than that by lignite char, especially at high temperature. When the pyrolysis temperature and holding time change, however, the results vary. Figures 22 through 25 show how the Mississippi lignite chars and Pittsburgh #8 coal chars react with NO under different pyrolysis serverities. The high severity char (produced at 1100°C, 2 h holding time) seems to have a lower k value than low severity chars (produced at 950°C, 5 min holding time and 1100°C, 5 min holding time). The possible reason for this result has been discussed in section V.A. Figures 26, 27, 28 and 29 show that the NO/char reaction rate is usually retarded by the presence of oxidants, except for the minimum effects of CO_2 on lignite char activity.

E. Comparison with Published Data

As shown in Tables 6 and 7, internal mass transfer limitations are not serious for most cases except for experiments at high temperatures. The intrinsic rates are illustrated in Figures 30 through 33. For comparison, a number of published rates are also included in these figures. Our data (char derived at 1100°C, 5 min holding time) are higher than most of the published results; there are a

number of possible reasons. First, our chars were "younger" than all the chars presented in the figures (these used 1 to 3 h pyrolysis times). In section V.A, we have shown the remarkable difference in reactivities between the young and the old chars. Second, possible mass transfer limitations have not been discussed in a number of studies. For example, rate measurement by TGA usually uses a sizeable amount of sample where internal mass transfer limitations may exist (Aarna and Suuberg, 1996). Third, gas/solid mixing and the temperature history of the various experimental setups can also play an important role in rate estimation. Specifically, our reactor tube has an 1.91 cm i.d., and particles have been injected into the reactor from a 0.635 cm o.d. tube. This design should provide better mixing than injecting particles from an 0.159 cm o.d. tube to a 5.08 cm i.d. reactor (Song, 1978). Fourth, our reactor measures the rate of the NO/char reaction in the first 0.2 s, while a fixed bed reactor measures rates after the stable surface oxygen complexes areformed. Due to the reasons discussed above, we carefully chose another condition for char pyrolysis. We use chars from both Pittsburgh #8 bituminous coal char and Mississippi lignite char which are derived from 1100°C, 2 h holding time. These chars can be regarded as "old chars", and the holding time falls in the range of 1 to 3 h for the published data. Results from experiments with the old chars are shown in Figures 31 and 34. To compare the rates from different temperature regions, some data have been extrapolated. The rate values from these "old char" fall into the region of the data from De Soete (1980), for both lignite char and bituminous coal char. This result suppots our claim about char history that high severity chars are less reactive than low severity chars.

F. Effects of Initial NO Concentration

Figures 34 and 35 show the k values from 5 different series for both lignite char and bituminous coal char. The initial concentrations in these series are 1000 ppm, 800 ppm, 600 ppm, 400

ppm, and 200 ppm. For the lignite char shown in Figure 34, the rate constants for each concentration fall into almost the same line. This indicates that the initial concentration effect for Mississippi lignite char is not obvious. If we take average the rate constantat each temperature, we can get the recommended rate expression for Mississippi lignite char

$$k = 2.41\times10^{5}\, exp(\frac{-33,768.8cal}{RT}), \quad in\ mole\, m^{-2} s^{-1} atm^{-1} \qquad \text{(VI-F-35)}$$

In Figure 35, the activation energy of the NO/bituminious coal char reaction with feed NO concentration at 1000 ppm changes steeply from a lower value to a much higher one at 950°C. The existence of this "breaking point" has been previously reported or discussed by a number of research groups (Farusawa *et al.*, 1980; Chan, 1980; Teng *et al.*, 1992), except the breaking point observed in the present study is noticeably higher than those in the literature, 600 to 680°C. The change in activation energy indicates change in controlling mechanisms in the low and high temperature regions, and transition to a higher value indicates the competition of parallel reactions. Teng *et al.* (1992) also reported that transition in activation energy is also accompanies with transition in product CO to CO_2 ratio at the breaking point. Based on their observations, they postualated a mechanisms involving three types of elementary reactions. The first type includes formation of surface complexes through two dissociative chemisorption reactions

$$2C + NO \rightarrow C(O) + C(N)$$

$$C + C(O) + NO \rightarrow C(O_2) + C(N)$$

where the atoms inside a bracket represent adsorbed atoms. These surface complexes undergo two sets of reactions at temperatures below and higher than the breaking point. At temperatures below the break point, three reactions are involved

$$C(O) \rightarrow CO + a\,C^*$$

$$C(O_2) \rightarrow CO_2 + b\,C^*$$

$$2C(N) \rightarrow N_2 + d\,C^*$$

where C* is a rapid turnover site. These three reactions are in accord with the observed products of gasification: CO, CO_2, and N_2. At temperatures higher than the breaking point, two other reactions with higher activation energies control the mechanisms

$$C^* + C(O) + NO \rightarrow CO_2 + C(N) + x\,C^*$$

$$C^* + NO \rightarrow CO + C(N) + y\,C^*$$

Note both of these high temperature reactions involve NO attack on the rapid turnover site, C*. Since NO is also involved in the initial stage of the chain reaction, i.e., the dissociative adsorptions, the resultant apparent NO reduction rate is nonlinear with respect to NO concentration. The calculated intrinsic rates presented in Figure 35 clearly shows a nonlinear rate dependence above 950°C for the experiments with feed NO at 1000 ppm. Although the nonliear dependence for the four other series of experiments with different feed NO concentrations is not clear, the high feed NO concentration seems to induce synergetic effects on NO reduction rate at temperatures above 1000°C, see Figure 11.

While our observed activation energies seem to be qualitatively consistent with the model developed by Teng *et al.* (1992), a number of questions remain to be explored:

1. Why is our breaking point much higher than others reported in the literature? Teng *et al.* (1992) reported that the breaking point shifted to a higher temperature when they increased the feed NO partial pressure. Our flow reactor indeed uses a higher NO/char ratio (about 6.7×10^3 ppm mg^{-1}) than that used in a fixed bed reactor adopted by Teng *et al.* (about 6.7×10^2 ppm

mg^{-1}), but the existence of breaking points is not clear when we reduce the feed NO concentration, see Figure 35.

2. The rate of NO reduction is much higher than those reported by Aarna and Suuberg (1996), which has been discussed earlier.

3. We also observed a maximum CO/CO_2 ratio at the breaking point, however, the ratio sharply decreases when temperature rises.

In Figure 35, the intrinsic rate for bituminious coal char appears to fall into a single region, except for the 1000 ppm series, for initial NO concerntration is 200 ppm, the rate expression at temperature range from 850 to 925°C is:

$$k = 4.79\, exp(\frac{-11{,}210\ cal}{RT}), \quad in\ mole\, m^{-2}\, s^{-1}\, atm^{-1} \tag{VI-F-36}$$

For temperatures from 925 to 1000 °C:

$$k = 2.65 \times 10^{5}\, exp(\frac{-31{,}620\ cal}{RT}), \quad in\ mole\, m^{-2}\, s^{-1}\, atm^{-1} \tag{VI-F-37}$$

For temperatures from 1000 to 1100 °C:

$$k = 3.24 \times 10^{5}\, exp(\frac{-38{,}230\ cal}{RT}), \quad in\ mole\, m^{-2}\, s^{-1}\, atm^{-1} \tag{VI-F-38}$$

For initial NO concerntration are 400, 600 and 800 ppm, the rate expression at temperature range from 850 to 925°C is:

$$k = 3.35 \times 10^{4}\, exp(\frac{-26{,}296\ cal}{RT}), \quad in\ mole\, m^{-2}\, s^{-1}\, atm^{-1} \tag{VI-F-39}$$

for temperature range from 925 to 1000°C:

$$k = 7.07 \times 10^{9} \exp\left(\frac{-48{,}343\ cal}{RT}\right), \quad in\ mole\ m^{-2}\ s^{-1}\ atm^{-1} \qquad \text{(VI-F-40)}$$

for temperature range from 1000 to 1100°C:

$$k = 3.51 \times 10^{11} \exp\left(\frac{-62{,}160\ cal}{RT}\right), \quad in\ mole\ m^{-2}\ s^{-1}\ atm^{-1} \qquad \text{(VI-F-41)}$$

The rate constants for the particular series (1000 ppm), can be divided into three sections: 850 to 925°C, 925 to 1000°C, and 1000 to 1100°C. The recommended rate expressions for each temperature region are:

for temperatures from 850 to 925°C

$$k = 1.53 \times 10^{-1} \exp\left(\frac{-7{,}680\ cal}{RT}\right), \quad in\ mole\ m^{-2}\ s^{-1}\ atm^{-1} \qquad \text{(VI-F-42)}$$

for temperatures from 925 to 1000°C:

$$k = 5.45 \times 10^{6} \exp\left(\frac{-49{,}250\ cal}{RT}\right), \quad in\ mole\ m^{-2}\ s^{-1}\ atm^{-1} \qquad \text{(VI-F-43)}$$

and for temperatures from 1000 to 1100°C:

$$k = 8.33 \times 10^{12} \exp\left(\frac{-61{,}158\ cal}{RT}\right), \quad in\ mole\ m^{-2}\ s^{-1}\ atm^{-1} \qquad \text{(VI-F-44)}$$

G. Comparison of the Rates of NO/Char and O_2/Char Reactions

One frequently discussed question in the combustion literature has been whether the rate of oxidation of char by oxygen is higher than that by NO. Therefore, a set of experiment is designed so that the rate of char oxidation can be compared with a well-referenced O_2/char rate reported by Smith (1982) at 1 atm of oxygen pressure

$k_{oxygen} = 305 \exp(-42{,}850 \text{ cal /RT})$ in $g_c\ cm^{-2}\ s^{-1}$, or

$k_{oxygen} = 0.336 \exp(-42{,}850 \text{ cal /RT})$ in mole $m^{-2}\ s^{-1}$

At 1100°C and 1 atm of O_2 pressure, this equation gives

$k_{oxygen,\ 1100C} = 4.6 \times 10^{-5}$ $g_c\ cm^{-2}\ s^{-1}$, or

$k_{oxygen,\ 1100C} = 3.83 \times 10^{-2}$ mole $m^{-2}\ s^{-1}$

In our experimental study, 1.95 volume% of O_2, or 0.1 volume% of NO are introduced in the feed. To compare the rates of the NO/char reaction and O_2/char reaction, Eqs. (VI-A-9) and (VI-C-21) are adopted in the calculation.

Both reactions are assumed to be first order with respect to oxidant partial pressure. For the O_2/char reaction, in an isothermal region, $P_{NO,\ in}$ can be replaced by $P_{oxygen,\ in}$ in Eq. (VI-A-9)

$$\ln(1 - X) = -\frac{k\ A\ W_t\ P_{oxygen,\ in}}{F_{oxygen,\ in}} \qquad \text{(VI-G-45)}$$

For a nonisothermal reacting system involving internal mass transfer limitations, rate constants can be related to conversion(s) similar to Eq. (VI-C-21)

$$\ln(1 - X_1) = 733.6 \left(- \int \frac{0.765}{T} W_1 A \eta k_0 e^{-\frac{E_a}{RT}} dT - t_h W_1 A \eta k_0 e^{-\frac{E_a}{RT_1}} \right.$$

$$\left. - \int - \frac{0.765}{T} W_1 A \eta k_0 e^{-\frac{E_a}{RT}} dT \right) \qquad \text{(VI-G-46)}$$

where X_1 is the O_2 conversion at different temperature,
W_1 is the char feeding rate, in g s^{-1},
A is the specific, internal surface area of char, in m^2 g^{-1},
k_0 is the frequency factor of the surface reaction, in mole s^{-1} m^{-2} atm^{-1},
E_a is the activation energy of the surface reaction, in kcal $mole^{-1}$,
T is temperature, in K,
t_h is gas residence time in the isothermal temperature region, in s.

Here conversion X for O_2/char reaction is defined as

$$X_{oxygen} = \frac{\left(conc.\ of\ CO_2 + \frac{conc.\ of\ CO}{2} \right)}{Feed\ oxygen\ conc.} \qquad \text{(VI-G-47)}$$

Equations (VI-G-46), (VI-G-47), (VI-C-22) and (VI-C-23) have been solved simultaneously by MathCad. Equation (VI-C-25) has been calculated for the effective diffusion coefficient, $D_{eff,\ oxygen}$. The value for lignite char is 1.529 cm^2/s and for bituminous coal char is 9.753 cm^2/s. The constants associated with k_0, $E_{0,\ oxygen}$, η and ϕ of O_2/char reaction, based on D-R CO_2 surface area are:

for lignite char

$k_{oxygen} = 2.936 \times 10^4 \exp(-34{,}570\ cal/RT)$ in mole m^{-2} s^{-1} atm^{-1}

$\eta = 0.536$, $\phi = 4.298$

for bituminous coal char

$k_{oxygen} = 6.226 \times 10^7 \exp(-55{,}620\ cal/RT)$ in mole m^{-2} s^{-1} atm^{-1}

$\eta = 0.971$, $\phi = 0.674$

It is interesting to note that the activation energies of char/O_2 reaction reported by Smith falls well within two activation energies for these two chars we tested. At 1100°C, these two rate expressions give the intrisic rates for two different chars.

$k_{oxygen,\ 1100C} = 9.217 \times 10^{-2}$ mole $m^{-2}\ s^{-1}\ atm^{-1}$ for the lignite char,

$k_{oxygen,\ 1100C} = 9.670 \times 10^{-2}$ mole $m^{-2}\ s^{-1}\ atm^{-1}$ for the bituminous coal char.

After converting these quantities to those with unit adopted by Smith (1982), the rate of O_2/char reactions based on D-R CO_2 surface area are

$k_{oxygen,\ 1100C} = 1.106 \times 10^{-4}$ $g_c\ cm^{-2}\ s^{-1}\ atm^{-1}$ for the lignite char,

$k_{oxygen,\ 1100C} = 1.047 \times 10^{-4}$ $g_c\ cm^{-2}\ s^{-1}\ atm^{-1}$ for the bituminous coal char.

The rates of NO/char reaction (based on D-R CO_2 surface area) for lignite char and bituminous coal char in Tables 6 and 7 give

$k_{NO} = 3.21 \times 10^{2} \exp(-24{,}608\ cal\ /RT)$ in mole $m^{-2}\ s^{-1}\ atm^{-1}$ for lignite char

$k_{NO} = 8.33 \times 10^{12} \exp(-84{,}430\ cal\ /RT)$ in mole $m^{-2}\ s^{-1}\ atm^{-1}$ for bituminous coal char

At 1100°C, these two rates give

$k_{NO,\ 1100C} = 3.88 \times 10^{-2}$ mole $m^{-2}\ s^{-1}\ atm^{-1}$ for the lignite char

$k_{NO,\ 1100C} = 3.03 \times 10^{-1}$ mole $m^{-2}\ s^{-1}\ atm^{-1}$ for the bituminous coal char

Converting the unit of rates of NO/char reactions based on D-R CO_2 surface area to that adopted by Smith (1982)

$k_{NO,\ 1100C} = 4.66 \times 10^{-5}$ $g_c\ cm^{-2}\ s^{-1}\ atm^{-1}$ for the lignite char

$k_{NO,\ 1100C} = 3.64 \times 10^{-4}$ $g_c\ cm^{-2}\ s^{-1}\ atm^{-1}$ for the bituminous coal char

These four data points are added into the Arrhenius plot for O_2/char reaction recommended

by Smith (1982), Figure 36. These data fit well with what Smith suggested. These results suggest that the gasification rate for char/NO reaction is about the same or even higher than the rate for char/O_2 reaction. This is a conclusion consistent with that Chu and Schmidt (1993) if we extrapolate their rates from 700 to 1100°C. However, Song (1978) and Teng *et al.*(1992) reported that the rate for char/O_2 reaction is about two orders of magnitude higher than the rate for char/NO reaction.

VII. CONCLUSIONS

Implications from experiments in pore structure analysis, parameters study, and kinetics analysis - reveal some significant information which are discussed below.

Implications from pore structure analysis suggest

- Higher pyrolysis severity (time and temp) causes demolition of reactive sites of char.Pyrolysis severity destroys reactive sites for CO_2-gasification before those for NO- and O_2-gasification.
- Pyrolysis severity destroys reactive sites for CO_2-gasification before those for NO- and O_2-gasification.
- Although the sites for CO_2-gasification are destroyed, chemisorption of CO_2 could still prevent NO attack their common reactive sites.
- Without CO_2 and O_2, the low reactivity of lignite char is accompanied by formation of stable surface oxygen complexes and closure of micropores.
- Neither BET-N_2 nor DR-CO_2 surface area is a good normalization factor for char reactivity, due to the formation of both stable and reactive surface complexes and closure of micropores.

Investigation on the parameters governing the heterogeneous reaction indicates

- Efficiency of heterogeneous reburning is governed by
  - origin of char
  - pyrolysis temperature & time
  - CO_2 and O_2 in reburning.
- Lignite char alone can be an effective reburning fuel. Bituminous coal and its char are poor reburning fuels.
- Without CO_2 and O_2, the reactivity of young bituminous coal char is comparable to (in terms of NO reduction) or higher than (in terms of per unit surface area) that of lignite char. The detrimental effects of CO_2 and O_2 on the active sites of lignite char for NO reduction are less severe than their effects on those of bituminous coal char. This renders lignite char a more efficient reburning fuel than bituminous coal char.

Study on kinetic analysis reveals

- Internal mass transfer limitation is important only at high temperatures near 1100°C. External mass transfer limitation appears insignificant.
- The rate of NO/char reactions are higher than published results. This may be caused by
  a) Young vs. old char,
  b) Reactor characteristics, such as
     - mass transfer limitations
     - solid mixing.
- The effect of initial concentration on NO reduction by bituminous coal char is obvious, but is not for lignite char.
- The rate of O_2/char reaction is consistent with that reported by Smith (1982).

- The NO/char reaction rate is in the same order of magnitude as the O_2/char reaction rate at 1100°C.

The results from this program reveal that heterogeneous reburning is a potentially significant approach for NO control. If high NO reduction can be achieved by reburning with char at higher oxidant/fuel stoichiometric ratios, less unburned carbon will enter the burnout stage. This observation, along with the demonstrated catalytic activity of calcium compounds in char oxidation, could lead to lower residual carbon and CO emissions. These emissions are typically of concern for other advanced NO control technologies. Moreover, results from the study on the effects of oxidants has provided insight into the competition of NO, CO_2, and O_2 for the reactive char surface, which suggests new, cost effective concepts for NO control.

This study show that lignite char is relatively insensitive to the presence of 16.8 volume % of CO_2. This observation appears to be important for NO reburning with mixed fuels containing both volatiles and solid carbon. Since the volatile fuels usually burn much faster than char, CO and CO_2 produced from burning of mixed fuels is not expected to compete with NO for the active sites on lignite char. Thus, with O_2 already depleted, the NO/char reaction will take place in an environment "richer" to NO than nominally observed, and the NO reduction will be more efficient. Furthermore, we have observed the catalytic conversion of HCN to NH_3 by lignite char or ash (Burch *et al.*, 1991b), which is a desired reaction when volatile fuel is used in reburning. Based on these observations, mixing lignite coal and char will be a more effective route for NO reduction.

REFERENCES

Aarna, I., and E.M. Suuberg, "A Comparison of the Reactivities of Different Carbons for Nitric

Oxide Reduction," Preprints of the Div. of Fuel Chem., Am. Chem. Soc., **41**, 284-288 (1996).
Allen, D., "The Removal of Gaseous Pollutants during Coal Combustion," Ph.D. Dissertation, University of Cambridge, Cambridge, England, 1991.
Aris, R. "On the Dispersion of a Solute in a Fluid Flowing through a Tube," Proc. Roy. Soc. (London), **A235**, 67-77 (1956)
Bedjai, G., H.K. Orbach, and F.C. Riesenfeld, "Reaction of Nitric Oxide with Activated Carbon and Hydrogen," Ind. & Eng. Chem., **50**, 1165-1168 (1958).
Beer, J.M., A.F. Sarofim, S.S. Sandhu, M. Andrei, D. Bachovchin, L.K. Chan, T.Z. Chaung, and A.M. Sprouse, "NO_x Emissions from Fluidized Coal Combustion," Report under Grant EPA/IERL-RTP #R804978020, 1980.
Bird, R.B., W.E. Stewart, and E.N. Lightfoot, "Transport Phenomena," John Wiley & Sons, New York, p.505 (1960).
Burch, T.E., R.B. Conway, and W.Y. Chen, "A Practical Pulverized Coal Feeder for Bench-Scale Combustion Requiring Low Feed Rates," Rev. Sci. Instrum., **62**, 480-483 (1991a).
Burch, T.E., F. R. Tillman, W.Y. Chen, T.W. Lester, R.B. Conway, and A.M. Sterling, "Partitioning of Nitrogenous Species in the Fuel-Rich Stage of Reburning," Energy & Fuels, **5**, 231-237 (1991b).
Burch, T.E., W.Y. Chen, T.W. Lester, and A.M. Sterling, "Interactions of Fuel Nitrogen with Nitric Oxide during Reburning with Coal," Combustion & Flame, **98**, 391-401 (1994).
Chan, L.K., A.F. Sarofim, and J.M. Beer, "Kinetics of the NO-Char Reaction at Fluidized Bed Combustor Conditions," Comb. & Flame, **52**, 37-45 (1983).
Chen, W.Y., T.W. Lester, L.M. Babcock, T.E. Burch, and F.R. Tillman, "Formation and Destruction of Nitrogen Oxides in Coal Combustion ," Final report submitted to U.S. Department of Energy under Contract DE-AC22-88PC88859, November, 1991.
Chen, W.Y., "Role of Char during Reburning of Nitrogen Oxide," First Quarterly Report submitted to the U.S. Department of Energy, under Grant DE-FG22-93PC93227, July, 1994.
Chen, W.Y., L.T. Fan, L. Ma, and M. Yashima, "Role of Char during Reburning of Nitrogen Oxide," Sixth Quarterly Report submitted to the U.S. Department of Energy, under Grant DE-FG22-93PC93227, July, 1995a.
Chen, W.Y., L.T. Fan, T.C. Lu, and M. Yashima, "Role of Char during Reburning of Nitrogen Oxide," Seventh Quarterly Report submitted to the U.S. Department of Energy, under Grant DE-FG22-93PC93227, August, 1995b.
Chen, W.Y., and L. Ma, "Extent of Heterogeneous Mechanisms during Reburning of Nitrogen Oxide," AIChE J, **42**, 1968-1976 (1995).
Chu, X., and L.D. Schmidt, "Intrinsic Rates of NO_x-Carbon Reactions," Energy & Fuels, **32**, 1359-1366 (1993).
De Soete, G.G., "Mechanisms of Nitric Oxide Reduction on Solid Particles; Comparative Study on Coal and Char Particles," Report on EERC Subcontract No. 8318-6, IFP Report No. 28136, June, 1980.
Dubinin, M.M. and L.V. Radushkevich, *Dokl. Adad. Nauk. SSSR*, **55**, 331 (1947).
Furusawa, T., D. Kunii, A. Oguma, and N. Yamada, "Rate of Reduction of Nitric Oxide by Char," Int'l. Chem. Eng., **20**, 239-241 (1980).
Gopalakrishnan, R., M.J. Fullwood, and C.H. Bartholomew, "Catalysis of Char Oxidation by Calcium

Minerals: Effects of Calcium Compound Chemistry on Intrinsic Reactivity of Doped Spherocarb and Zap Chars," Energy & Fuels, **8**, 984-989 (1994).

Hansen, P.F.B., K. Dam-Johansen, J.E. Johnson, and T. Hulgaard, "Catalytic Reduction of NO and N_2O on Limestone during Sulfur Capture under Fluidized Bed Combustion Conditions," Chem. Eng. Sci., **47**, 2419-2424 (1992).

Hansen, P.F.B., and K. Dam-Johansen, "Limestone Catalyzed Reduction of NO and N_2O under Fluidized Bed Combustion Conditions," Proceedings of the 1993 Int'l Conf. on Fluidized Bed Combustion, ASME, **2**, 779-787, 1993.

Howard, J.B., "Fundamentals of Coal Pyrolysis and Hydropyrolysis," in Chemistry of Coal Utilization, Second Supplementary Volume, M. A. Elliot (ed.), John Wiley, New York, pp.665-784, 1981.

Huffman, G.P., F.E. Huggins, N. Shah and A. Shah, "Behavior of Basic Elements during Coal Combustion," Prog. Energy Combustion Sci., **16**, 243-251 (1990).

Illan-Gomez, M. J., A. Linares-Solano, L. R. Radovic, C. Salinas-Martinez de Lecea, and J.M. Calo, "NO Reduction by Activated Carbons. 1. The Role of Carbon Porosity and Surface Area," Energy & Fuels, **7**, 146-154 (1993).

Johnson, J.E., "Formation and Destruction of Nitrogen Oxides in Fluidized-Bed Combustion," Fuel, **73**, 1398-1415 (1994).

Kramlich, J.C., Cole, J. A., McCarthy, J. M., Lanier, W.S. and McSorley, J. A. "Mechanisms of nitrous oxide formation in coal flames," Combust. Flame, 77, 375-384 (1989)

Laine, N.R., F.J. Vastola, and P.L. Walker, Jr., J. Phys. Chem., **67**, 2030-2034 (1963).

Levenspiel, O., and K.B. Bischoff, "Backmixing in the Design of Chemical Reactors," Ind. & Eng. Chem., **51**, 1431-1432 (1959).

Levy, J.M., L.K. Chan, A.F. Sarofim, and J.M. Beer, "NO/Char Reactions at Pulverized Coal Flame Conditions," 18th Symp. (Int'l) on Combustion, The Combustion Institute, pp.111-120, 1981.

Lin, W., J.E. Johnsson, K. Dam-Johansen, and C. M. Van den Bleek, "Interactions between NO_x Emission and Desulfurization in FBC," Proceedings of the 1993 Int'l Conf. on Fluidized Bed Combustion, ASME, **2**, 1093-1100, 1993.

Lizzio, A.A., "The Concept of Reactive Surface Area Applied to Uncatalyzed Carbon (Char) and Catalyzed Carbon (Char) Gasification in Carbon Dioxide and Oxygen," Ph.D. dissertation, Department of Fuel Science, Pennsylvania State University, December, 1990.

Lizzio, A.A., H. Jiang, and L.R. Radovic, "On the Kinetics of Carbon (Char) Gasification: Reconciling Models with Experiments," Carbon, **28**, 7-19 (1990).

Low, M.J.D., and R.T. Yang, "Reactions of Gaseous Pollutants with Solids, V. Infrared Study of the Sorption of NO on CaO," J. Catalysis, **34**, 479-489 (1974).

Lowell, S., *Introduction to Powder Surface Area*, pp.80-89, Wiley, New York, NY (1979).

Mahajan, O.P., and P.L. Walker, "Porosity of Coals and Coal Products," in "Analytical Methods for Coal and Coal Products, Volume 1," C. Karr ed., Academic press, New York, NY, pp.125-188, 1978.

Miller, J.A., and C.T. Bowman, "Mechanism and Modeling of Nitrogen Chemistry in Combustion," Prog. Energy & Combustion Sci., **15**, 287-337 (1989).

Payne, R., D.K. Moyeda, P. Maly, T. Glavicic, and B. Weber, "The Use of Pulverized Coal and Coal-Water-Slurry in Reburning NO_x Control," Proceedings of the EPRI/EPA 1995 Joint

Symposium on Stationary Combustion NO_x Control, Book 4, Kansas City, Missouri, May 16-19, 1995.

Pershing, D.W., and J.O.L. Wendt, "Relative Contributions of Volatile Nitrogen and Char Nitrogen to NO_x Emissions from Pulverized Coal Flames," Ind. Eng. Chem., Process Des. Dev., **18**, 60-67 (1979).

Pershing, D.W., personal communication, November, 29,1995.

Pohl, J.H., "Fate of Coal Nitrogen," Ph.D. Dissertation, Chemical Engineering, Massachusetts Institute of Technology, Boston, MA, June, 1976

Radovic, L. R., P. L. Walker, Jr., and R. G. Jenkins, "Importance of Catalyst Dispersion in the Gasification of Lignite Chars," J. of Catalysis, **82**, 382-394 (1983a).

Radovic, L. R., P. L. Walker, Jr., and R. G. Jenkins, "Importance of Carbon Active Sites in the Gasification of Coal Chars," Fuel, **62**, 849-856 (1983b).

Radovic, L., H. Jiang, and A.A. Lizzio, "A Transient Kinetic Study of Char Gasification in Carbon Dioxide and Oxygen," Energy & Fuels, **5**, 68-74 (1991).

Sahu, R., Y.A. Levendis, R.C. Flagan, and G.R. Gavalas, "Physical Properties and Oxidation Rates of Chars from Three Bituminous Coals," Fuel, **67**, 275-283 (1988).

Satterfield, C.N., "Mass Transfer in Heterogeneous Catalysis," MIT Press, Cambridge, MA, 1970.

Sellars, J.R., M. Tribus, and J.S. Klein, "Heat Transfer to Laminar Flow in a Flat - The Graetz Problem Extended," Trans. ASME, **78**, 441-448 (1956).

Shimizu, T., D. Fujita, K. Ishizu, S. Kobayashi, and M. Inagaki, "Effects of Limestone Feed on Emissions of NO_x and N_2O from a Circulating Fluidized Bed Combustor," Proceedings of the 1993 Int'l Conf. on Fluidized Bed Combustion, Vol. 1, ASME, pp.611-617, 1993.

Smith, R.N., J. Swinehart, and D. Lesnini, "The Oxidation of Carbon by Nitric Oxide," J. Phys. Chem., **63**, 544-547 (1959).

Smith, I.W., "The Combustion Rates of Coal Chars: A Review," 19th Symp. (Int'l) on Combustion, The Combustion Institute, Pittsburgh, PA, pp.1045-1065, (1982).

Song, Y.H., "Fate of Fuel Nitrogen during Pulverized Coal Combustion," D.Sc. dissertation, Chemical Engineering, Massachusetts Institute of Technology, Boston, MA, April, 1978.

Strickland-Constable, R.F., Trans. Faraday Soc., **34**, 1074-1080 (1938).

Suuberg, E.M., H. Teng, and J.M. Calo, "Studies on the Kinetics and Mechanism of the Reaction of NO with Carbon," 23rd Symp. (Int'l) on Combustion, The Combustion Institute, Pittsburgh, PA, pp.1199-1205, 1990.

Takahashi, Y., M. Sakai, T. Kunimoto, S. Ohme, H. Haneda, T. Kawamura, and S. Kaneko, "Development of MACT In-Furnace NO_x Removal Process for Steam Generators," Proc. 1982 Joint Symp. Stationary Combustion NO_x Control, Vol. 1," EPRI Report No. CS-3182, July, 1983.

Taylor, G., "Dispersion of Soluble Matter in Solvent Flowing Slowing through a Tube," Proc. Roy. Soc., **A219**, 186-203 (1953).

Teng, H., E.M. Suuberg, and J.M. Calo, "Studies on the Reduction of Nitric Oxide by Carbon: The NO-Carbon Gasification Reaction," Energy & Fuels, **6**, 398-406 (1992).

Wen, C.Y., and L.T. Fan, "Models for Flow Systems and Chemical Reactors," Marcel-Dekker, New York, pp.68-112 (1975).

Wendt, J.O.L., C.V. Sternling, and M.A. Matovich, "Reduction of Sulfur Trioxide and Nitrogen

Oxides by Secondary Fuel Injection," 14th Symp. (Int'l) on Combustion, The Combustion Inst., Pittsburgh, PA, p.897-904 (1973).

Winter, E.R.S., "The Catalytic Decomposition of Nitric Oxide by metallic Oxides," J. of Catalysis, **22**, 158-170 (1971).

Wissler, E.H., "On the Applicability of the Taylor-Aris Axial Diffusion Model to Tubular Reactor Calculation," Chem. Eng. Sci., **24**, 527-539 (1969).

Wong, B.A., G.R. Gavalas, and R.C. Flagan, "Effects of Char Formation Temperature on the Densification of a Bituminous Coal Char during Gasification," Energy & Fuels, **9**, 493-499 (1995).

APPENDIX A. Surface Area Measurement

For this study, there are two different methods used measure the surface area: the BET-N_2 method and the CO_2 D-R equation. For the BET-N_2 method, we were used the Quantachrome NOVA-1200 BET apparatus. This apparatus reduces the operating time approximately 80% compared to that required by our original BET apparatus (Micrometrics, Flowsorb 2300); moreover, it does not require helium gas.

The BET-surface areas of nine samples were measured with nitrogen (N_2) as the adsorbate at a temperature of 77 K. Measurements were carried out under six different relative pressures, P/P_0, with the multi-point method. The P/P_0 ranged from 0.05 to 0.30 , within the region of the adsorption isotherm. Each P/P_0 leads to the weight of gas, W, adsorbed on the sample. The surface area of each sample has been recovered from the Brunauer-Emmett-Teller (BET) equation,

$$\frac{1}{W[(P_0/P)-1]} = \frac{1}{W_m C} + \frac{C-1}{W_m C}\left(\frac{P}{P_0}\right) \qquad \text{(A-1)}$$

where W_m is the weight of adsorbate constituting a monolayer of surface coverage, and C is a constant. Both W_m and C are simultaneously recovered from the slope, s, and the intercept, i, of a linear plot of $1/[W(P/P_0-1]$ against P/P_0. This gives

$$s = \frac{C-1}{W_m C} \qquad \text{(A-2)}$$

and

$$i = \frac{1}{W_m C} \qquad \text{(A-3)}$$

Summing Eqs. (A-2) and (A-3) yields W_m as

$$W_m = \frac{1}{s + i} \tag{A-4}$$

Thus, the total surface area, A, is

$$A = \frac{W_m N_0 \sigma}{M} \tag{A-5}$$

where N_0 is the Avogadro number; σ, the effective cross-sectional area of an adsorbate molecule; and M, the molar weight of the adsorbate. The results is shown in Table 2.

Another measurement method, the CO_2 D-R equation, was carried out with carbon dioxide (CO_2) as the adsorbate at a temperature of 273 K. The P/P_0 ranging from 0.001 to 0.010 was within the region of the adsorption isotherm. The P/P_0 is small compared to that of the above measurements because the adsorbate saturation vapor pressure, P_0, at 273 K is much larger than the atmospheric pressure. Measurements were carried out under eleven different levels of P/P_0 with the multi-point method. The surface area of each sample has been estimated with the BET equations. Furthermore, the micropore volume and micropore surface area of each sample have been calculated with the Dubinin-Radushkevich (D-R) equation (see, e.g., Lowell, 1979). Dubinin and Radushkevich (1947) postulated that the fraction of the adsorption volume, V, occupied by a liquid adsorbate at various adsorption potentials, E, can be expressed as a Gaussian function

$$V = V_0 e^{-K(E/\beta)^2} \tag{A-6}$$

where V_0 is the adsorption volume of a reference liquid adsorbate; K, a constant related to the shape of the pore size distribution; and β, an affinity coefficient relating E to that of the reference adsorbate, E_0, or

$$\beta = \frac{E}{E_0} \tag{A-7}$$

When the adsorbate is in the liquid state, the adsorption potential is given by

$$E = RT \left[\ell n \frac{P_0}{P}\right] \tag{A-8}$$

If the above expression is substituted into Eq. (A-6), then

$$V = V_0 \, e^{-K \left[\frac{RT}{\beta} \ell n \frac{P_0}{P}\right]^2} \tag{A-9}$$

or

$$\ell og \; V = \log \; V_0 - k \left[\ell og \frac{P_0}{P}\right]^2 \tag{A-10}$$

where

$$k = 2.303 \; K \left[\frac{RT}{\beta}\right]^2 \tag{A-11}$$

The micropore volume is recovered from the intercept of a plot of ℓog V against $[\ell \text{og } P_0/P]^2$. The results are summarized in Table 3.

APPENDIX B . Stoichiometric Ratio (SR) of Reburning Zone

The stoichiometric ratio of a reburning zone depends on the composition of the reburning fuel. Here, Mississippi lignite char is used as an example. Only C, H, and O are involved in the calculation of the stoichiometric ratio. Therefore, from Table 1, the following atomic ratios can be calculated for Mississippi lignite char.

	wt.%	Atomic wt.	Aomic ratio	Atomic ratio normalized to carbon
C	51.55	12	4.2958	1
H	0.67	1	0.67	0.1559
O	1.38	16	0.08625	0.02
C+H+O	53.60			

Therfore, the equivalent formula of Mississippi lignite char can be written as: $C_1H_{0.1559}\ O_{0.02}$. The stoichiometric equation in reburning zone can be wriiten as

$$CH_{0.1559}\ O_{0.02} + 1.07795O_2 \rightarrow CO_2 + 0.07795\ H_2O$$

Assuming Pittsburgh #8 bituminous coal is burned in the primary combustion zone at stoichiometric ratio 1.1 and with He, not N_2, as the offset gas in the oxidant, then the chemical reaction can be written in the following form

$$CH_{0.793}\ O_{0.109} + 1.258\ O_2 + 4.8303\ He \rightarrow CO_2 + 0.3965\ H_2O + 0.1148\ O_2 + 4.8303\ He$$

When the x units of Mississippi lignite char is used as reburning fuel, then the feed for the reburning zone include the following

$$xCH_{0.1559}\ O_{0.02} + CO_2 + (0.3965\ H_2\ O) + 0.1148\ O_2 + 4.8303\ He \qquad \text{(B-1)}$$

The stoichiometric ratio in the reburning zone, SR2, can be defined as

$$SR2 = \frac{\frac{O(\text{as atom}) \text{ actually used}}{\text{total fuel}}}{\frac{O(\text{as atom}) \text{ theoretically required}}{\text{total fuel}}}$$

or, in terms of reburning with x units of lignite char, the oxygen quanties in the above expressin can be written as

$$SR2 = \frac{0.02x + 2 + 0.2296}{\frac{2 + 0.2296}{1.1} + (1.1866)(2)x}$$

where the first, second and third terms in the numerator represent the oxygen atoms from the reburning fuel, CO_2 from the primary zone, and excess oxygen from the primary zone, respectively. Similarly, the two terms in the denominator represent the theoretically required oxygen for burning the primary fuel and reburning fuel (which can be obtained by balancing a chemical reaction involving burning lignite char), respectively. Rearranging the above equation, we obtain

$$SR2 = \frac{0.2306x + 2.2296}{2.0269 + 2.3732x}$$

This equation has been used in the calculation of required feeding rate of reburning fuel when a particular SR2 is selected. For example, at SR2 = 0.9, the equation above becomes

$$1.8242 + 2.1359\,x = 0.02\,x + 2.2296$$

or,

$$x = 0.1916$$

This is the number of moles of lignite char, $CH_{0.1559}\,O_{0.02}$, required to achieve a SR2=0.9 when one

mole of $CH_{0.793}\ O_{0.109}$ in the primary zone is burned. This number can be further related to the feed rate of reburning fuel, as discussed below.

Since the reactor is operated at a flowrate 2000 cc/min, the molar flowrate is

$$n = \frac{PV}{RT} = \frac{1 \times \frac{2000}{1000}}{0.0821 \times 298} = 0.0818\ moles/min$$

Assuming the gas contains mainly CO_2, O_2, and He, the required feeding rate of lignite char for one minute operation is

$[(0.0818)/(1 + 0.1148 + 4.8303)]\ (0.1916) = 2.636 \times 10^{-3}$ "moles" of reburning fuel

Note the quantities of gases and reburning fuels in moles are consistent with the stoichiometric coefficients in Eq. (B-1). Furthermore, the "molecular weight" of lignite char can be written as

$[12 + 0.1559 + 0.02 \times 16] = 12.476$ g/mole

Therefore, the feeding rate of char in term of three elements, C, H, and O, is

$2.636 \times 10^{-3} \times 12.476 = 0.0329$ g/min.

The three elements (C, H, and O) consist only part of the char weight (see Table 1) and, taking the mineral content into consideration, we obtain the corresponding feeding rate for lignite char

$0.0329/0.536 = 0.064$ g/min of dried lignite char.

Table 1. Ultimate Analysis of Coals and Chars

Contents, %	MS lignite	Pitt #8 bituminous coal	MS lignite char (Low temperature 950°C)	Pitt #8 coal char (Low temperature 950°C)	MS lignite char (High temperature 1100°C)	Pitt #8 coal char (High temperature 1100°C)
Moisture	0.29	1.75	0.55	0.304	0.11	0.7
Carbon	53.07	77.23	56.54	90.63	51.55	88.28
Hydrogen	5.34	5.34	0.77	0.53	0.67	0.61
Oxygen	0*	8.75	0*	0*	1.38	0.43
Nitrogen	0.58	1.55	0.41	1.05	0.31	1.31
Sulfur	0.94	0.71	1.33	2.38	1.79	1.14
Ash	23.75	6.42	45.2	8.93	53.01	9.99

* by difference.

Moisture was determinted by loss on drying in air at 105°C for one hour.Char results are reported on a dried sample basis.

Table 2. Char preparation conditions

4-1L lignite char pyrolyzed at 1100°C and 5 min holding time
4-2L lignite char pyrolyzed at 1100°C and 5 min holding time followed by reaction with NO at 1100°C
4-3L lignite char pyrolyzed at 1100°C and 5 min holding time followed by reaction with NO at 800°C
4-4L lignite char pyrolyzed at 1100°C and 5 min holding time followed by reaction with ($NO+CO_2+O_2$) at 1100°C
6-3L lignite char pyrolyzed at 950°C and 5 min holding time
7-1L lignite char pyrolyzed at 950°C and zero holding time
7-2L lignite char pyrolyzed at 1100°C and 5 min holding time followed by reaction with ($NO+CO_2$) at 1100°C
7-3L lignite char pyrolyzed at 1100°C and 2 h holding time

4-1P bituminous coal char pyrolyzed at 1100°C and 5 min holding time
4-2P bituminous coal char pyrolyzed at 1100°C and 5 min holding time followed by reaction with NO at 1100°C
4-3P bituminous coal char pyrolyzed at 1100°C and 5 min holding time followed by reaction with NO at 800°C
4-4P bituminous coal char pyrolyzed at 1100°C and 5 min holding time followed by reaction with ($NO+CO_2+O_2$) at 1100°C
6-2P bituminous coal char pyrolyzed at 950°C and 5 min holding time
7-1P bituminous coal char pyrolyzed at 9500°C and zero holding time
7-3P bituminous coal char pyrolyzed at 1100°C and 5 min holding time followed by reaction with ($NO+CO_2$) at 1100°C
7-4P bituminous coal char pyrolyzed at 1100°C and 2 h holding time

Table 3. Comparison of surface areas measured by various methods

Sample	N_2-BET[a] 77 K (m^2/g)	CO_2-BET[b] 273 K (m^2/g)	CO_2-DR[c] 273 K (m^2/g)
4-1L	86.86	136	255
4-2L	12.18	125	235
4-3L	9.37	124.5	245.5
4-4L	16.48	26.4	49.9
6-3L	82.11	158.15	311.46
7-1L	11.45	124.55	252.50
7-2L	56.54	80.59	158.31
7-3L	18.29	116.74	239.11
4-1P	4.18	31.2	36.2
4-2P	4.65	N/A	24.6
4-3P	4.15	24.2	22.1
4-4P	69.19	137	270.7
6-2P	2.33	6.11	30.12
7-1P	2.6	6.59	33.15
7-3P	2.27	7.00	36.16
7-4P	1.92	4.27	25.54

[a] measured volumetrically and evaluated with multi-point BET equation.
[b] measured volumetrically and evaluated with multi-point BET equation.
[c] measured volumetrically and evaluated with DR equation for micro-pore surface area.

Table 4. Micropore volume, total pore volume, and average pore radius with adsorbate N_2 at 77 K

sample	micro[a] pore volume (cc/g)	total[b] pore volume (cc/g)	volume ratio of micro pore to total pore (%)	average[c] pore radius (A)	micro[d] pore volume (cc/g)
4-1L	0.0418	0.0715	58.46	16.46	0.093
4-2L	0.0049	0.0286	17.13	46.96	0.086
4-3L	0.0036	0.0180	20.00	38.42	0.089
4-4L	0.0065	0.0332	19.58	40.29	0.018
6-3L	0.0417	0.0951	43.85	23.16	0.1129
7-1L	0.0051	0.0351	14.53	61.31	0.0915
7-2L	0.0351	0.0613	57.26	21.68	0.0574
7-3L	0.0075	0.0373	20.11	40.79	0.0867
4-1P	0.0012	0.0065	18.46	31.10	0.013
4-2P	0.0011	0.0061	18.03	26.24	0.009
4-3P	0.0010	0.0062	16.13	29.88	0.008
4-4P	0.0335	0.0483	69.36	13.96	0.098
6-2P	0.0010	0.0046	21.74	39.48	0.0109
7-1P	0.0010	0.0051	19.61	39.23	0.0120
7-3P	0.0011	0.0041	26.83	36.12	0.0131
7-4P	0.0007	0.0040	17.50	41.67	0.0093

[a]measured volumetrically and evaluated with DR equation.
[b]volume measured directly when P/P^0 is close to 1.
[c]evaluated from total pore volume and surface area, $r=2V_T/S$.
[d]with adsorbate CO_2 at 273 K.

Table 5. Yield of Nitrous Oxide for different chars

Temperature, °C	Yield of N_2O from NO+MS lignite char reaction char pyrolysis temp. 1100 °C, 5 min holding time ppm	Yield of N_2O from NO+Pitt #8 coal char reaction char pyrolysis temp. 1100 °C, 5 min holding time ppm
800	13.5	10.4
850	13.4	10.1
900	13.3	9.9
950	13.0	9.3
1000	12.9	9.2
1050	11.5	9
1100	10.0	8.7

* The feeding rate of high temp. (1100 °C, 5 min holding time) Mississippi lignite char is 0.064 g/min.

† The feeding rate of Pitt #8 bituminous coal char at $[NO]_{in}$ = 1000 ppm is 0.0446 g/min.

Table 6. Summary of Arrhenius' constants and mass transfer limitations of NO reaction with Mississippi lignite char at various temperatures based on CO_2 surface areas. (reaction time about 0.2s)

Reactants	Temp. Range, °C	k_0, mole/(s m^2 atm)	E_a, Kcal/mole	ϕ	η
MS Lignite Char (1100°C, 5min)+NO $[NO]_{in}$ = 1000 ppm w/ CO_2	800-850	13.752	15.9	1.458	0.882
	850-900			1.781	0.837
	900-925			1.922	0.817
	925-950			1.965	0.811
	950-1000			2.480	0.739
	1000-1050			2.622	0.720
	1050-1100			2.547	0.730
MS Lignite Char (950°C,5min)+NO $[NO]_{in}$ = 1000 ppm	800-850	1.16×10^1	15.92	1.637	0.857
	850-900			2.005	0.805
	900-925			2.169	0.782
	925-950			2.224	0.774
	950-1000			2.829	0.693
	1000-1050			2.856	0.687
	1050-1100			2.991	0.683
MS Lignite Char (1100°C,5min)+NO $[NO]_{in}$ = 1000 ppm	800-850	321.815	24.608	1.088	0.828
	850-900			1.345	0.897
	900-925			1.451	0.883
	925-950			1.548	0.865
	950-1000			1.842	0.828
	1000-1050			2.367	0.754
	1050-1100			2.881	0.686
MS Lignite Char (1100°C,5min)+NO $[NO]_{in}$ = 800 ppm	800-850	1520.333	28.811	0.958	0.944
	850-900			1.199	0.916
	900-925			1.291	0.904
	925-950			1.406	0.889
	950-1000			1.741	0.843
	1000-1050			2.158	0.784
	1050-1100			3.123	0.657

Reactants	Temp. Range, °C	k_0, mole/(s m^2 atm)	E_a, Kcal/mole	ϕ	η
MS Lignite Char (1100°C,5min)+NO $[NO]_{in}$ = 600 ppm w/ CO_2	800-850	3,933.423	31.586	0.872	0.953
	850-900			1.043	0.934
	900-925			1.159	0.920
	925-950			1.261	0.908
	950-1000			1.482	0.879
	1000-1050			2.052	0.799
	1050-1100			3.233	0.644
MS Lignite Char (1100°C,5min)+NO $[NO]_{in}$ = 400 ppm	800-850	93,523.57	39.5	0.628	0.975
	850-900			0.929	0.947
	900-925			1.182	0.918
	925-950			1.357	0.895
	950-1000			1.540	0.858
	1000-1050			2.531	0.732
	1050-1100			2.995	0.672
MS Lignite Char (1100°C,5min)+NO $[NO]_{in}$ = 200 ppm	800-850	1,107,058	44.359	0.788	0.961
	850-900			1.203	0.915
	900-925			1.319	0.900
	925-950			1.465	0.881
	950-1000			2.376	0.753
	1000-1050			2.906	0.683
	1050-1100			4.913	0.486
MS Lignite Char (1100°C, 2 h)+NO $[NO]_{in}$ = 1000 ppm	1000-1050	402.22	28.45	1.183	0.918
	1050-1100			1.428	0.886
MS Lignite Char (1100°C,5min)+NO $[NO]_{in}$ = 1000 ppm w/ CO_2, O_2	1000-1050	1.990	11.794	0.923	0.947
	1050-1100			0.996	0.940

* The feeding rate of high temp. (1100°C, 5 min & 2 h holding time) Mississippi lignite char is 0.064 g/min.

† The feeding rate of low temp. (950°C, 5 min holding time) Mississippi lignite char is 0.0325 g/min.

Table 7. Summary of Arrhenius' constants and mass transfer limitations of NO reaction with Pitt #8 bituminous coal char at various temperatures based on CO_2 surface areas. (reaction time about 0.2s)

Reactants	Temp. Range, °C	k_0, mole/(s m^2 atm)	E_a, Kcal/mole	ϕ	η
Pitt #8 Coal Char (1100°C,5min)+NO $[NO]_{in}$ = 1000 ppm w/ CO_2	800-925 925-1000 1000-1100	1.35×10^{-1} 3.12×10^{6} 4.20×10^{12}	7.671 47.802 82.91	0.170 0.309 0.991	0.998 0.994 0.940
Pitt #8 Coal Char (950°C,5min)+NO $[NO]_{in}$ = 1000 ppm	800-925 925-1000 1000-1100	7.83×10^{2} 6.31×10^{5} 9.32×10^{9}	20.06 35.47 65.84	0.265 0.732 1.408	0.995 0.996 0.889
Pitt #8 Coal Char (1100°C,5min)+NO $[NO]_{in}$ = 1000 ppm	800-925 925-1000 1000-1100	1.53×10^{-1} 5.45×10^{6} 8.33×10^{12}	7.68 49.25 84.43	0.159 0.284 0.929	0.998 0.995 0.947
Pitt #8 Coal Char (1100°C,5min)+NO $[NO]_{in}$ = 800 ppm	800-925 925-1000 1000-1100	1.67×10^{3} 3.01×10^{6} 3.17×10^{9}	25.784 43.605 61.158	0.444 0.733 1.737	0.987 0.966 0.843

Reactants	Temp. Range, °C	k_0, mole/(s m^2 atm)	E_a, Kcal/mole	ϕ	η
Pitt #8 Coal Char (1100°C,5min)+NO $[NO]_{in}$ = 600 ppm	800-925 925-1000 1000-1100	9.89×10^4 3.87×10^5 1.05×10^{12}	35.339 36.269 76.708	0.998 0.995 0.947	0.993 0.976 0.830
Pitt #8 Coal Char (1100°C,5min)+NO $[NO]_{in}$ = 400 ppm	800-925 925-1000 1000-1100	4.23×10^1 2.12×10^{10} 2.84×10^7	17.71 65.15 48.61	0.369 0.831 1.642	0.991 0.957 0.857
Pitt #8 Coal Char (1100°C,5min)+NO $[NO]_{in}$ = 200 ppm	800-925 925-1000 1000-1100	4.79×10^0 2.65×10^5 3.24×10^5	11.21 31.62 38.23	0.490 0.713 1.216	0.984 0.968 0.913
Pitt #8 Coal Char (1100°C, 2 h)+NO $[NO]_{in}$ = 1000 ppm	1000-1050 1050-1100	4.57×10^{-1}	6.75	0.300	0.993
Pitt #8 Coal Char (1100°C,5min) $[NO]_{in}$ = 1000 ppm w/CO_2, O_2	1000-1050 1050-1100	1.58×10^{-1}	9.06	0.448	0.987

*The feeding rate of Pitt #8 bituminous coal char at $[NO]_{in}$ = 1000 ppm is 0.0446 g/min.

Table 8. Summary of Arrhenius' constants and mass transfer limitations of NO reaction with Mississippi lignite char at various temperatures based on N_2 surface areas. (reaction time about 0.2s)

Reactants	Temp. Range, °C	k_0, mole/(s m^2 atm)	E_a, Kcal/mole	ϕ	η
MS Lignite Char (1100°C,5min)+NO $[NO]_{in}$ = 1000 ppm w/ CO_2	800-850	8.024	13.68	0.674	0.971
	850-900			0.694	0.969
	900-925			0.773	0.962
	925-950			0.833	0.957
	950-1000			1.033	0.935
	1000-1050			1.009	0.938
	1050-1100			1.034	0.935
MS Lignite Char (950°C,5min)+NO $[NO]_{in}$ = 1000 ppm	800-850	2.98×10^1	15.39	0.794	0.960
	850-900			0.95	0.945
	900-925			1.017	0.937
	925-950			1.040	0.935
	950-1000			1.270	0.907
	1000-1050			1.331	0.899
	1050-1100			1.431	0.885
MS Lignite Char (1100°C,5min)+NO $[NO]_{in}$ = 1000 ppm	800-850	318.702	22.24	0.625	0.975
	850-900			0.756	0.964
	900-925			0.813	0.959
	925-950			0.881	0.952
	950-1000			1.011	0.938
	1000-1050			1.259	0.908
	1050-1100			1.487	0.878
MS Lignite Char (1100°C,5min)+NO $[NO]_{in}$ = 800 ppm	800-850	1.35×10^3	26.16	0.556	0.980
	850-900			0.686	0.970
	900-925			0.732	0.966
	925-950			0.787	0.961
	950-1000			0.965	0.943
	1000-1050			1.164	0.920
	1050-1100			1.589	0.864

Reactants	Temp. Range, °C	k_0, mole/(s m^2 atm)	E_a, Kcal/mole	ϕ	η
MS Lignite Char (1100°C,5min)+NO $[NO]_{in}$ = 600 ppm w/ CO_2	800-850	3376.69	28.82	0.501	0.984
	850-900			0.595	0.977
	900-925			0.658	0.972
	925-950			0.712	0.968
	950-1000			0.829	0.829
	1000-1050			1.112	0.926
	1050-1100			1.635	0.858
MS Lignite Char (1100°C,5min)+NO $[NO]_{in}$ = 400 ppm	800-850	71258.62	32.40	0.364	0.991
	850-900			0.533	0.982
	900-925			0.671	0.971
	925-950			0.764	0.963
	950-1000			0.905	0.906
	1000-1050			1.334	0.898
	1050-1100			1.535	0.871
MS Lignite Char (1100°C,5min)+NO $[NO]_{in}$ = 200 ppm	800-850	292984.87	38.90	0.454	0.987
	850-900			0.982	0.970
	900-925			0.744	0.965
	925-950			0.82	0.958
	950-1000			1.263	0.908
	1000-1050			1.494	0.877
	1050-1100			2.285	0.766
MS Lignite Char (1100°C, 2 h)+NO $[NO]_{in}$ = 1000 ppm	1000-1050	1.913	8.695	0.267	0.995
	1050-1100			0.280	0.995
MS Lignite Char (1100°C,5min)+NO $[NO]_{in}$ = 1000 ppm w/ CO_2, O_2	1000-1050	1.193	11.89	0.546	0.981
	1050-1100			0.587	0.978

* The feeding rate of high temp. (1100 °C, 5 min & 2 h holding time) Mississippi lignite char is 0.064 g/min.

† The feeding rate of low temp. (950 °C, 5 min holding time) Mississippi lignite char is 0.0325 g/min.

Table 9. Summary of Arrhenius' constants and mass transfer limitations of NO reaction with Pitt #8 bituminous coal char at various temperatures based on N_2 surface areas. (reaction time about 0.2s)

Reactants	Temp. Range, °C	k_0, mole/(s m^2 atm)	E_a, Kcal/mole	ϕ	η
Pitt #8 Coal Char (1100°C,5min)+NO $[NO]_{in}$ = 1000 ppm w/ CO_2	800-925	1.18×10^{0}	7.706	0.058	1.000
	925-1000	2.46×10^{7}	47.604	0.605	0.999
	1000-1100	1.64×10^{13}	80.950	0.545	0.981
Pitt #8 Coal Char (950°C,5min)+NO $[NO]_{in}$ = 1000 ppm	800-925	2.55×10^{0}	5.63	0.073	1.000
	925-1000	5.68×10^{1}	20.79	0.194	0.997
	1000-1100	5.50×10^{13}	76.19	0.368	0.991
Pitt #8 Coal Char (1100°C,5min)+NO $[NO]_{in}$ = 1000 ppm	800-925	1.11×10^{0}	7.66	0.056	1.000
	925-1000	1.24×10^{22}	128.97	0.262	0.995
	1000-1100	8.49×10^{9}	57.66	0.588	0.978
Pitt #8 Coal Char (1100°C,5min)+NO $[NO]_{in}$ = 800 ppm	800-925	1.47×10^{1}	10.257	0.116	0.999
	925-1000	1.53×10^{10}	59.830	0.239	0.996
	1000-1100	8.35×10^{9}	58.328	0.544	0.981
Pitt #8 Coal Char (1100°C,5min)+NO $[NO]_{in}$ = 600 ppm	800-925	4.97×10^{3}	24.388	0.106	0.999
	925-1000	4.79×10^{8}	51.770	0.205	0.997
	1000-1100	1.29×10^{12}	71.833	0.572	0.979

Reactants	Temp. Range, °C	k_0, mole/(s m^2 atm)	E_a, Kcal/mole	ϕ	η
Pitt #8 Coal Char (1100°C,5min)+NO $[NO]_{in}$ = 400 ppm	800-925 925-1000 1000-1100	8.04×10^5 1.00×10^8 4.70×10^7	34.77 46.18 44.51	0.125 0.277 0.576	0.999 0.995 0.983
Pitt #8 Coal Char (1100°C,5min)+NO $[NO]_{in}$ = 200 ppm	800-925 925-1000 1000-1100	1.78×10^2 3.29×10^5 3.65×10^5	14.51 26.76 31.74	0.175 0.241 0.396	0.998 0.997 0.990
Pitt #8 Coal Char (1100°C, 2 h)+NO $[NO]_{in}$ = 1000 ppm	1000-1050 1050-1100	4.59×10^{-1}	6.75	0.300 0.331	0.993 0.994
Pitt #8 Coal Char (1100°C,5min)+NO $[NO]_{in}$ = 1000 ppm w/ CO_2, O_2	1000-1050 1050-1100	1.36×10^0	9.03	0.055 0.058	1.000 1.000

*The feeding rate of Pitt #8 bituminous coal char at $[NO]_{in}$ = 1000 ppm is 0.0446 g/min.

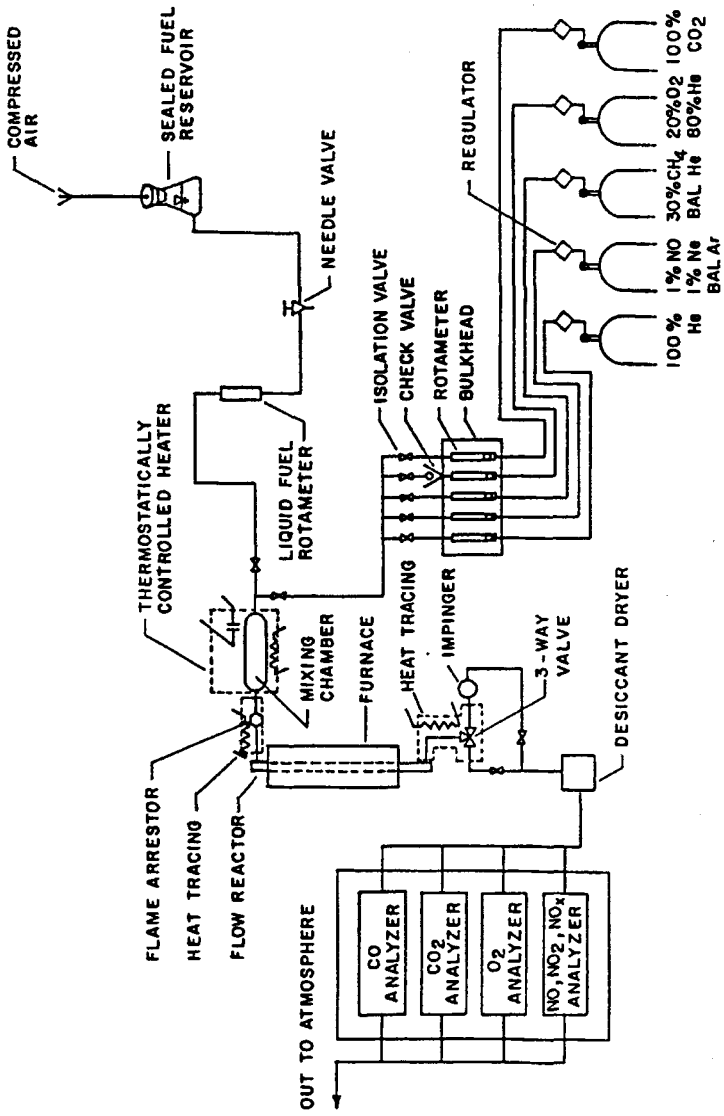

Figure 1. Experimental apparatus.

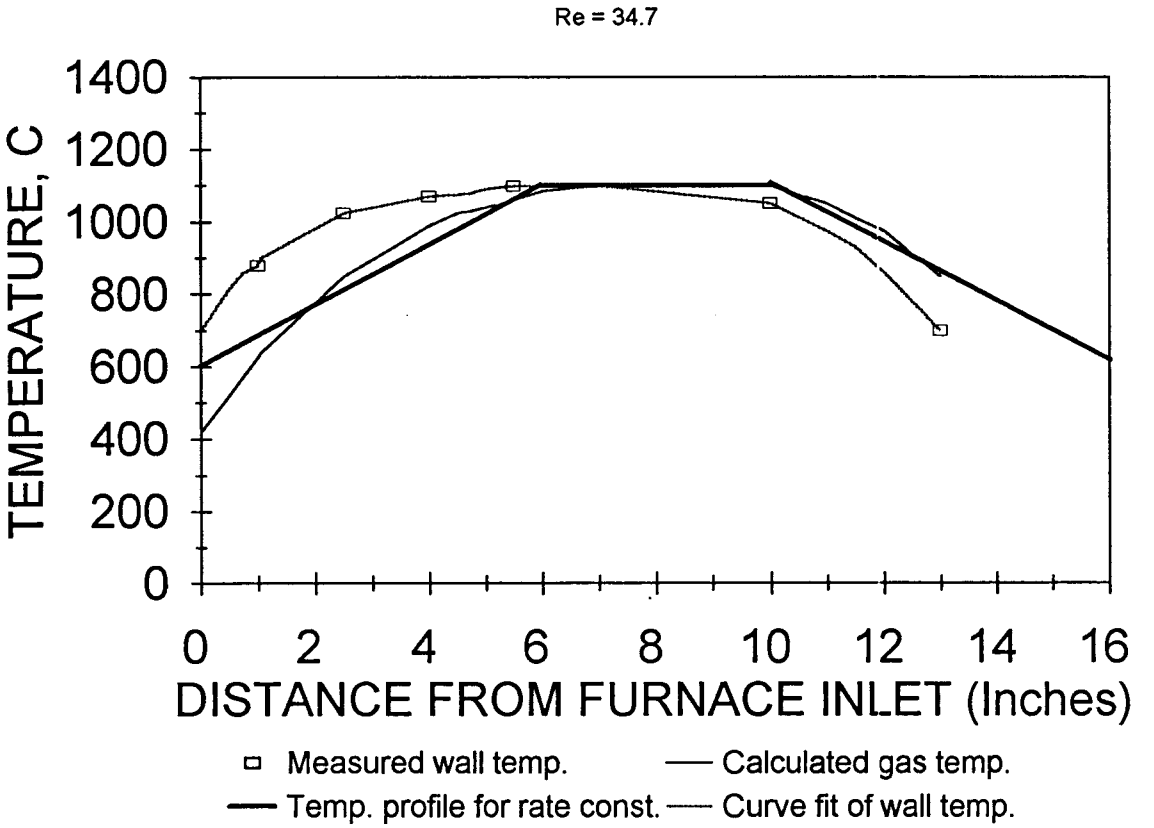

Figure 2. Furnace temperature profile.

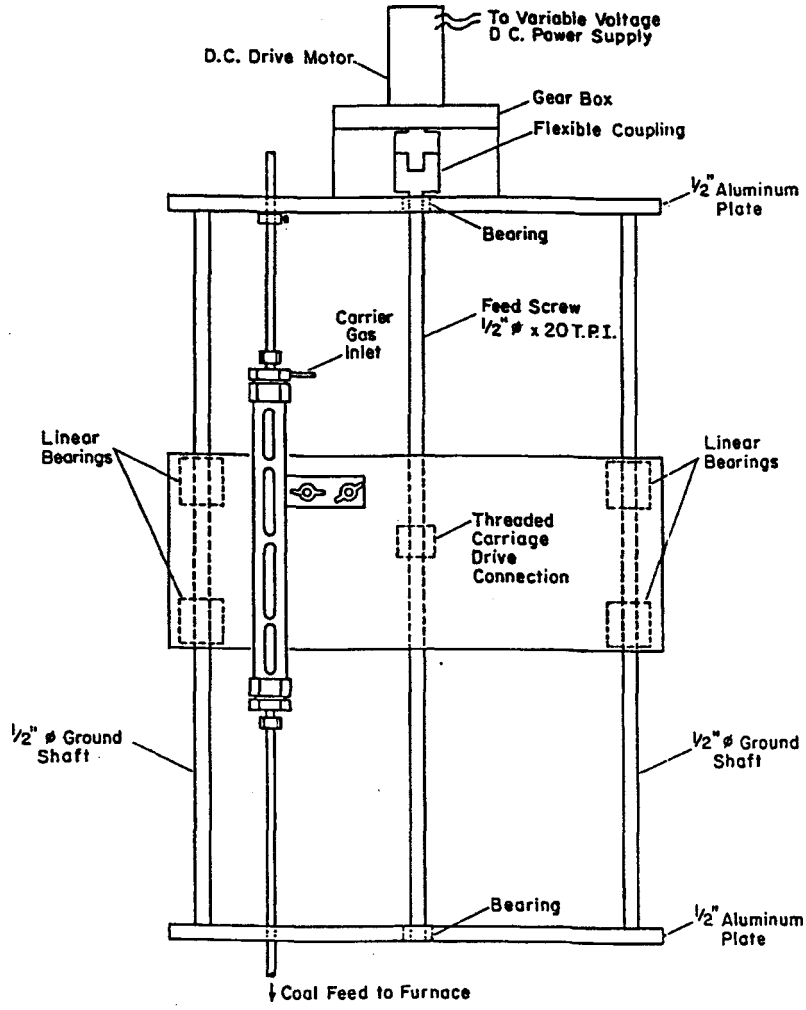

Figure 3. Exploded view of the coal feeder assembly.

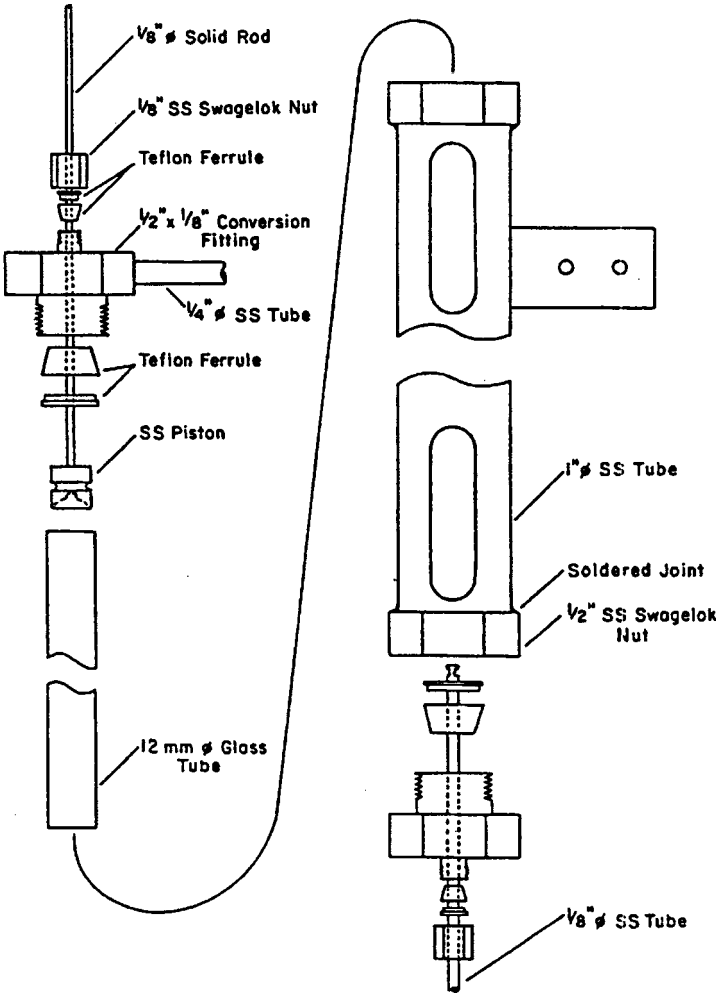

Figure 4. Coal feeder with carriage and drive mechanism.

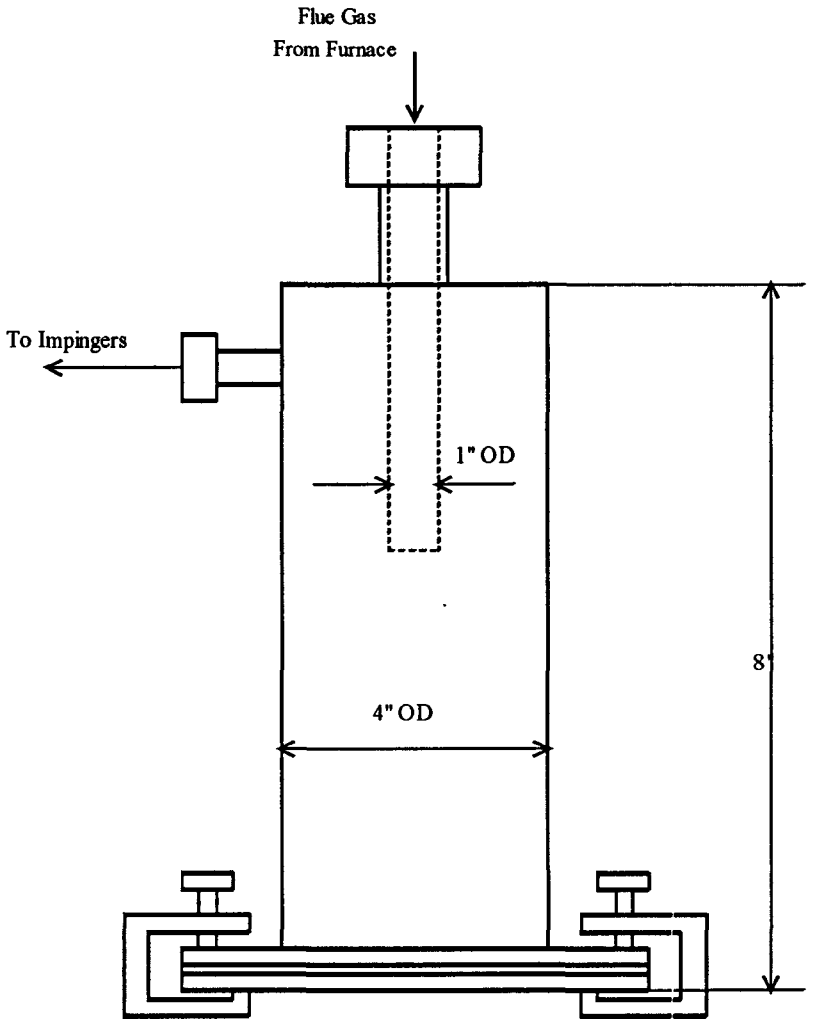

Figure 5. Char/ash collection unit.

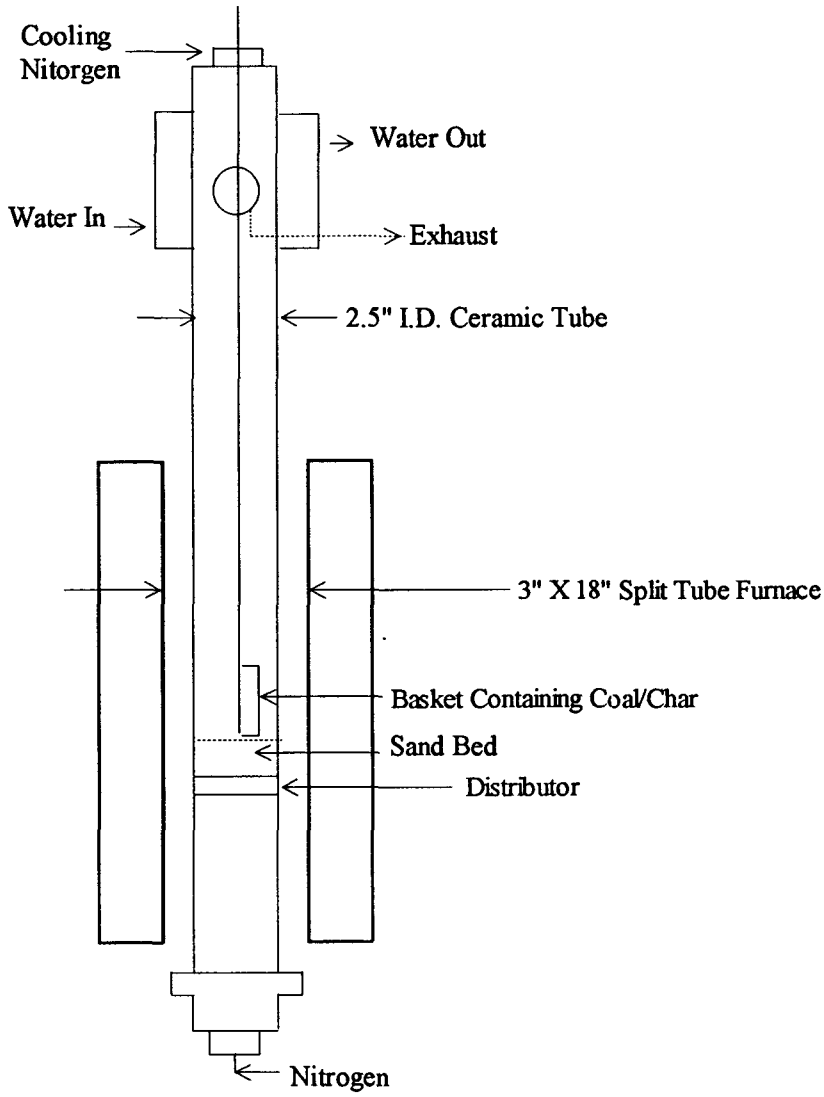

Figure 6. Char preparation system.

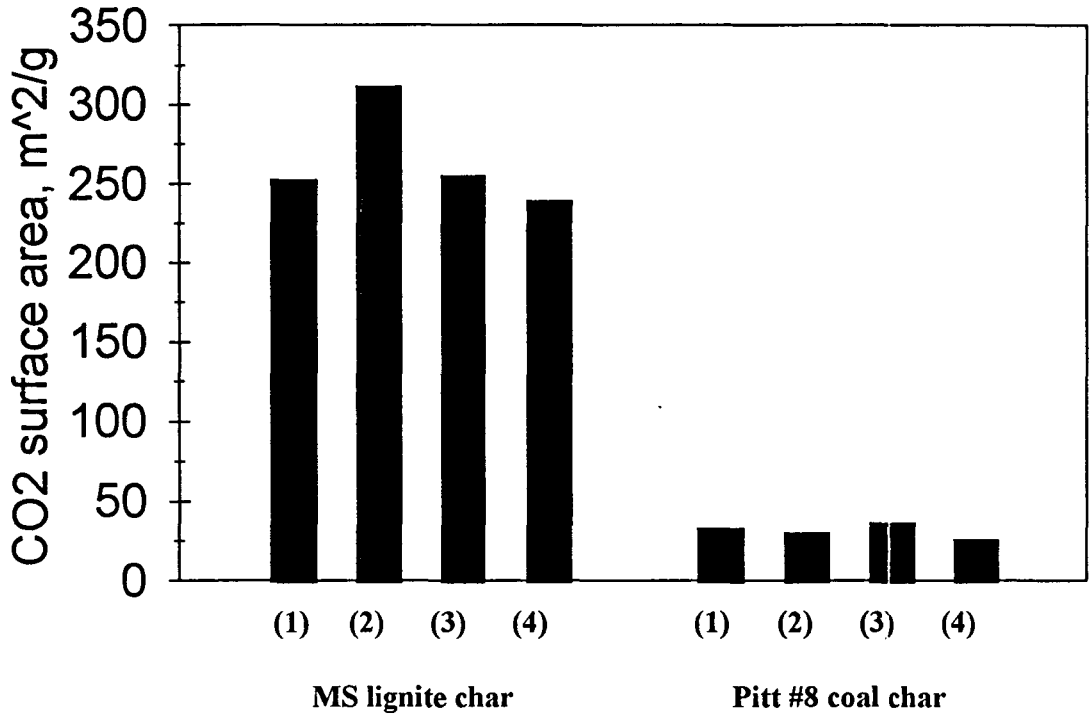

(1). Char py. temp. at 950 C, zero holding time
(2). Char py. temp. at 950 C, 5 min holding time
(3). Char py. temp. at 1100 C, 5 min holding time
(4). Char py. temp. at 1100 C, 2 h holding time

Figure 7. Comparison of surface areas of different chars at different pyrolysis temperatures (Based on CO_2 surface area)

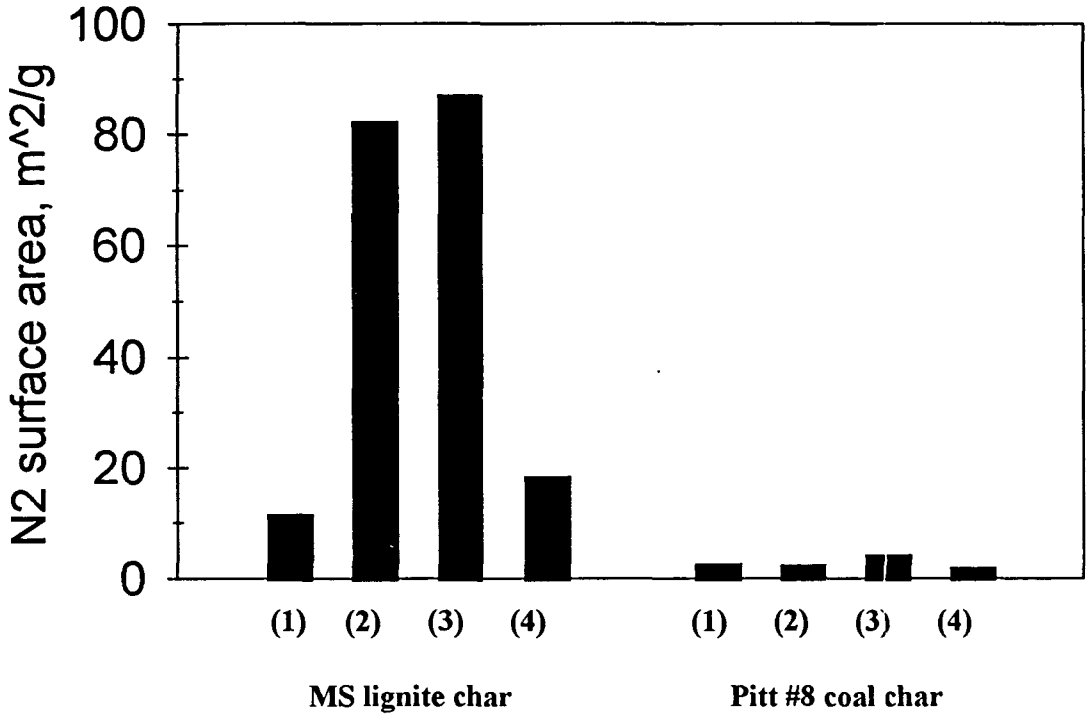

(1). Char py. temp. at 950 C, zero holding time
(2). Char py. temp. at 950 C, 5 min holding time
(3). Char py. temp. at 1100 C, 5 min holding time
(4). Char py. temp. at 1100 C, 2 h holding time

Figure 8. Comparison of surface areas of different chars at different pyrolysis temperatures (Based on N_2 surface area)

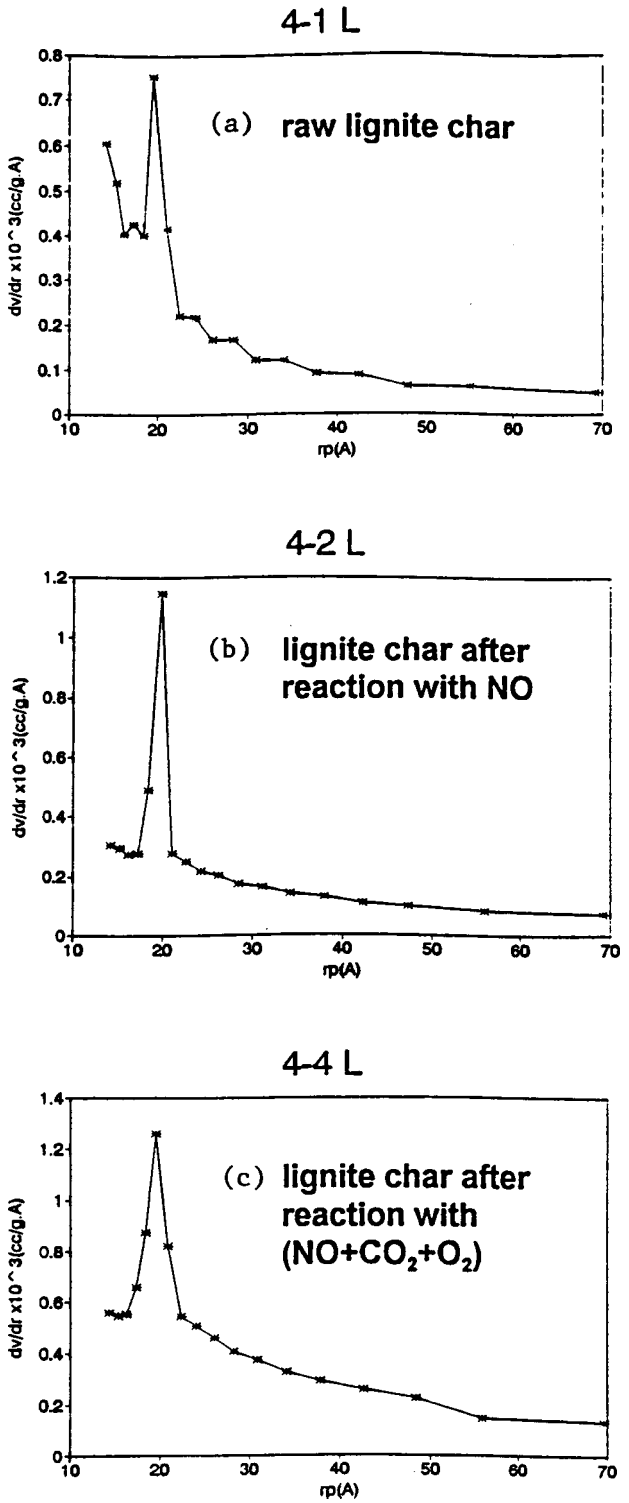

Figure 9. Pore size distribution of lignite char

(a). Char pyrolyzed at 1100°C and 5 min holding time.

(b). Char pyrolyzed at 1100°C and 5 min holding time followed by reaction with NO at 1100°C

(c). Char pyrolyzed at 1100°C and 5 min holding time followed by reaction with ($NO+CO_2+O_2$) at 1100°C

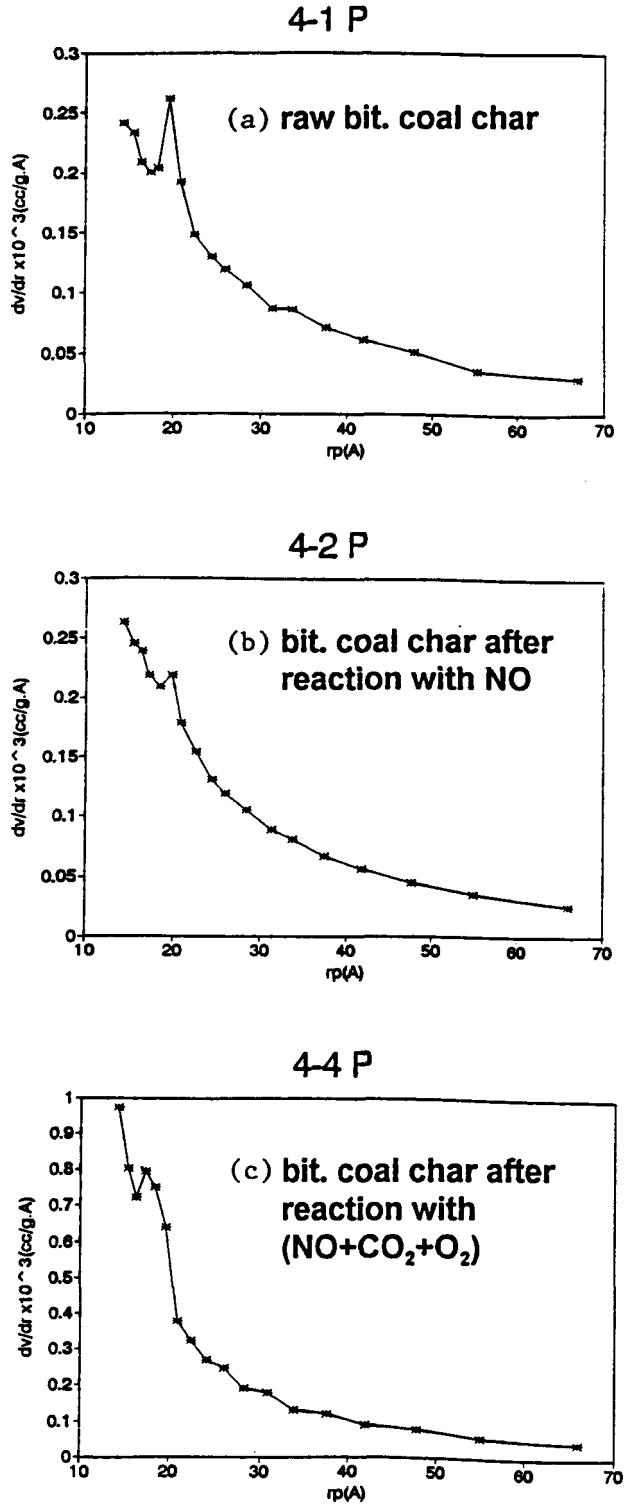

Figure 10. Pore size distribution of bituminous coal char

(a). Char pyrolyzed at 1100°C and 5 min holding time

(b). Char pyrolyzed at 1100°C and 5 min holding time followed by reaction with NO at 1100°C

(c). Char pyrolyzed at 1100°C and 5 min holding time followed by reaction with ($NO+CO_2+O_2$) at 1100°C

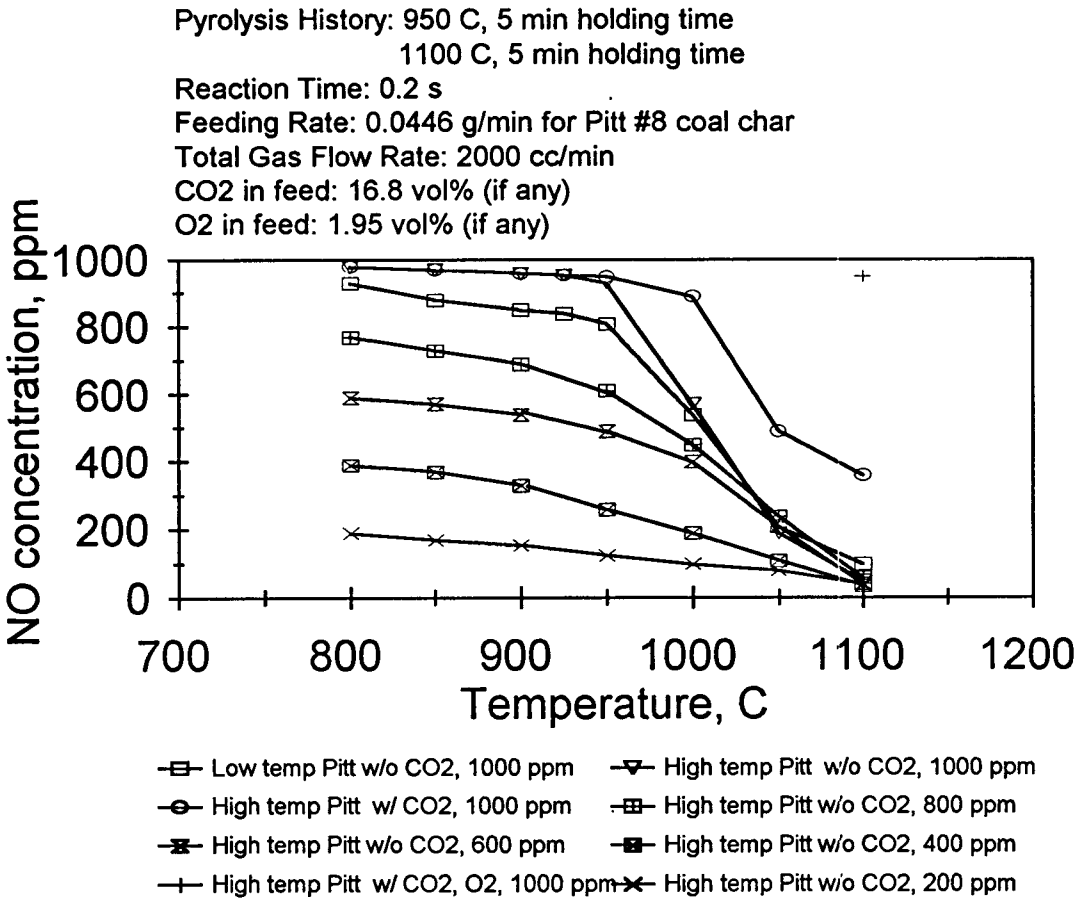

Figure 11. Effects of char origins, char history on exit NO concentration

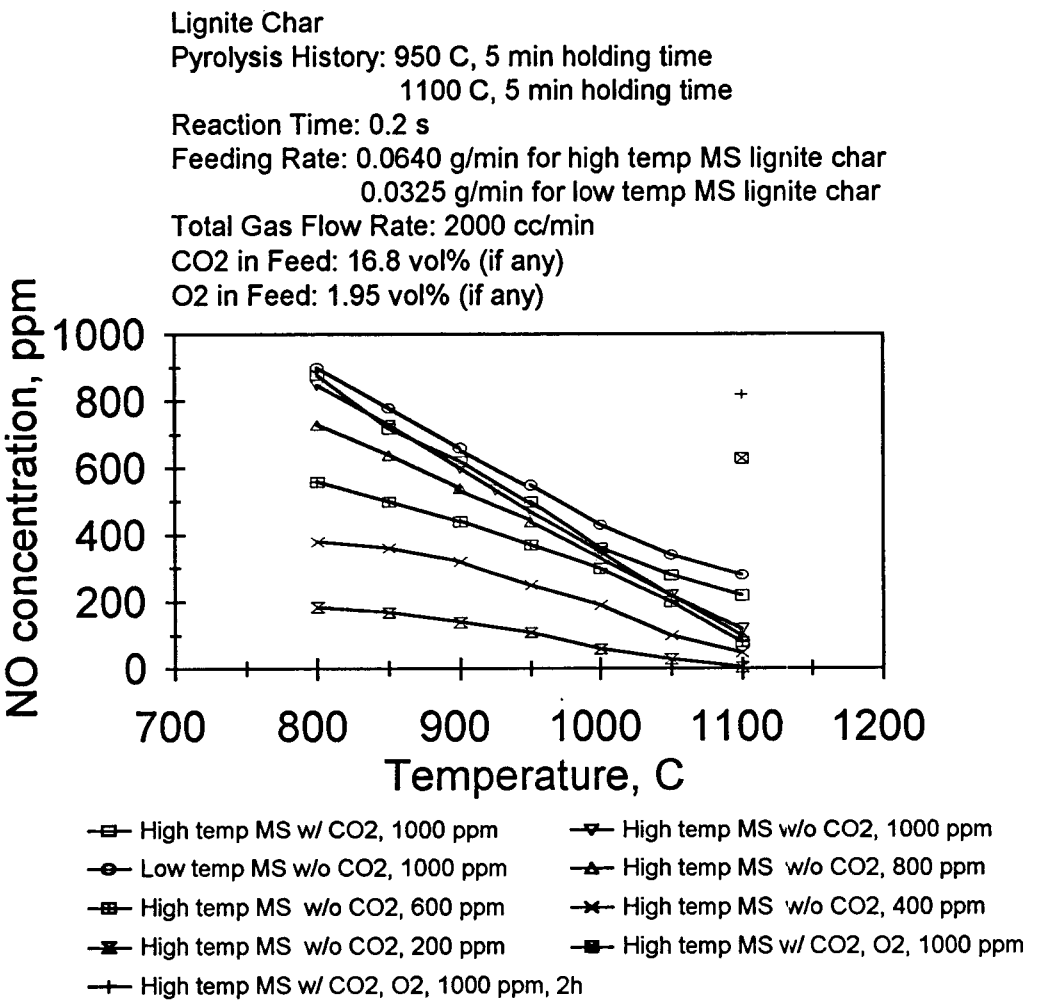

Figure 12. Effects of char origins, char history on exit NO concentration

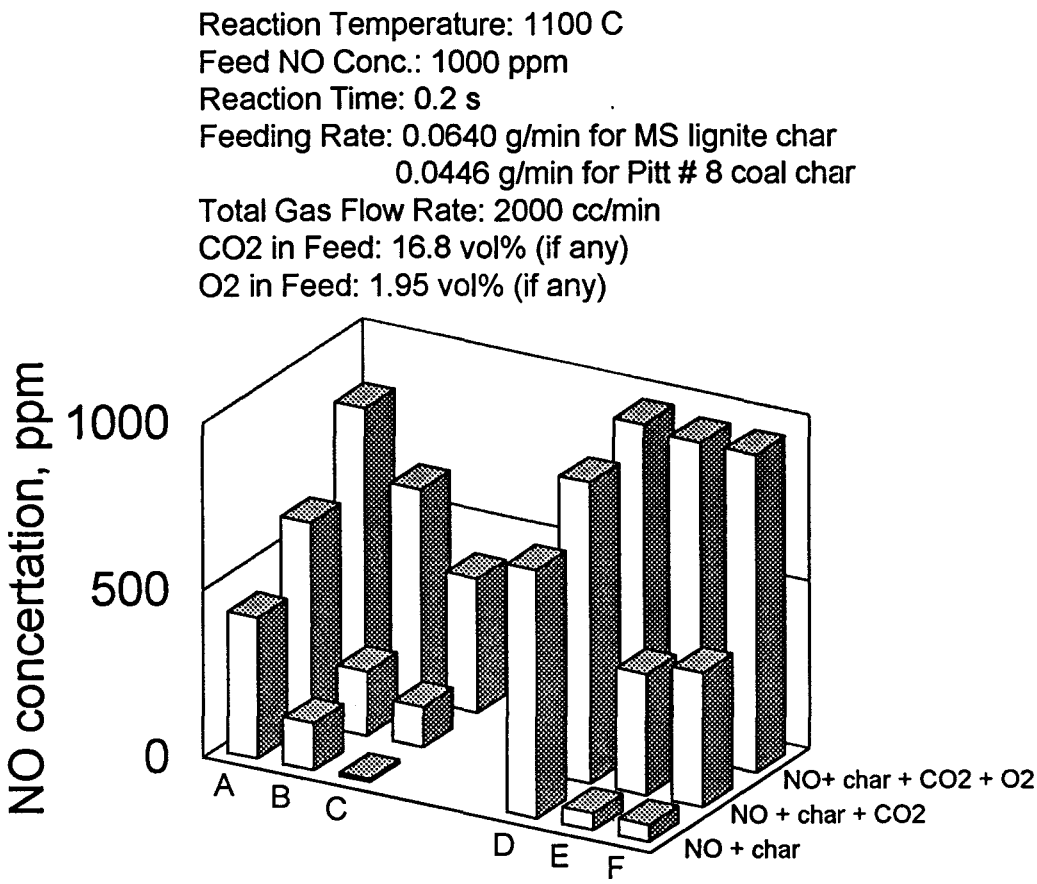

A : MS lignite char, py. temp. 1100 C, 2 h holding time
B : MS lignite char, py. temp. 1100 C, 5 min holding time
C : MS lignite char, py. temp. 950 C, 0 holding time
D : Pitt # 8 coal char, py. temp. 1100 C, 2 h holding time
E : Pitt # 8 coal char, py. temp. 1100 C, 5 min holding time
F : Pitt # 8 coal char, py. temp. 950 C, 0 holding time

Figure 13. Effects of char origins, char history, and oxidants on exit NO concentration. The NO to char ratios correspond to agent used in reburning at SR = 0.95 and 0.90 for the lignite char and bituminous coal char, respectively.

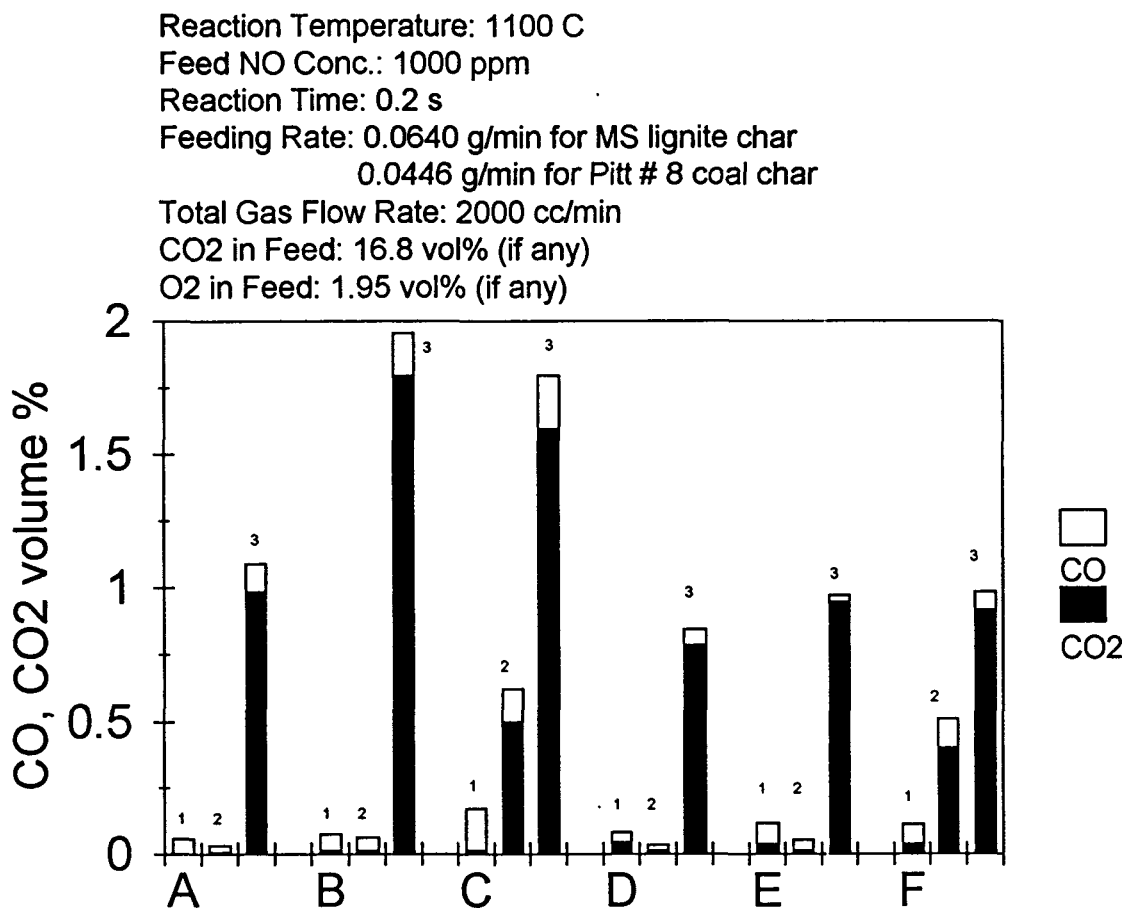

1 : NO+char reaction, 2 : NO+char+CO2 reaction, 3 : NO+char+CO2+O2 reaction
A : MS lignite char py. temp. 1100 C, 2 h holding time
B : MS lignite char py. temp. 1100 C, 5 min holding time.
C : MS lignite char py. temp. 950 C, 0 holding time.
D : Pitt #8 coal char py. temp 1100 C, 2 h holding time
E : Pitt #8 coal char py. temp 1100 C, 5 min holding time
F : Pitt #8 coal char py. temp 950 C, 0 holding time.

Figure 14. Effects of char origins, char history, and oxidants on yields of carbon oxides (in volume percentage) from the reactions of NO with the chars. The NO to char ratios correspond to agent used in reburning at SR = 0.95 and 0.90 for the lignite char and bituminous coal char, respectively.

Reaction Temperature: 1100 C
Feed NO Conc.: 1000 ppm
Reaction Time: 0.2 s
Feeding Rate: 0.0640 g/min for MS lignite char
0.0446 g/min for Pitt # 8 coal char
Total Gas Flow Rate: 2000 cc/min
CO2 in Feed: 16.8 vol% (if any)
O2 in Feed: 1.95 vol% (if any)

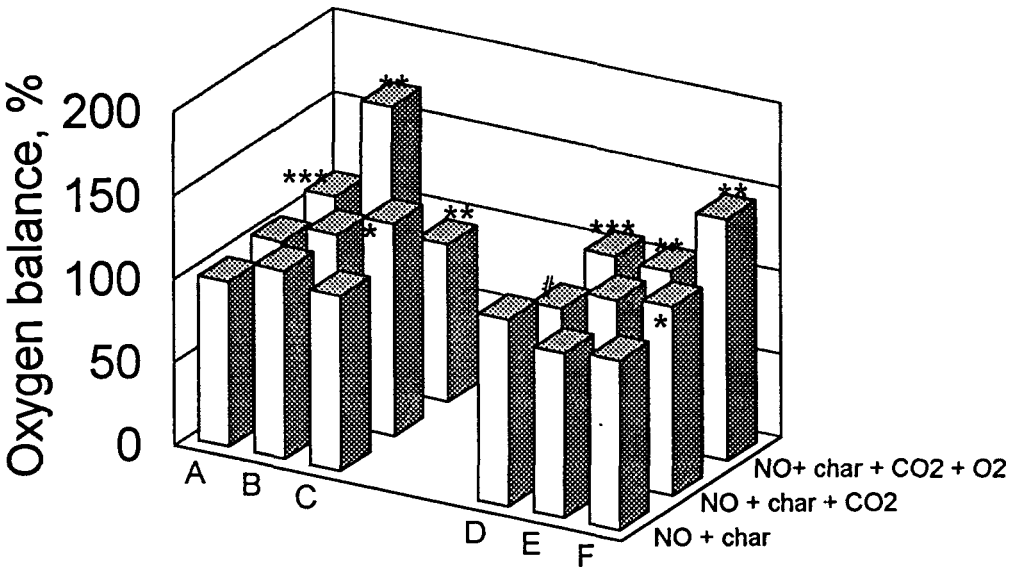

A : MS lignite char, py. temp. 1100 C, 2 h holding time
B : MS lignite char, py. temp. 1100 C, 5 min holding time
C : MS lignite char, py. temp. 950 C, 0 holding time
D : Pitt # 8 coal char, py. temp. 1100 C, 2 h holding time
E : Pitt # 8 coal char, py. temp. 1100 C, 5 min holding time
F : Pitt # 8 coal char, py. temp. 950 C, 0 holding time
: value/5
* : value/16
** : value/60
*** : value/120
**** : value/600

Figure 15. Effects of char origins, char history, and oxidants on percentage conversion of oxygen in feed NO to the gasification products, CO and CO_2. The NO to char ratios correspond to agent used in reburning at SR = 0.95 and 0.90 for the lignite char and bituminous coal char, respectively.

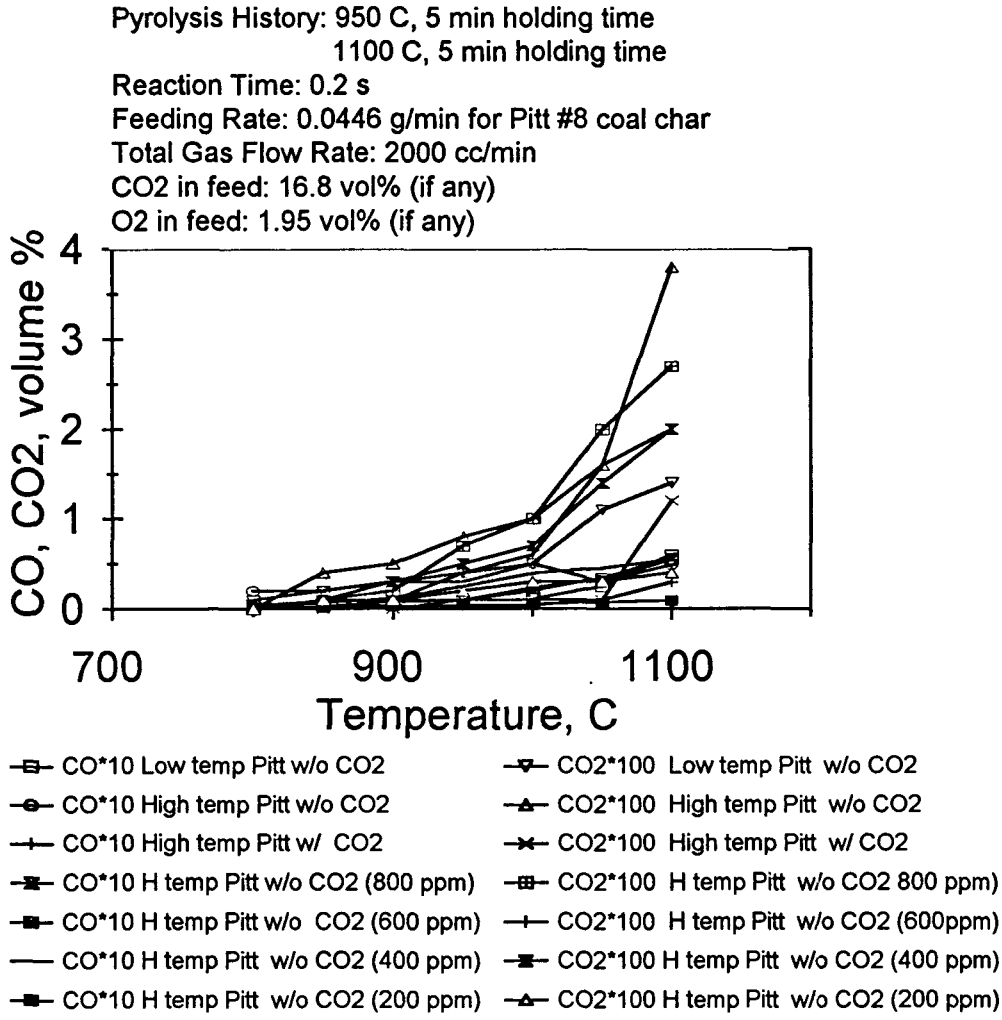

Figure 16. Yields of carbon oxides (in volume percentage) from the reaction of NO for Pittsburgh #8 coal char

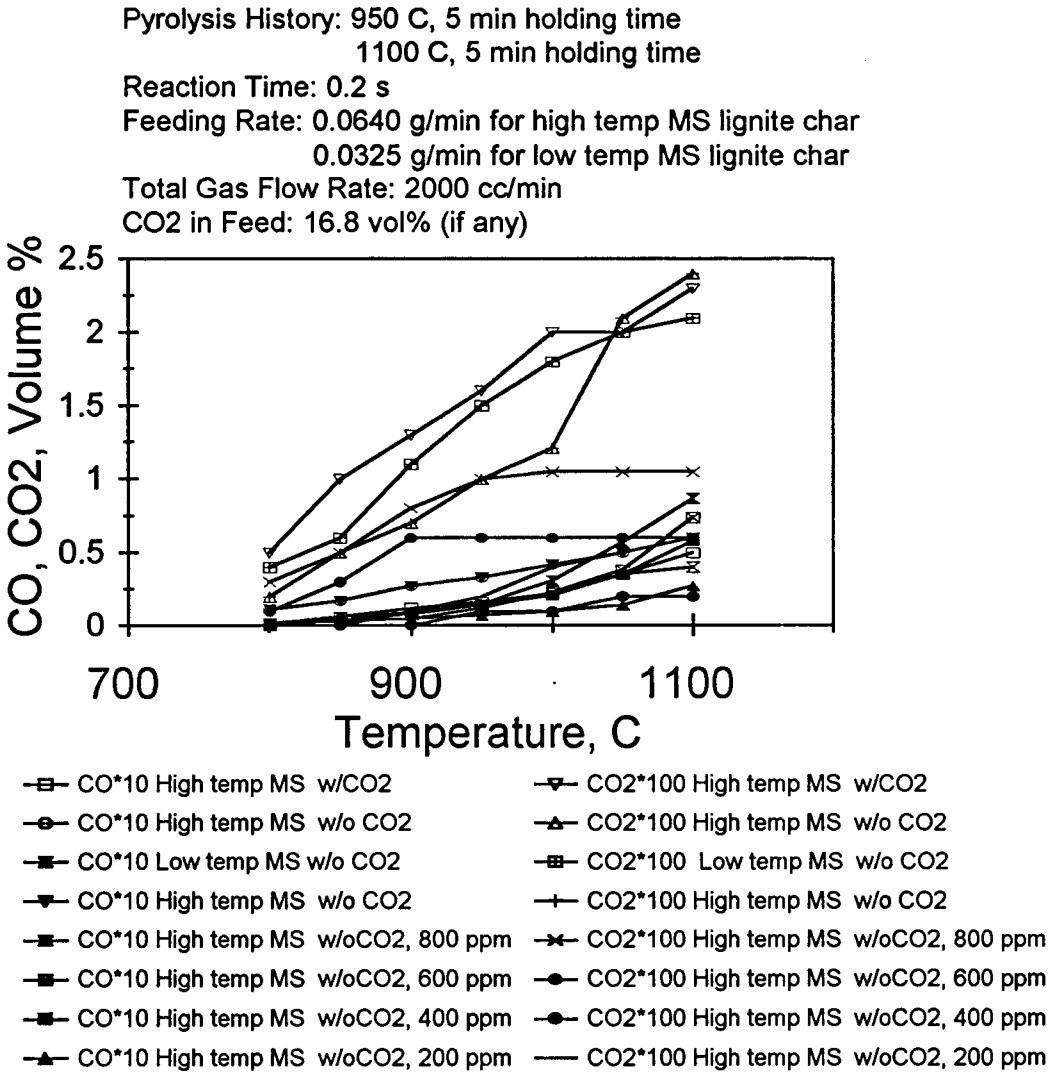

Figure 17. Yields of carbon oxides (in volume percentage) from the reaction of NO for Mississippi lignite char

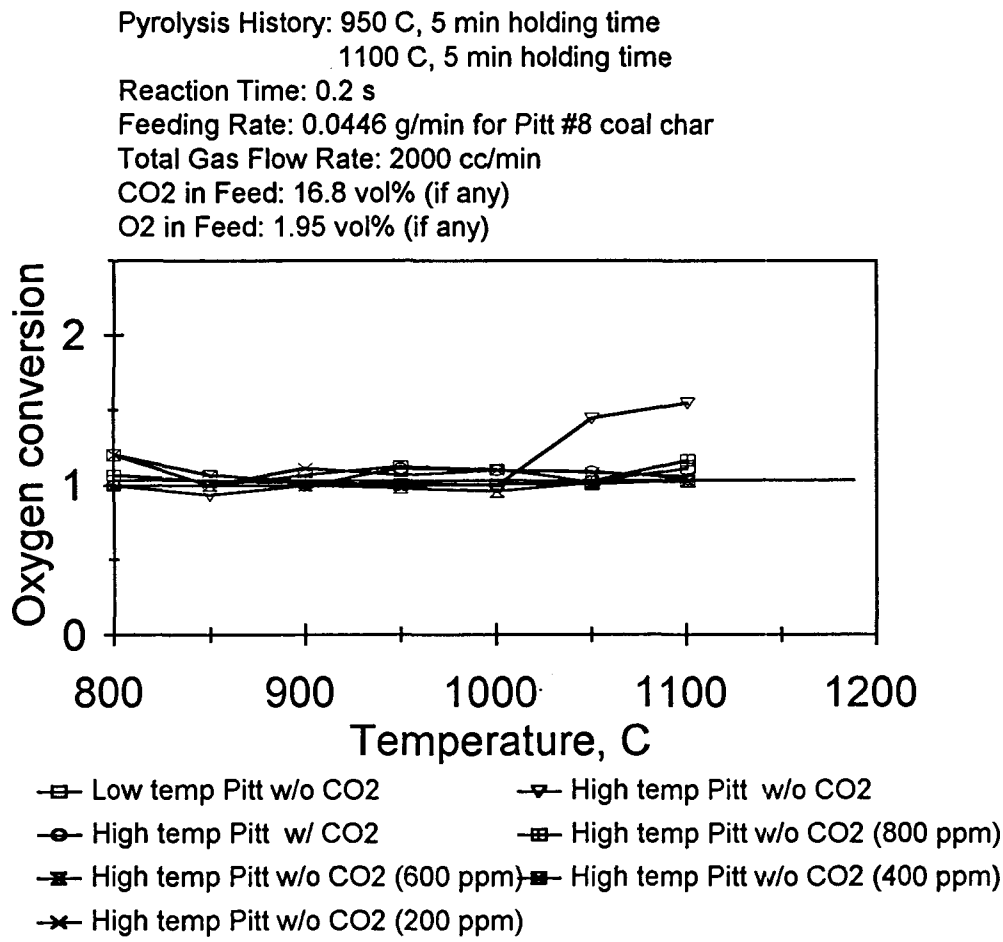

Figure 18. Conversions of oxygen of NO during reactions with the Pittsburgh #8 coal char and different gas compositions

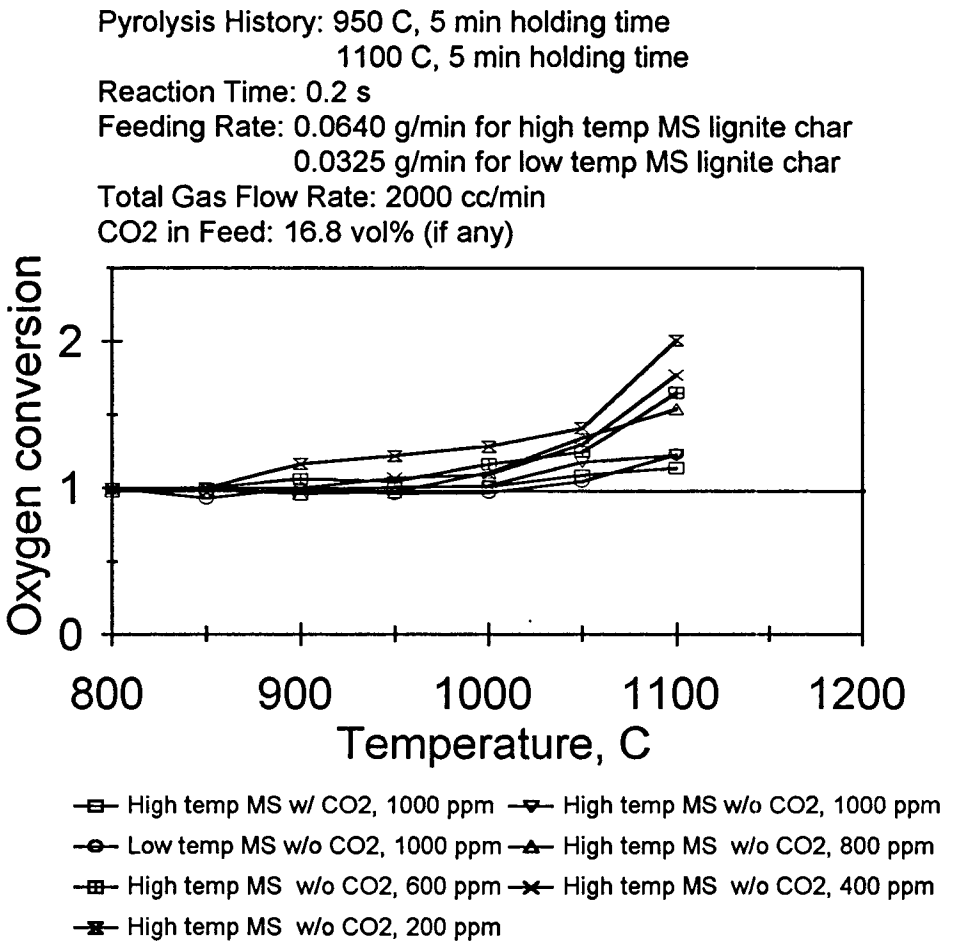

Figure 19. Conversions of oxygen of NO during reactions with the Mississippi lignite chars and different gas compositions

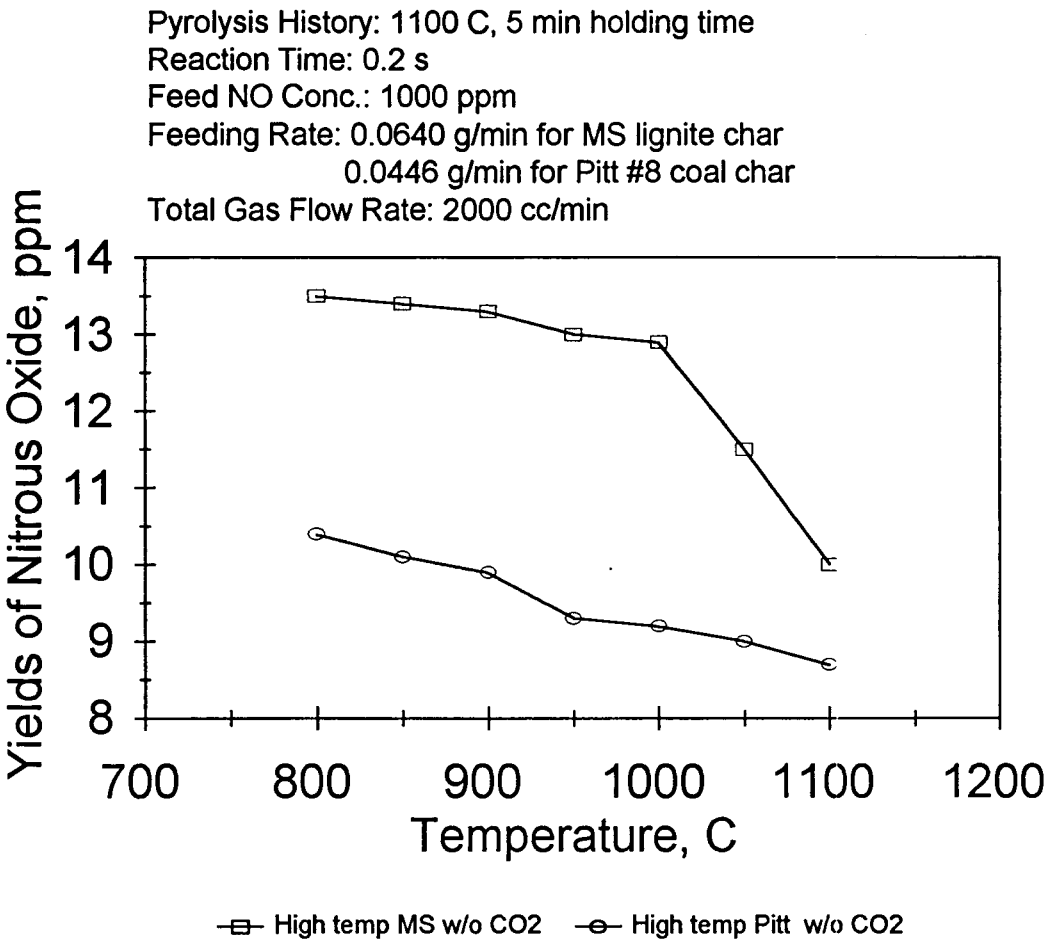

Figure 20. Yields of nitrous oxide for Pittsburgh #8 coal char and Mississippi lignite char

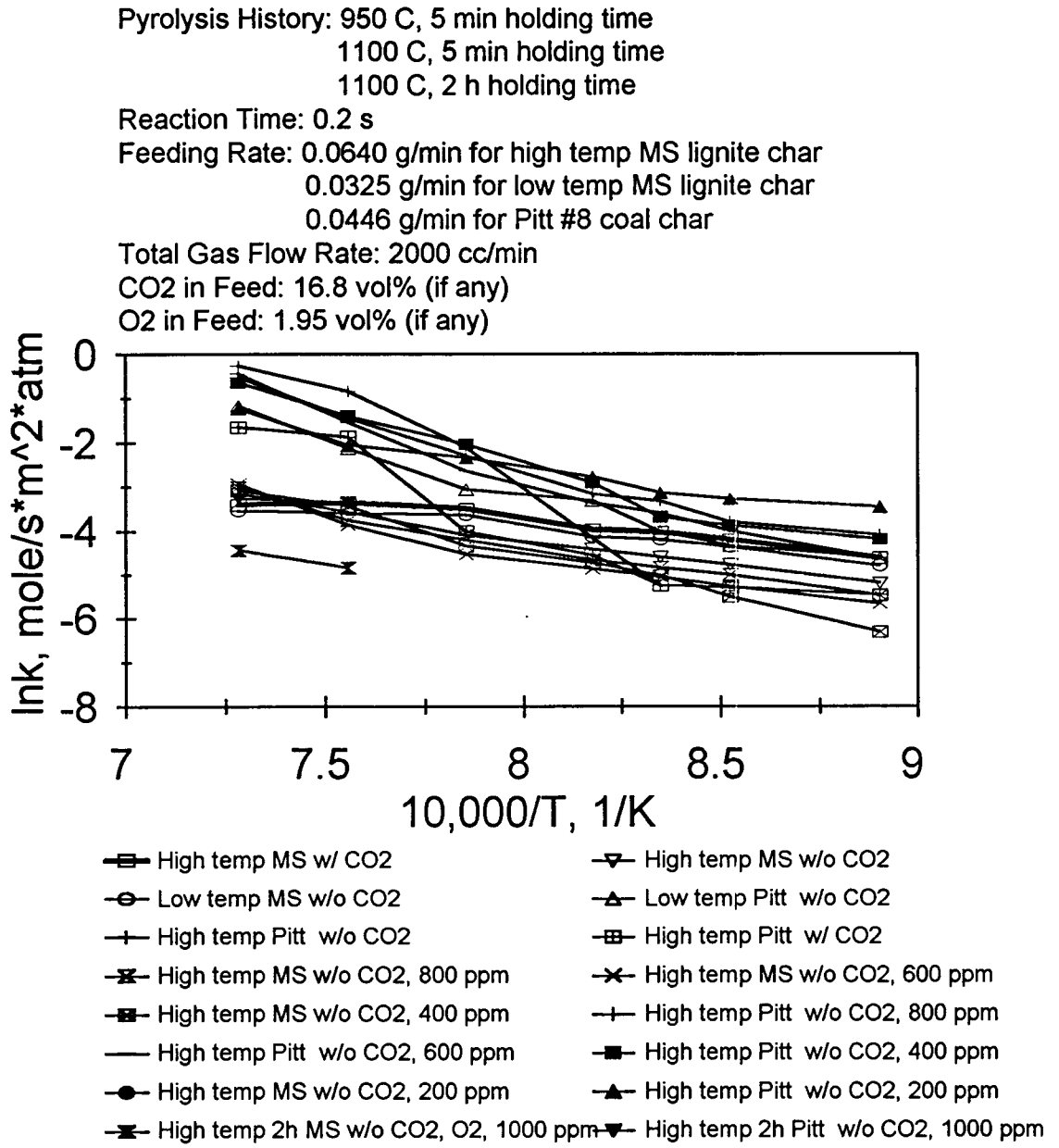

Figure 21. Arrhenius plots for the reactions with chars of different origins and different feed compositions (based on CO_2 surface area)

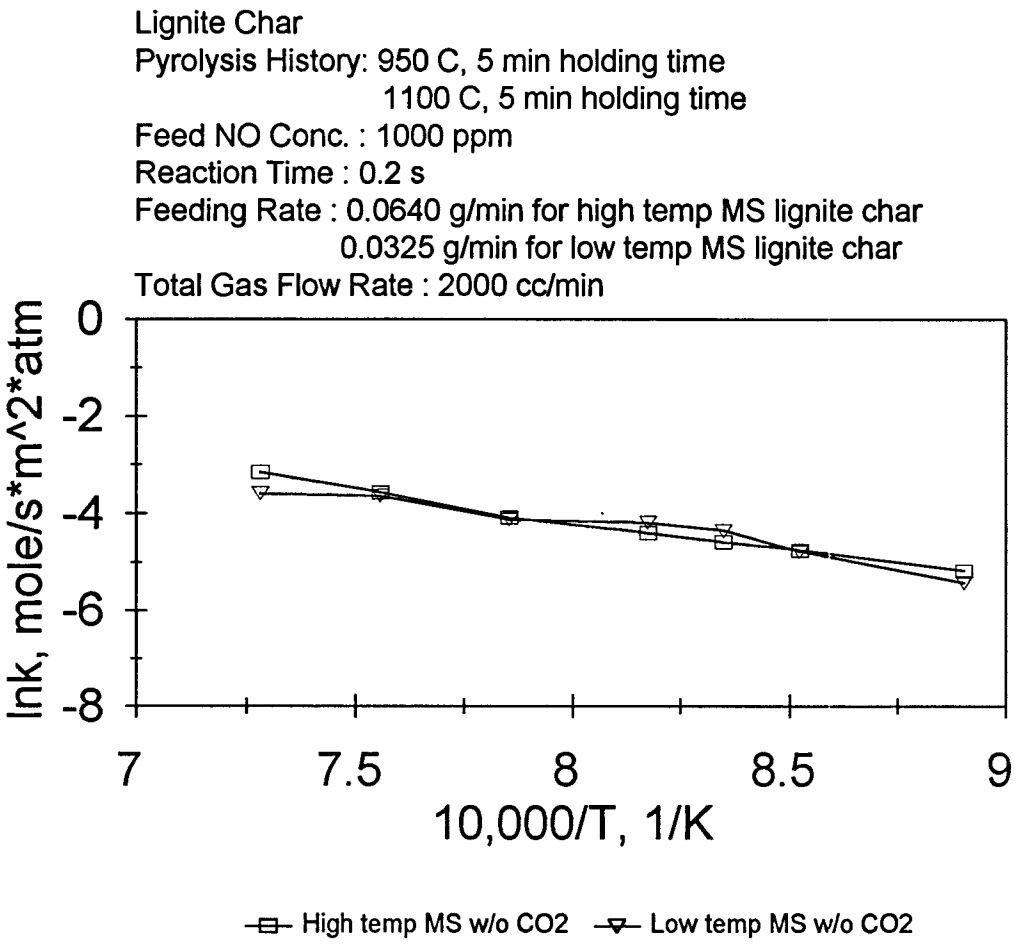

Figure 22. Arrhenius plots for the reactions of Mississippi lignite chars with NO of different pyrolysis temperatures (based on CO_2 surface area)

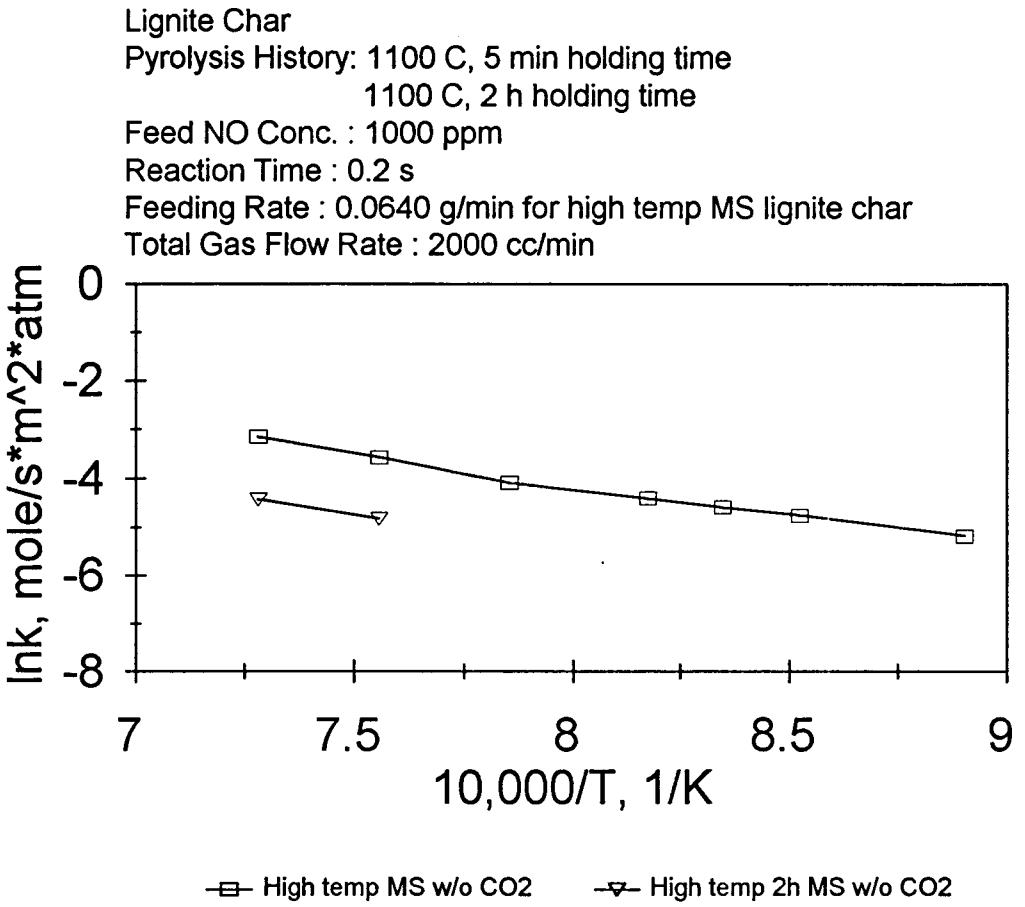

Figure 23. Arrhenius plots for the reactions of Mississippi lignite chars with NO of different holding time (based on CO_2 surface area)

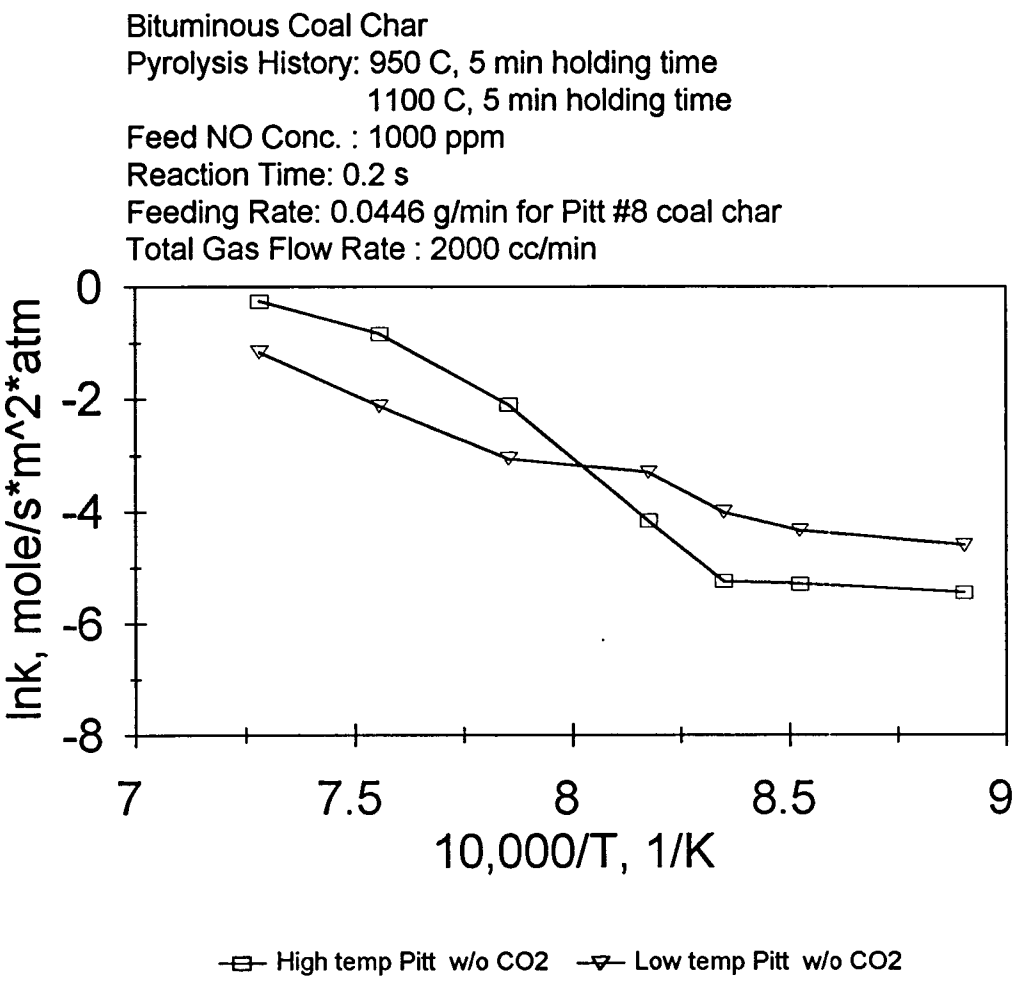

Figure 24. Arrhenius plots for the reactions of Pittsburgh #8 coal chars with NO of different temperatures (based on CO_2 surface area)

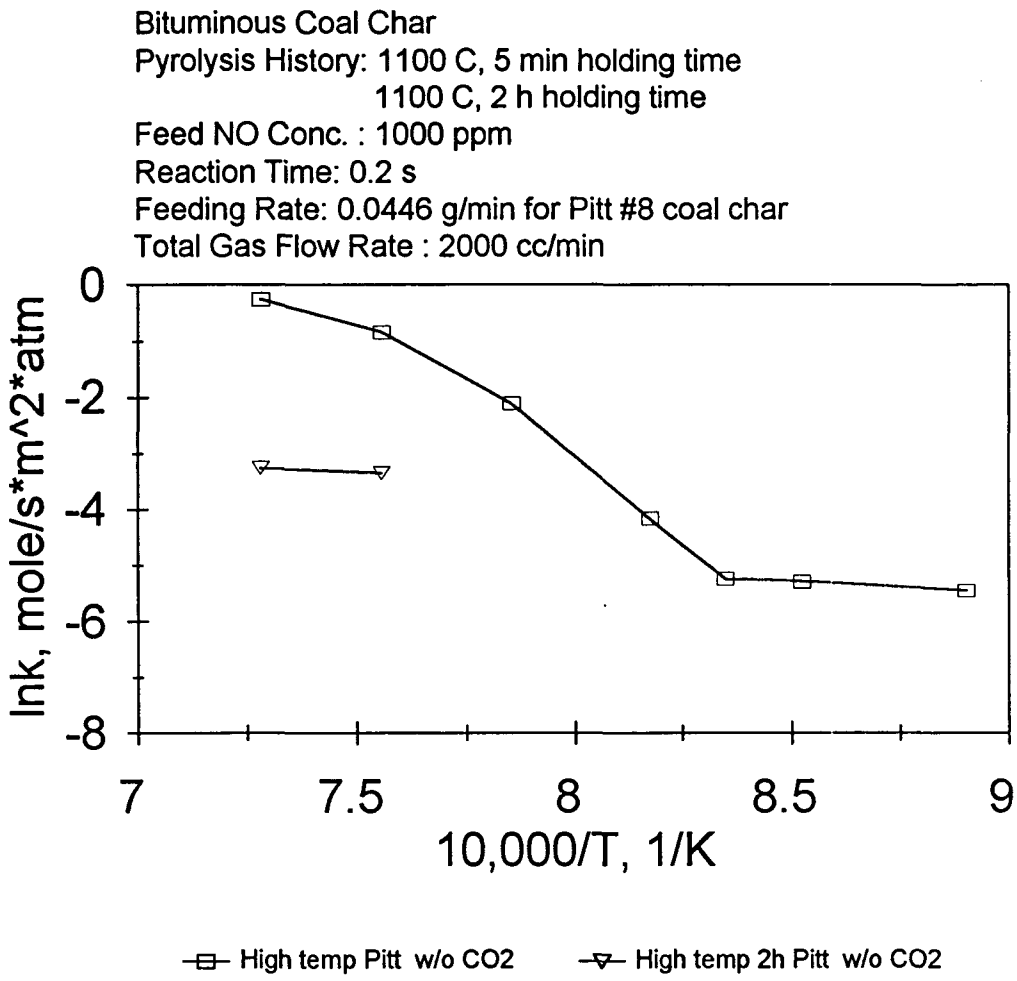

Figure 25. Arrhenius plots for the reactions of Pittsburgh #8 coal chars with NO of different holding time (based on CO_2 surface area)

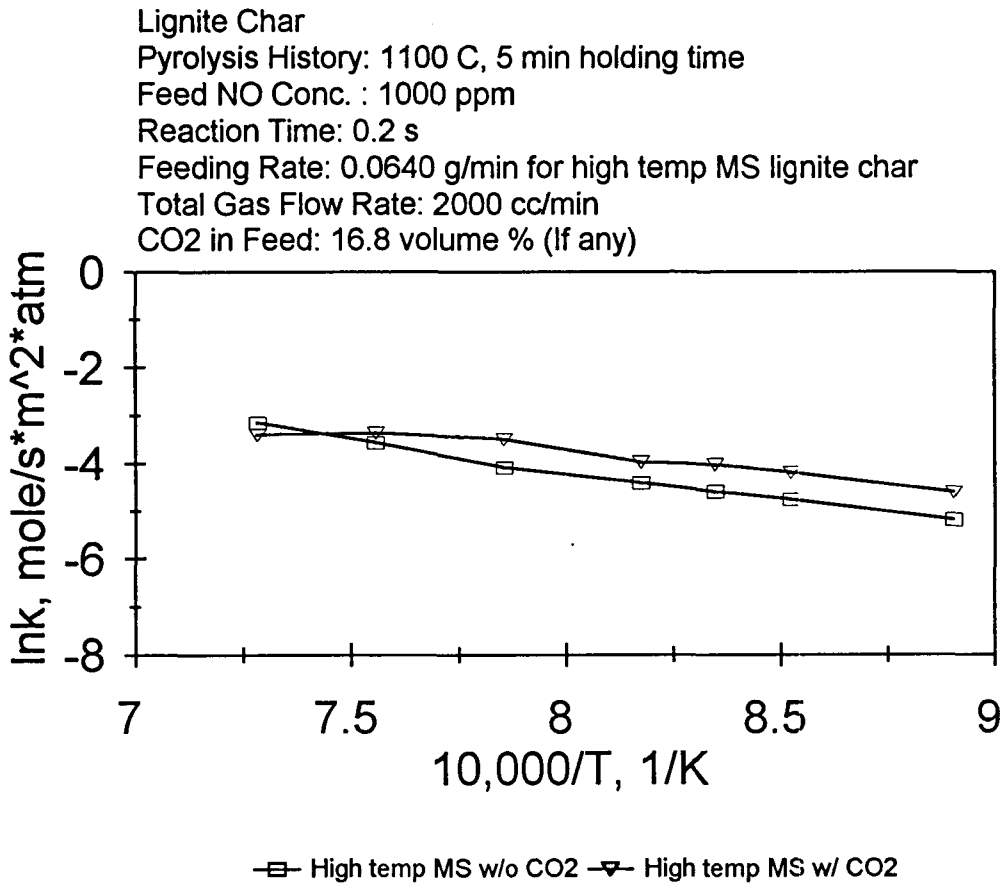

Figure 26. Arrhenius plots for the reactions of Mississippi lignite char with NO and $NO+CO_2$ (based on CO_2 surface area)

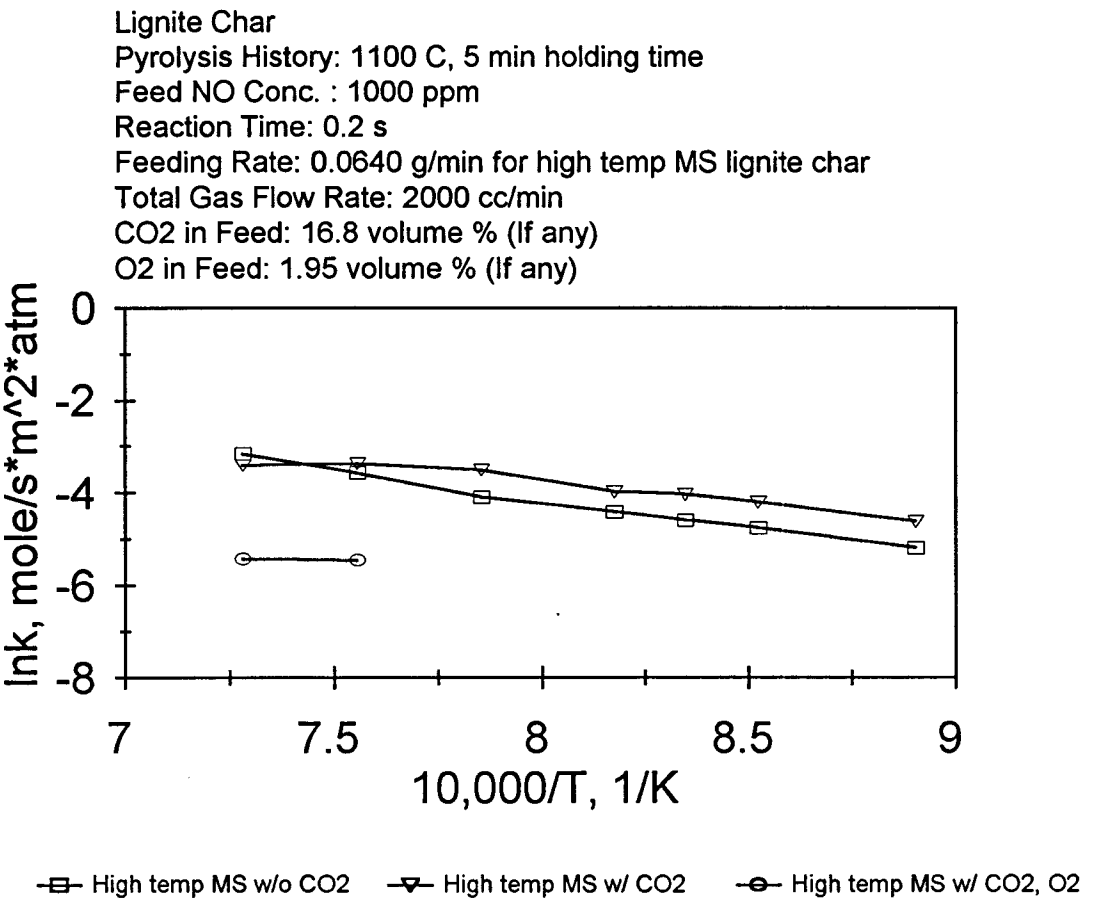

Figure 27. Arrhenius plots for the reactions of Mississippi lignite char with NO, $NO+CO_2$ and $NO+CO_2+O_2$ (based on CO_2 surface area)

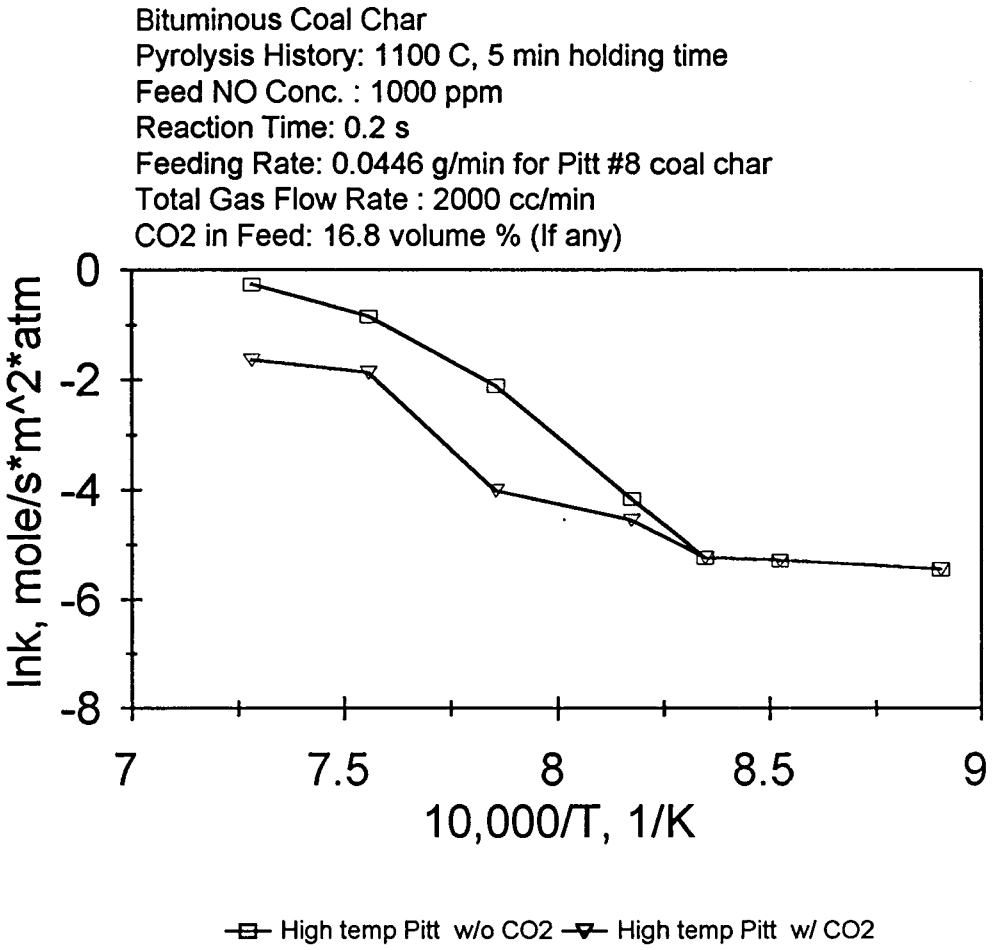

Figure 28. Arrhenius plots for the reactions of Pittsburgh #8 coal char with NO and $NO+CO_2$ (based on CO_2 surface area)

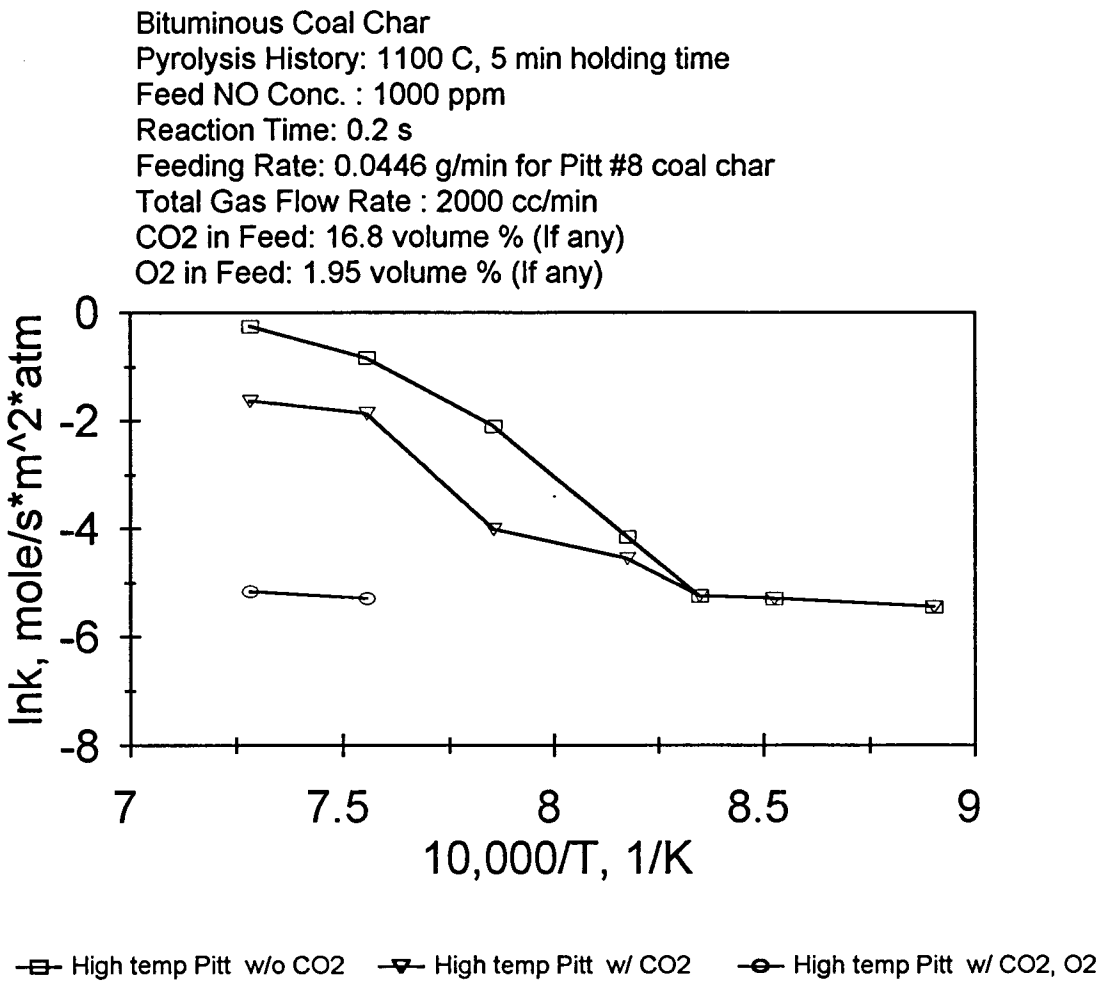

Figure 29. Arrhenius plots ofor the reactions of Pittsburgh #8 coal char with NO, $NO+CO_2$ and $NO+CO_2+O_2$ (based on CO_2 surface area)

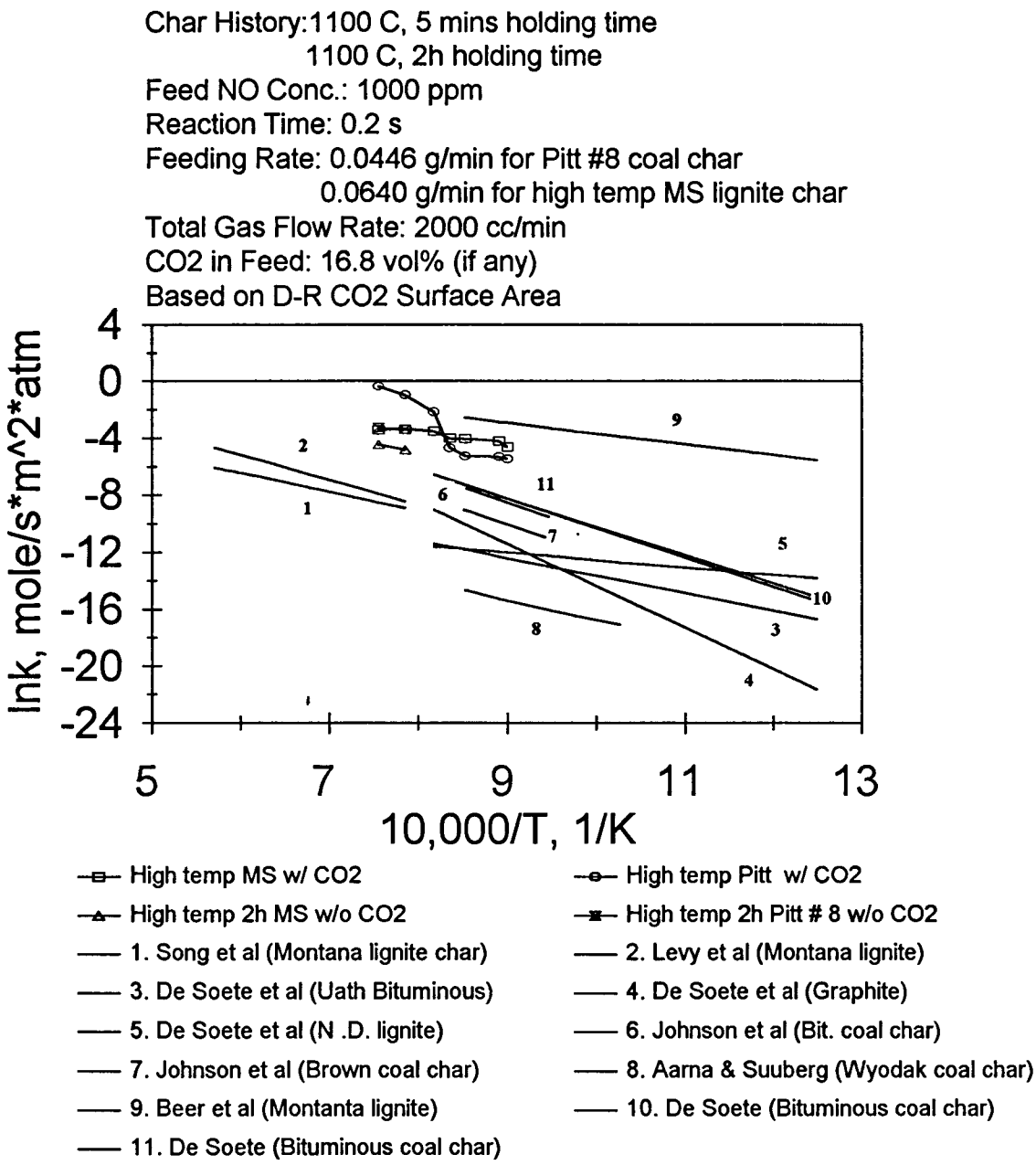

Figure 30. Arrhenius plots of NO reactions with chars of two different origins in the presence of CO_2 based on CO_2 surface areas. Published data in the literature are included for comparison

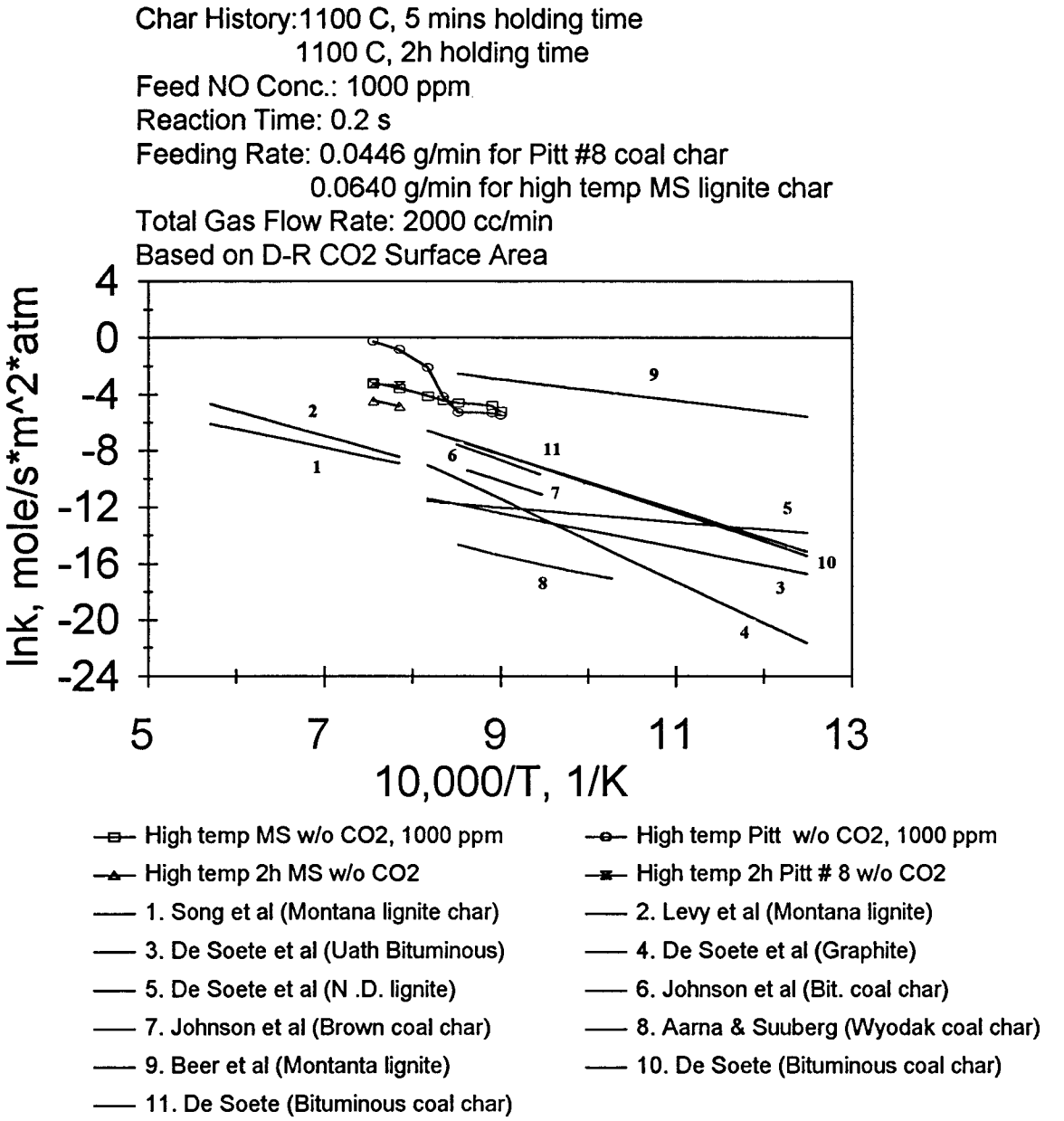

Figure 31. Arrhenius plots of NO reactions with chars of two different origins in the absence of CO_2 based on CO_2 surface areas. Published data in the literature are included for comparison

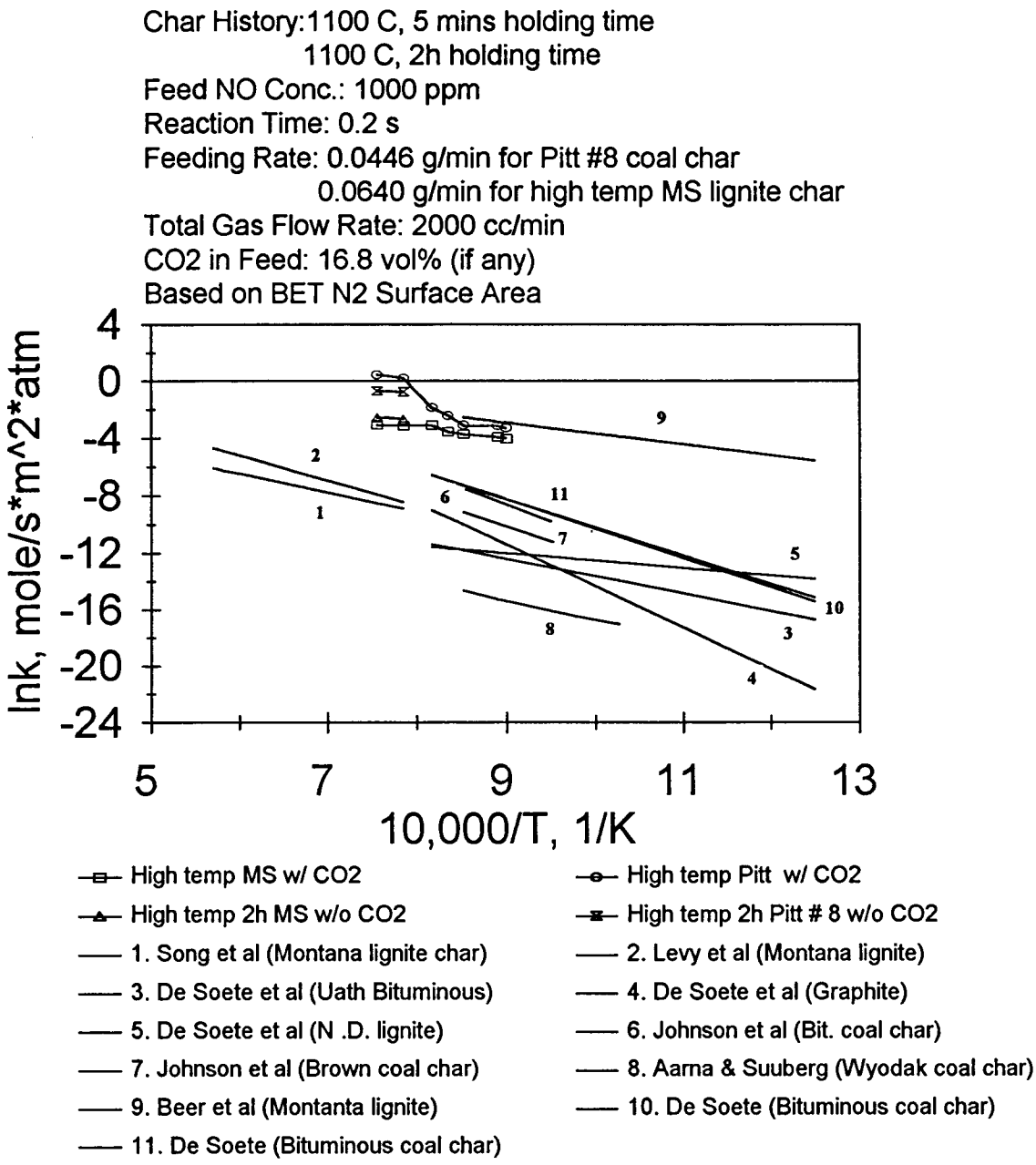

Figure 32. Arrhenius plots of NO reactions with chars of two different origins in the presence of CO_2 based on N_2 surface areas. Published data in the literature are included for comparison

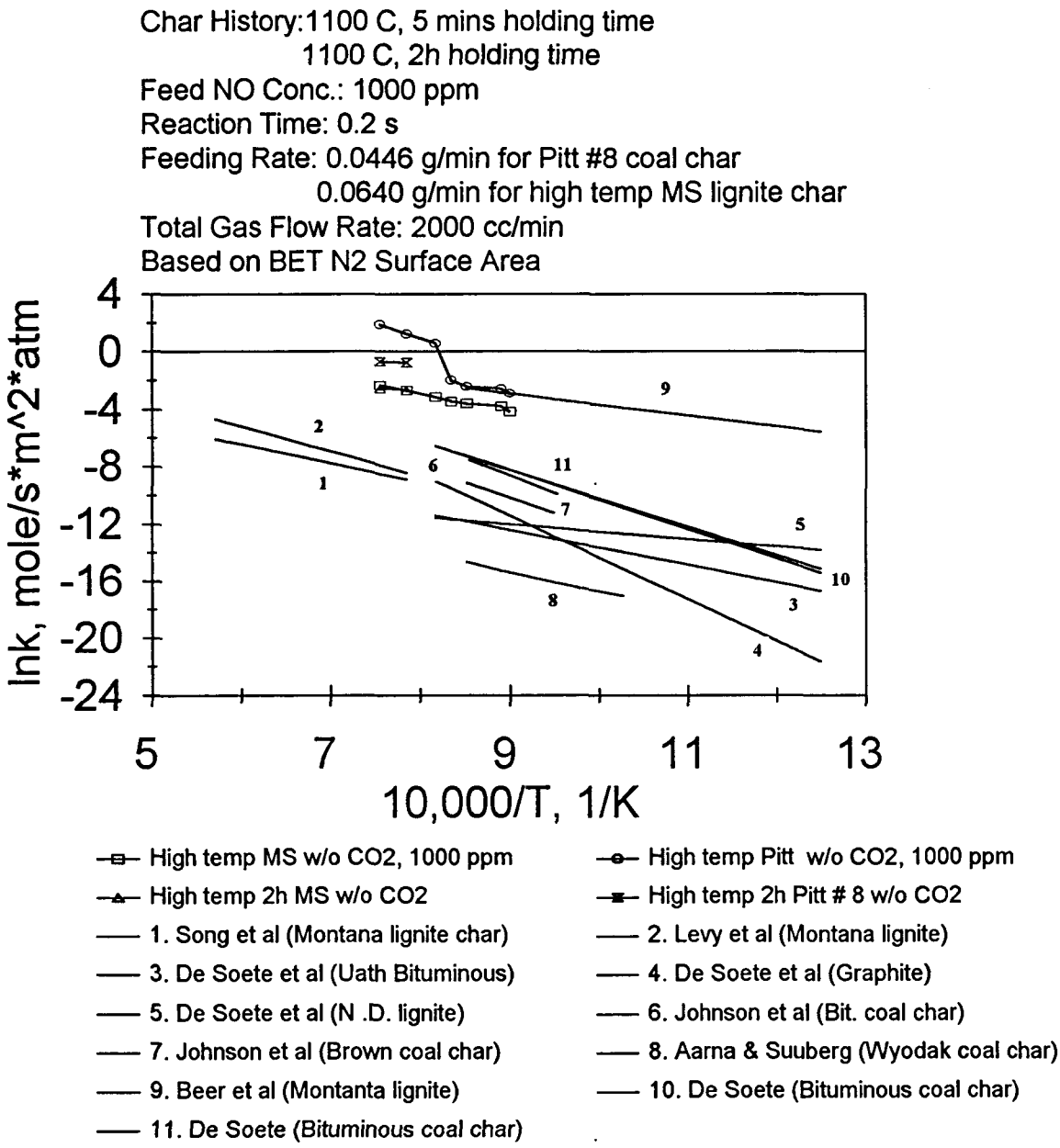

Figure 33. Arrhenius plots of NO reactions with chars of two different origins in the absence of CO_2 based on N_2 surface areas. Published data in the literature are included for comparison

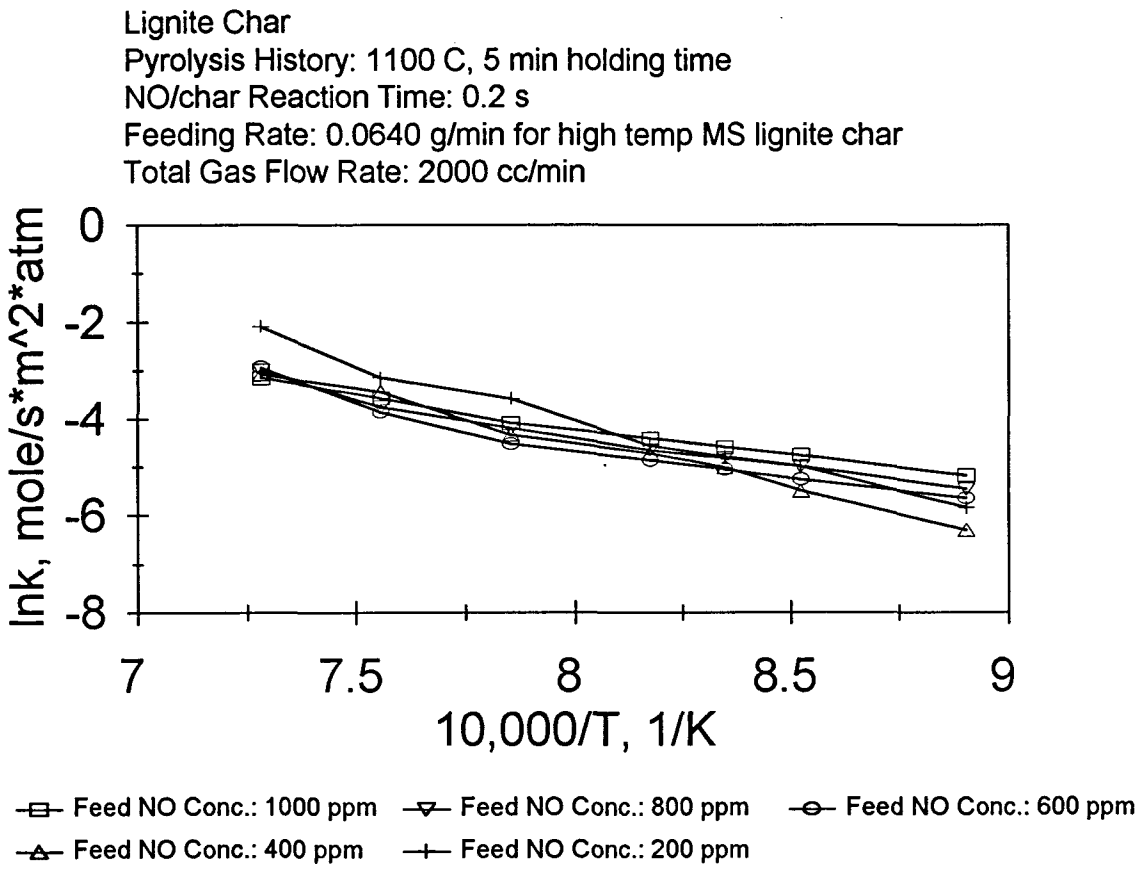

Figure 34. Arrhenius plots for the reactions of Mississippi lignite char reacts with NO for different initial NO concentrations (based on CO_2 surface area)

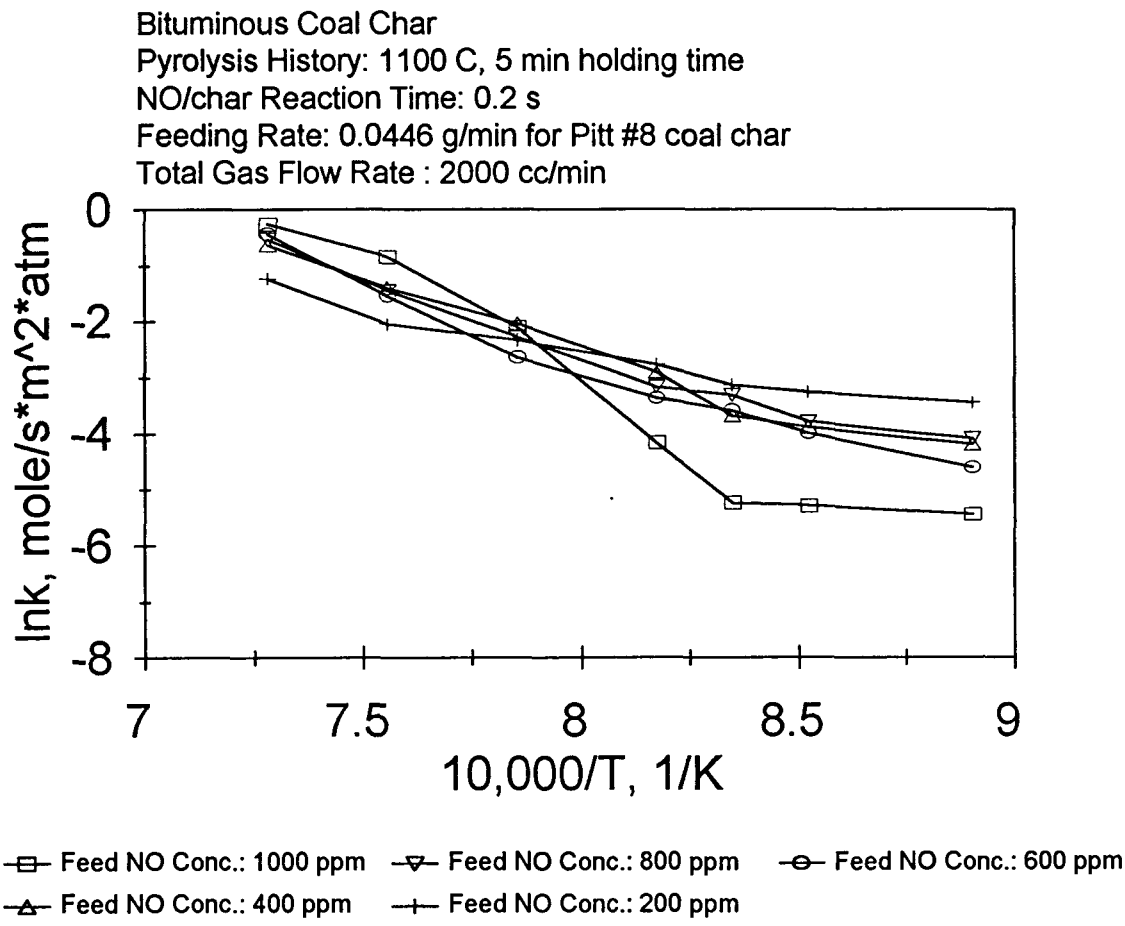

Figure 35. Arrhenius plots for the reactions of Pittsburgh #8 coal char reacts with NO for different initial NO concentrations (based on CO_2 surface area)

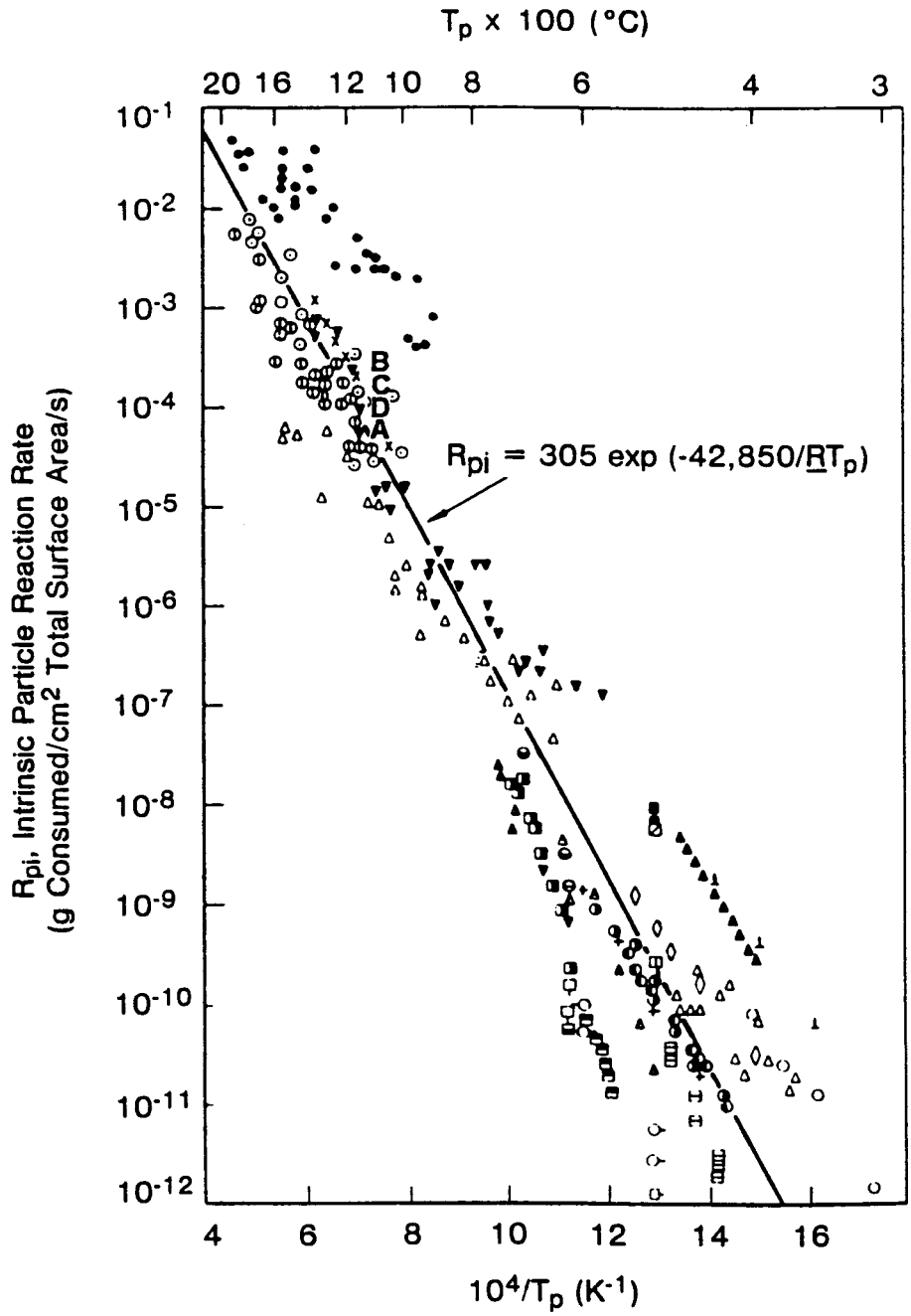

Figure 36. Comparison of NO/Char and O_2/Char reaction with published data (based on CO_2 surface area)

A: NO/Mississippi lignite char reaction B: NO/Pittsburgh # 8 coal char reaction

C: O_2/Mississippi lignite char reaction D: O_2/Pittsburgh # 8 coal char reaction